

**New Insights into Hepatitis C Virus Induced Changes
of the Host Cell Lipidome and the Impact of
Fatty Acid Remodeling on the Viral Life Cycle**

Dissertation

submitted to the

Department of Chemistry

Faculty of Mathematics, Informatics, and Natural Sciences

University of Hamburg

In fulfillment of the requirements

for the degree of

Doctor of Natural Sciences (Dr. rer. nat.)

by

Sarah Hofmann

Hamburg, 2017

Reviewer of the dissertation:

Dr. rer. nat. Eva Herker

PD Dr. rer. nat. habil. Markus Perbandt

Oral defence:

March 17, 2017

This dissertation was conducted between February 2012 and January 2017 at the Heinrich Pette Institute, Leibniz Institute for Experimental Virology, under the supervision of Dr. rer. nat. Eva Herker and PD Dr. rer. nat. habil. Markus Perbandt.

Contents

Abstract.....	1
Zusammenfassung.....	3
1. Introduction.....	5
1.1. Hepatitis C virus (HCV) infection.....	5
1.2. HCV life cycle.....	7
1.2.1. The lipovirion and cell entry.....	7
1.2.2. Viral RNA translation and protein function.....	10
1.2.3. Viral RNA replication.....	12
1.2.4. Viral assembly and release.....	13
1.3. Lipid metabolism.....	14
1.3.1. Fatty acids.....	14
1.3.2. Glycerolipids.....	19
1.3.3. Membrane lipids.....	20
1.3.4. Localization of lipid synthesis.....	22
1.3.5. Lipid transport is performed by lipoproteins.....	24
1.3.6. Lipid storage takes place in lipid droplets.....	26
1.4. HCV causes an alteration in the lipid composition of the host cell.....	27
1.5. Aim of the project.....	28
2. Results.....	31
2.1. HCV infection shifts the lipid profile of the host cell.....	31
2.1.1. Preparation of whole cell extracts for mass spectrometry.....	31
2.1.2. HCV-infected cells contain a higher portion of membrane lipids compared to neutral lipids.....	33
2.1.3. HCV-infected cells contain a higher relative abundance of lipids with longer fatty acyl chains.....	34
2.1.4. The absolute amount of polyunsaturated fatty acids is increased upon HCV infection.....	36
2.2. Metabolomic screen of HCV-infected Huh7.5 cells.....	37

Contents

2.2.1. HCV infection changes the phosphatidylcholine composition and decreases sphingomyelins	37
2.2.2. Analysis of amino acids and biogenic amines	39
2.3. Free cholesterol accumulates in the perinuclear region upon HCV infection	41
2.4. HCV infection alters the lipid profile but not the morphology of lipid droplets.....	42
2.4.1. HCV infection has no impact on lipid droplet morphology in Huh7.5 cells.....	42
2.4.2. Preparation of lipid droplet extracts for mass spectrometry	45
2.4.3. Lipids with longer fatty acyl chains have a higher abundance in lipid droplets isolated from HCV-infected cells	47
2.5. Different lipid species have diverse effects on HCV replication	49
2.5.1. Cholesterol has a dose- and time-dependent impact on HCV infection	49
2.5.2. The triglyceride level is altered upon fatty acid treatment in HCV-infected and uninfected cells in a similar manner	51
2.5.3. Fatty acids have diverse effects on HCV replication depending on fatty acyl chain length and desaturation	52
2.5.4. Lauric acid has no impact on HCV particle density.....	55
2.5.5. Polyunsaturated fatty acids cause alterations of the membranous web in HCV-infected cells.....	56
2.6. Fatty acid elongation and desaturation is necessary for viral replication	57
2.6.1. Fatty acid elongases and desaturases are differentially expressed in HCV-infected cells	57
2.6.2. Knockdown of elongases and desaturases has diverging effects on the HCV life cycle	59
2.7. FADS2 inhibition impairs HCV replication	61
2.7.1. SC-26196 has no impact on cell viability and <i>FADS2</i> expression.....	61
2.7.2. FADS2 inhibition has diverging dose- and time-dependent effects on HCV infection	62
2.7.3. FADS2 inhibition increases the surface expression of SR-BI	65
2.7.4. FADS2 inhibition has no impact on viral particle density	65
2.7.5. FADS2 inhibition increases intracellular ApoE levels.....	67
3. Discussion.....	69

Contents

3.1. HCV infection causes a higher abundance of lipids with longer fatty acyl chains in Huh7.5 cells	69
3.2. Fatty acid incorporation is comparable in HCV-infected and uninfected cells upon prolonged fatty acid treatment.....	74
3.3. Fatty acids have diverse effects on viral replication depending on chain length and desaturation	74
3.4. Cholesterol plays a role in the HCV life cycle	76
3.5. Fatty acid elongation and desaturation is important for HCV replication.....	77
3.6. FADS2 has a dose- and time-dependent effect on the HCV life cycle	79
3.7. Conclusion	82
3.8. Outlook	82
4. Materials.....	85
4.1. HCV full replicating cell culture system	85
4.2. Plasmids	85
4.3. Oligonucleotides	86
4.4. Bacteria	88
4.5. Cell lines and cell culture materials	88
4.6. Solvents and buffers for biochemical methods.....	91
4.6.1. Agarose gel electrophoresis.....	91
4.6.2. SDS-PAGE	91
4.6.3. DNA and protein ladder.....	93
4.6.4. Cell lysis.....	93
4.6.5. Buffers used for lipid droplet isolation.....	94
4.6.6. Solutions used for acidified Bligh & Dyer.....	94
4.6.7. Density gradient.....	95
4.7. Solutions and stainings utilized for microscopy	95
4.8. Antibodies	96
4.9. Enzymes.....	96
4.10. Inhibitors	97
4.11. Chemicals	97

Contents

4.12. Kits.....	101
4.13. Consumables.....	102
4.14. Devices.....	104
4.15. Software.....	105
5. Methods	107
5.1. Molecular biology.....	107
5.1.1. Overlap-extension polymerase chain reaction and cloning of Jc1 ^{Flag-E2 NS5AB-EGFP} ..	107
5.1.2. Colony PCR.....	110
5.1.3. Agarose gel electrophoresis.....	111
5.1.4. Miniprep.....	111
5.1.5. Maxiprep.....	111
5.1.6. Sequencing.....	111
5.1.7. Glycerol stocks.....	111
5.2. Cell biology.....	112
5.2.1. Thawing of eukaryotic cells.....	112
5.2.2. Cell culture.....	112
5.2.3. Freezing of eukaryotic cells.....	112
5.2.4. Electroporation of Huh7.5 cells with <i>in vitro</i> transcribed RNA.....	112
5.2.5. HCV stock production.....	113
5.2.6. Viral titer assay.....	113
5.2.7. Production of lentivirus stocks and lentiviral transduction.....	113
5.2.8. Flow cytometry.....	114
5.2.9. Surface receptor staining for flow cytometry.....	115
5.2.10. Cell viability assay.....	115
5.2.11. Luciferase assays to study HCV replication.....	115
5.2.12. Gradient centrifugation.....	119
5.2.13. Preparation of samples for lipidomic analysis.....	120
5.2.14. Lipid droplet isolation for lipidomics.....	120
5.3. Biochemical methods.....	121
5.3.1. RNA <i>in vitro</i> transcription.....	121

Contents

5.3.2. Phenol/chloroform extraction using 5 Prime Phase Lock Gel tube	121
5.3.3. RNA isolation with TriReagent/Stat60	122
5.3.4. cDNA synthesis.....	122
5.3.5. HCV PCR standard preparation	123
5.3.6. Real-time quantitative PCR	123
5.3.7. Coomassie staining.....	123
5.3.8. Silver staining	123
5.3.9. Western blot.....	124
5.3.10. Lipid extraction, shotgun lipidomics and free fatty acid measurement	124
5.3.11. Metabolite extraction and analysis	125
5.3.12. Bligh & Dyer lipid extraction for triglyceride measurement.....	126
5.4. Microscopic analysis	127
5.4.1. Determination of z-elongation factor.....	127
5.4.2. Microscopy and volumetric analysis of lipid droplets	127
5.4.3. Microscopy analysis of unesterified cholesterol.....	128
5.4.4. Electron microscopy.....	128
5.5. Statistical analysis.....	129
Bibliography	131
Appendix	141
A. Abbreviations.....	141
B. List of figures	146
C. List of tables	148
D. Presentations	150
E. Toxicity of chemicals	152

Abstract

Hepatitis C virus (HCV) infection often progresses to a chronic disease that causes liver pathologies including the accumulation of lipids, known as steatosis. Neutral lipids are stored in cellular organelles termed lipid droplets. Furthermore, HCV utilizes lipid droplets for its own purpose as virus assembly platform. In addition, several lipid synthesis pathways have been described to be required for viral replication. Examples are the cholesterol synthesis pathway and the desaturation of palmitic and stearic acid. Furthermore, HCV has the capability to interfere with the lipid metabolism causing changes in the host cell lipid composition.

The first aim of this study was the generation of lipid profiles from HCV-infected and uninfected cells by shotgun lipidomics. HCV-infected cells revealed a higher abundance of membrane lipids compared to neutral lipids, likely due to the formation of the membranous web for HCV RNA replication. Detailed lipid profiles revealed a lower abundance of triglycerides and phosphatidylcholines with shorter fatty acyl chains and an increased abundance of triglycerides and phosphatidylcholines with longer fatty acyl chains in HCV-infected cells compared to uninfected cells. These changes were observed in whole cell extracts as well as in isolated lipid droplet fractions. In addition, the free fatty acids arachidonic acid, eicosapentaenoic acid, and docosahexaenoic acid were increased in HCV-infected cells. Subsequently, the impact of free fatty acid supplementation on the viral life cycle was further elucidated. Interestingly, the influence of fatty acids on the viral life cycle was dependent on the fatty acid chain length and the degree of desaturation. Only the shortest fatty acid tested, lauric acid, promoted viral RNA replication and virus production. Two saturated fatty acids, myristic acid and palmitic acid, had an impact on late stages of the viral life cycle (production of viral progeny) without affecting viral RNA replication. Mono- and polyunsaturated fatty acids inhibited viral RNA replication and consequently virus production. Subsequent investigation of fatty acid modulating enzymes underlined the importance of a functional fatty acid homeostasis. This study revealed that a diminished fatty acid elongation or desaturation impairs mainly viral replication, while only the knockdown of the $\Delta 6$ -desaturase FADS2 reduced virion production. Dose- and time dependent FADS2 inhibition indicates a dual role of FADS2 in the viral life cycle. Short-term FADS2 inhibition increased the surface expression of the HCV entry receptor SR-BI, and in low doses the FADS2 inhibitor was capable to promote viral replication. Prolonged treatment with high FADS2 inhibitor doses, but not with the low inhibitor dose, caused a reduction in virus production. Taken together, this thesis provides new insights into the lipid composition of HCV-infected cells, including the lipid composition of lipid droplets. The role of fatty acids in the HCV life cycle was elucidated in greater detail and, importantly, FADS2 was discovered as a novel host factor that influences HCV replication.

Zusammenfassung

Eine Infektion mit dem Hepatitis C Virus (HCV) nimmt häufig einen chronischen Verlauf, der zu krankhaften Veränderungen der Leber führen kann. Zu diesen Veränderungen gehört die als Steatose bezeichnete Akkumulierung von Lipiden in der Leber. Neutrallipide werden in cytoplasmatischen Organellen, den sogenannten *lipid droplets*, gespeichert. HCV verwendet *lipid droplets* als Plattform für die Virusassemblierung. Zudem spielt die zelluläre Lipidsynthese eine wichtige Rolle in der viralen Replikation. Beispiele sind die Cholesterolsynthese sowie die Desaturierung von Palmitin- und Stearinsäure. Des Weiteren führt eine Infektion mit HCV zu Veränderungen in der zellulären Lipidkomposition.

Zu Beginn dieser Arbeit wurden detaillierte Lipidprofile von HCV-infizierten und nicht-infizierten Zellen mittels *shotgun lipidomics* generiert. Im Vergleich zu nichtinfizierten Zellen enthielten HCV-infizierte Zellen einen höheren Anteil an Membranlipiden gegenüber Neutrallipiden. Grund hierfür könnten die von HCV induzierten Membranveränderungen sein. Die detaillierten Lipidprofile zeigten, dass HCV-infizierte Zellen im Vergleich zu nicht-infizierten Zellen einen verminderten Anteil an Triglyceriden und Phosphatidylcholinen mit kurzen Fettsäureketten aufweisen. Der Anteil an Triglyceriden und Phosphatidylcholinen mit längeren Fettsäureketten ist in HCV-infizierten Zellen erhöht. Diese Veränderungen waren sowohl in Extrakten aus der gesamten Zelle als auch in isolierten *lipid droplets* nachweisbar. Zudem trat in HCV-infizierten Zellen eine erhöhte Menge an Arachidonsäure, Eicosapentaensäure und Docosahexaensäure auf. Bei diesen drei Lipiden handelt es sich um freie Fettsäuren. Basierend auf diesen Ergebnissen wurde der Einfluss einzelner freier Fettsäuren auf verschiedene Schritte des HCV-Lebenszyklus untersucht. Laurinsäure, die kürzeste untersuchte Fettsäure, steigerte die virale RNA-Replikation sowie die Virusproduktion. Zwei gesättigte Fettsäuren, Myristinsäure und Palmitinsäure, zeigten einen negativen Effekt auf späte Schritte des viralen Lebenszyklus (Virusproduktion), ohne dabei die virale RNA-Replikation zu beeinträchtigen. Einfach und mehrfach ungesättigte Fettsäuren inhibierten die virale RNA-Replikation und demzufolge auch die Virusproduktion. Folglich haben Fettsäuren in Abhängigkeit von Kettenlänge und Grad der Desaturierung unterschiedliche Effekte. Die Untersuchung fettsäuremodulierender Enzyme zeigte, dass eine verminderte Elongation oder Desaturierung von Fettsäuren überwiegend die virale Replikation verringert. Ausschließlich der *knockdown* von FADS2 führte zu einer reduzierten Virusproduktion. Die Inhibierung von FADS2 zeigte einen dosis- und zeitabhängigen Effekt auf den HCV-Lebenszyklus: Eine kurze FADS2-Inhibierung erhöhte die Expression des HCV-Eintrittsrezeptors SR-BI und eine geringe Inhibitorkonzentration hatte einen positiven Effekt auf die virale Replikation. Eine länger andauernde Inhibierung mit einer hohen Inhibitorkonzentration führte hingegen zu einer reduzierten Virusproduktion.

Zusammengefasst konnten in dieser Studie neue Erkenntnisse über die Lipidkomposition von HCV-infizierten Zellen, sowie deren *lipid droplets*, gewonnen werden. Außerdem wurden weitere Details über die Rolle verschiedener Fettsäuren und die Bedeutung der Fettsäurehomöostase für den HCV-Lebenszyklus ermittelt. Insbesondere wurde FADS2 als neuer zellulärer Faktor mit einem Einfluss auf die HCV-Replikation identifiziert.

1. Introduction

1.1. Hepatitis C virus (HCV) infection

HCV belongs to the family of *Flaviviridae*. Other well-known members of this family are yellow fever and dengue virus (Moradpour et al., 2007). HCV is a blood-borne virus that infects human hepatocytes and is mostly transmitted via transfusion of blood products and sharing drug injection needles. Sexual and mother to child transmission are less frequent (Shepard et al., 2005; Syriopoulou et al., 2005). Some patients spontaneously clear the virus, but in 75–85% of the cases the infection becomes chronic (Chen and Morgan, 2006). Around 184 million people are chronically infected with HCV worldwide, which is 2.8% of the world population (Mohd Hanafiah et al., 2013). Seven different HCV genotypes, with several subgenotypes (a, b, etc.), are known. Genotype 1 is most prevalent amongst all HCV genotypes and accounts for 46.2% of all HCV infections worldwide. It is followed by genotype 3 with a rate of 30.1% of the infections. Genotype 2 (9.1%), genotype 4 (8.3%), and genotype 6 (5.4%) are less frequent. Genotype 5 causes the lowest amount of cases with 0.8% of all infections (Messina et al., 2015). Recently, a 7th genotype was identified in central Africa (Murphy et al., 2015). However, the frequency of the HCV genotypes differs between geographic regions. Genotype 1 accounts for most infections in Europe, North and South America, as well as in East Asia. Genotype 2 is mainly found in East Asia, South America, and western sub-Saharan Africa. Genotype 3 has the highest prevalence in South Asia. Genotype 4 is mainly found in patients in central sub-Saharan Africa, North Africa, and the Middle East. Genotype 5 is most prevalent in southern sub-Saharan Africa and genotype 6 in East Asia (Messina et al., 2015; Scheel and Rice, 2013) (Figure 1).

Over a long period, the standard HCV therapy was a combination of ribavirin and pegylated-interferon alpha, which caused strong side effects and in only 56% of the cases viral RNA remained absent in the serum of the patients 24 weeks after the end of the treatment (Fried et al., 2002). In the past years, several direct acting antivirals (DAAs) were approved. These are inhibitors of different viral proteins, like the protease NS3/NS4A, the protein NS5A, or the RNA-dependent RNA polymerase NS5B. DAAs have fewer side effects than ribavirin and interferon and have a high potency to clear the virus. However, due to the extremely high costs of the DAA, their access is limited (Bidell et al., 2016).

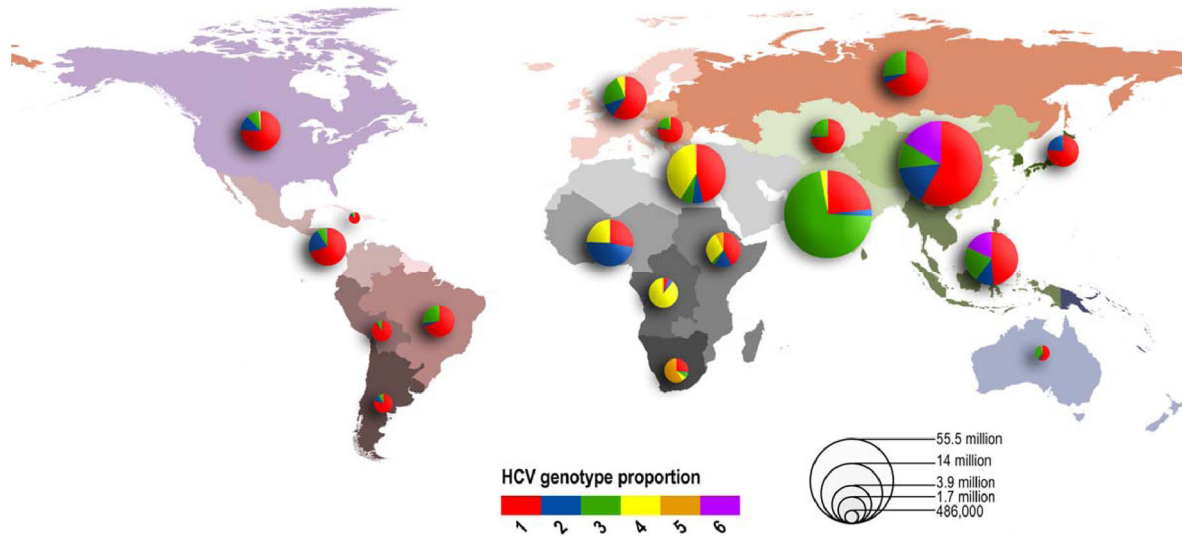


Figure 1: HCV genotype distribution

The map shows the distribution and abundance of the six different HCV genotypes. The prevalence of cases is depicted by the size of the pie chart, while the slices represent the abundance of the genotypes. Taken from (Messina et al., 2015).

In most of the cases the acute HCV infection is either asymptomatic or causes mild symptoms like fever. But the chronicity can cause severe liver diseases like liver cirrhosis, steatosis, or hepatocellular carcinoma (Chen and Morgan, 2006). Steatosis, also termed fatty liver, is a symptom caused by the accumulation of lipids in the hepatocytes (Yoon and Hu, 2006). Steatosis indicates an alteration of the lipid metabolism caused by HCV and up to now several studies have shown a strong connection between the HCV life cycle and the cellular lipid metabolism (Herker and Ott, 2011).

1.2. HCV life cycle

The HCV life cycle comprises several steps: entry, RNA translation and polyprotein processing, RNA replication, assembly and release (Figure 2) (Herker and Ott, 2012).

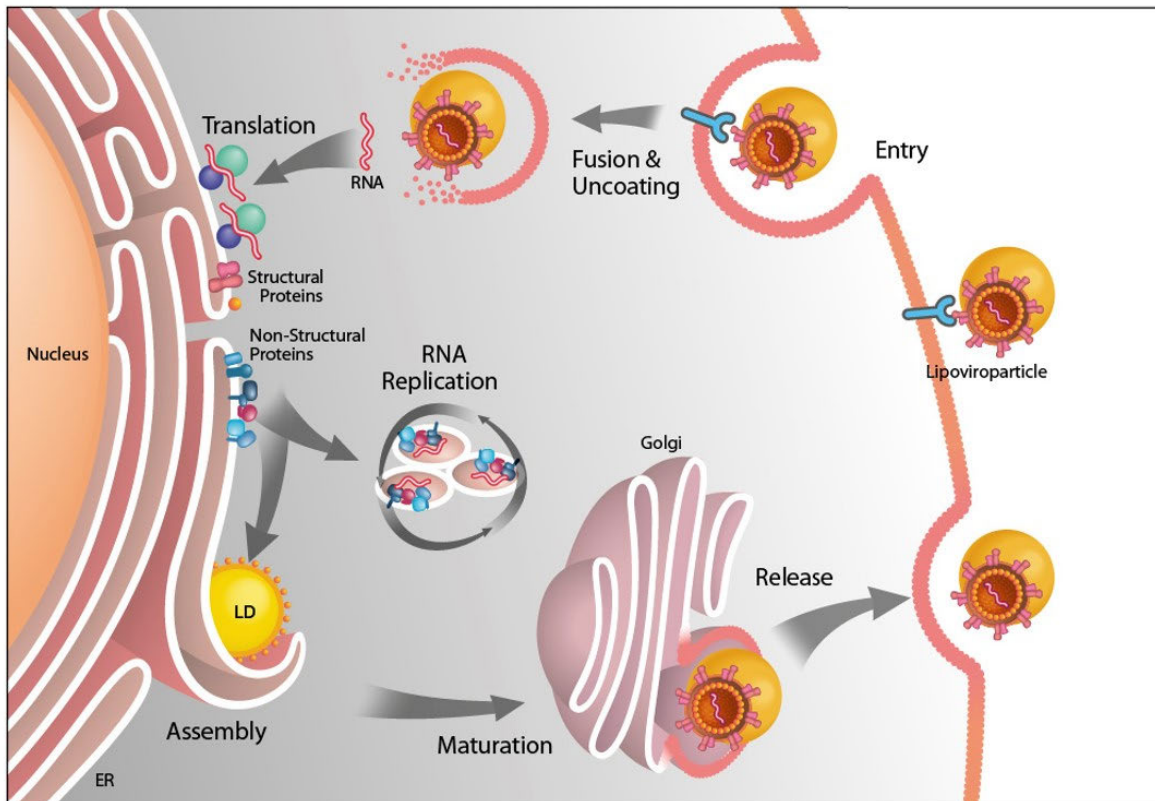


Figure 2: The HCV life cycle.

This scheme depicts the different steps of the viral life cycle. HCV circulates in blood as a lipoviroparticle and enters the cell via receptor-mediated endocytosis. Afterwards, the viral RNA is released and translated at the ER into a polyprotein. This polyprotein is then further processed. The viral RNA replication occurs in the membranous web and the virus uses lipid droplets as assembly sites. It is suggested that HCV uses the secretory pathway for exiting the cell. Taken from (Herker and Ott, 2012).

1.2.1. The lipoviroparticle and cell entry

The HCV particle comprises the viral RNA that is enclosed by the capsid composed of the protein core. A membrane bilayer surrounds this capsid and carries the envelope glycoproteins E1 and E2 (Figure 3 A) (Lindenbach and Rice, 2013). Viral particles circulate in blood in tight association with lipoproteins, coining the term lipoviroparticles. First hints regarding this association resulted from the observation that viral particles isolated from the blood of patients have a variable density from 1.03–1.20 g/cm³ and that low-density particles

co-precipitate with lipoproteins (Thomssen et al., 1992). Later, the interaction of viral particles with different apolipoproteins (Apo) as ApoA-I, ApoB-48, ApoB-100, ApoC-I, and ApoE was discovered (Lindenbach and Rice, 2013). In addition, a lipidomic approach further supported these findings. Cell culture–derived HCV particles (HCVcc) were rich in cholesteryl esters (CE), cholesterol, phosphatidylcholine (PC), and sphingomyelin (SM). The lipid composition of HCVcc particles revealed high similarities to very low–density lipoproteins (VLDL) and low-density lipoproteins (LDL) (Merz et al., 2011). It is still unclear in which manner the viral particle associates with the lipoproteins. One model suggests a common membrane that surrounds the lipoprotein and the viral particle, while another model describes a transient association of the viral particle and the lipoprotein (Figure 3 B) (Lindenbach and Rice, 2013). HCV entry into hepatocytes occurs via receptor-mediated endocytosis (Figure 3 C). Several receptors are important for virus entry: Initial attachment likely occurs through the LDL-receptor (LDLR) and glycosaminoglycans (GAG), which bind to ApoE of the associated lipoprotein. Scavenger receptor BI (SR-BI) was identified as another co-receptor. It binds to the lipoprotein as well as to the envelope glycoprotein E2 in the early entry stage and is additionally required for the binding of E2 to cluster of differentiation 81 (CD81). Bound to CD81 the viral particle laterally diffuses to tight junctions, where it associates with claudin-1 (CLDN1) and triggers the clathrin-dependent endocytosis (Ding et al., 2014). Another tight-junction protein that was identified as an entry factor is occludin (OCLN), but its function has not been clarified so far. Nevertheless, OCLN together with CD81 determines the species tropism in regard to virus entry (Lindenbach and Rice, 2013). Several other factors were described to be important for viral entry, like the epidermal growth factor receptor (EGFR) and the Niemann-Pick C1 like1 (NPC1L1), even though their precise role is unknown (Lindenbach and Rice, 2013). NPC1L1 is a sterol transporter and absorbs cholesterol from the bile into the cell (Betters and Yu, 2010). It has been suggested that its role in HCV entry is connected with this function in cholesterol uptake (Lindenbach and Rice, 2013). After HCV has entered the cell, the vesicle is acidified and the viral membrane fuses with the vesicle membrane followed by the release of the viral RNA (Scheel and Rice, 2013). The described process refers to cell-free virus entry, but HCV can also infect neighboring cells by cell-to-cell transmission. This route relies on host factors also needed in cell-free virus entry, such as SR-BI, CLDN1, OCLN, EGFR, NPC1L1, and eventually CD81 (Ding et al., 2014).

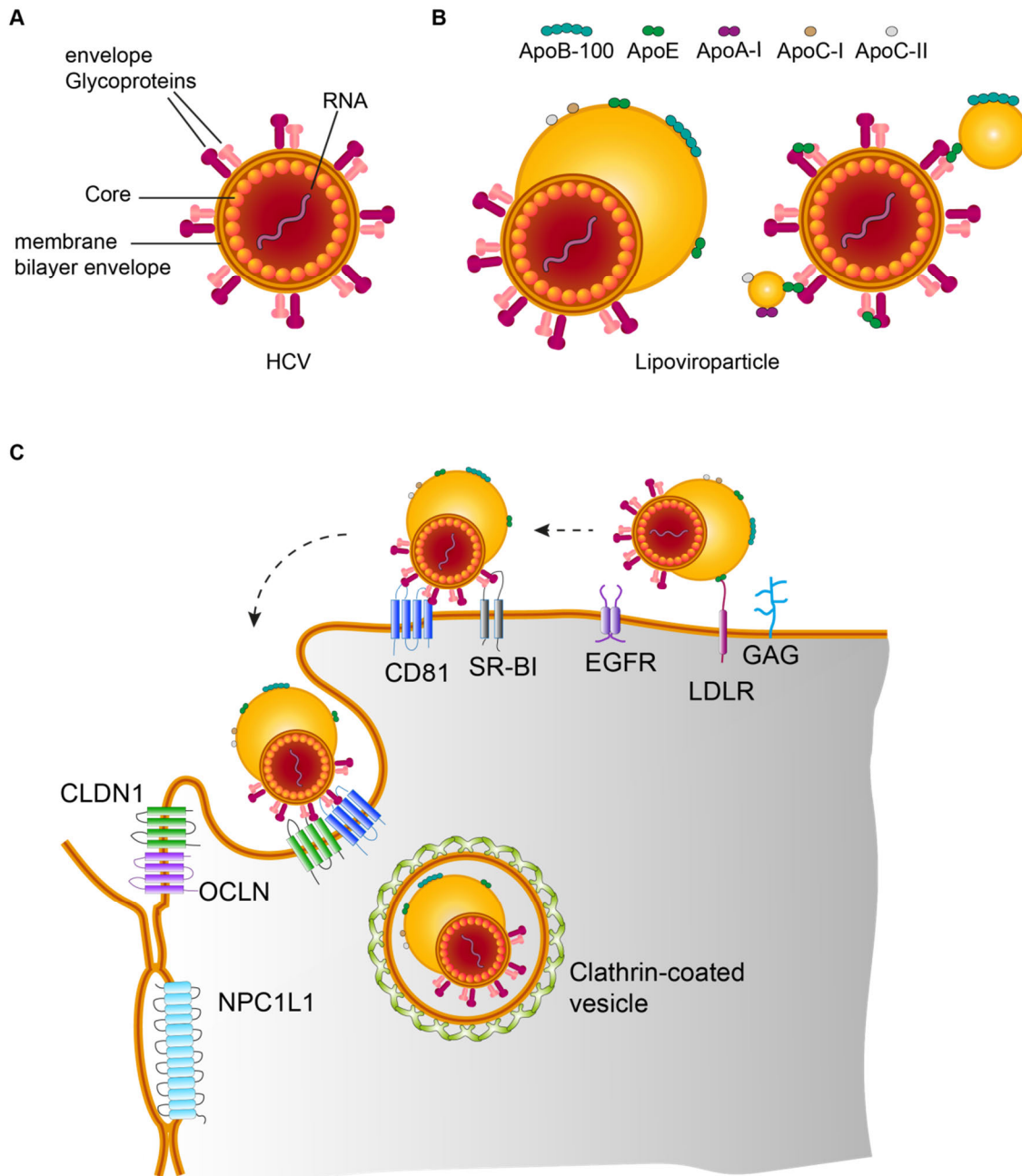


Figure 3: Structure of the virions and HCV entry.

A) The viral particle contains its RNA genome that is surrounded by the capsid protein core. It carries an envelope with the envelope glycoproteins E1 and E2. B) Current models of the lipoviroparticles suggest a shared membrane between the viral particle and the lipoprotein or a transient association. C) HCV attaches to several cell surface receptors before it is endocytosed. GAG, glycosaminoglycan; LDLR, low-density lipoprotein receptor; EGFR, epidermal growth factor receptor; SR-BI, scavenger receptor BI; CD81, cluster of differentiation 81; CLDN1, claudin-1; OCLN, occluding; NPC1L1, Niemann-Pick C1 like1 (Lindenbach and Rice, 2013; Scheel and Rice, 2013).

1.2.2. Viral RNA translation and protein function

The HCV RNA is positive and single-stranded with a size of 9.6 kb. It contains a 5'- and 3'-untranslated region (UTR) that flank a single open reading frame (ORF). At the ER the RNA translation is initiated by the internal ribosome entry site (IRES) in the 5'-UTR (Moradpour et al., 2007). The resulting polyprotein is co- and post-translationally processed at the ER membrane into three structural and seven non-structural proteins. The structural proteins are cleaved by the ER signal peptidase and signal peptide peptidase and the non-structural proteins are cleaved by the viral proteases NS2 and NS3-NS4A (Figure 4) (Scheel and Rice, 2013). The structural proteins are core, E1, and E2 and the non-structural comprise p7, NS2, NS3, NS4A, NS4B, NS5A, and NS5B.

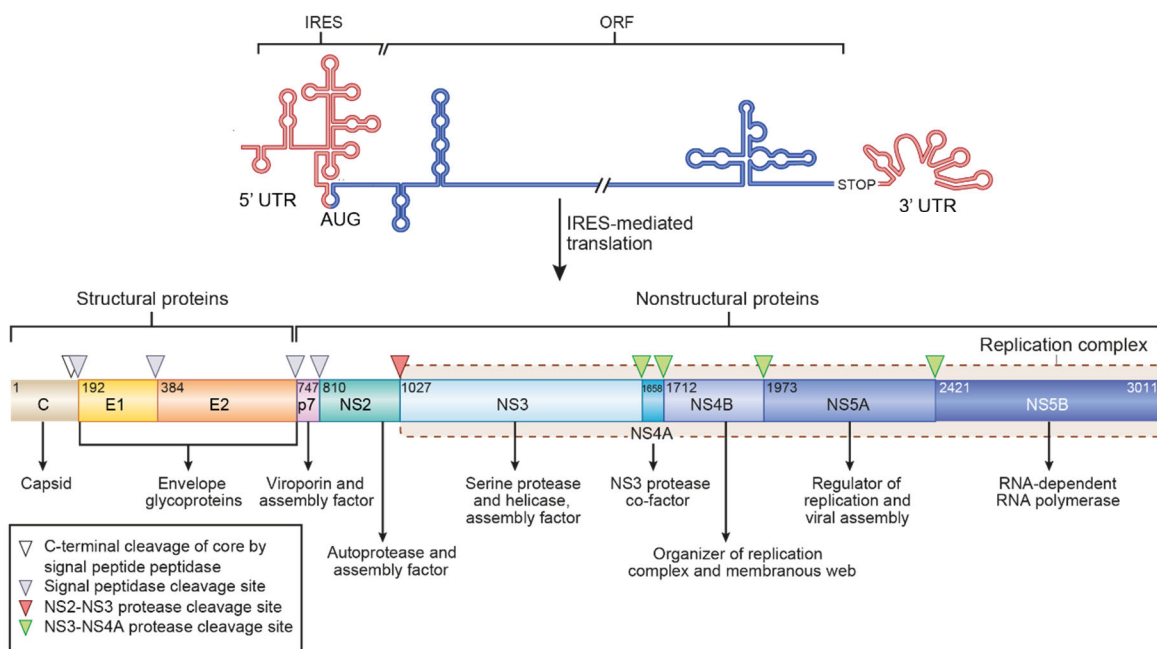


Figure 4: Viral genome organization and polyprotein processing.

The HCV genome is a single-stranded positive sense RNA that is flanked by a 5' and 3' untranslated region (UTR). The 5' UTR contains an internal ribosome entry site (IRES) for translation initiation. The resulting polyprotein is processed by host and viral proteases into three structural and seven non-structural proteins. Modified from (Scheel and Rice, 2013).

The core protein forms the viral capsid. It dimerizes at the ER, a feature that is necessary for particle production. Mature core protein contains two domains; one domain (DII) facilitates the binding to membranes and is necessary for the localization of core to lipid droplets. The

other domain (DI) has been described to have an RNA chaperone activity acting in the packaging process of the viral RNA (Moradpour and Penin, 2013).

The envelope E1 and E2 play an important role in viral entry, amongst others. The two proteins are connected by disulfide bonds to form heterodimers. E1 and E2 are anchored into the ER membrane, while their ectodomain resides in the ER lumen. They are post-translationally glycosylated, a modification that is necessary for their proper folding (Voisset and Dubuisson, 2004). E2 contains two hypervariable regions and one of them has been described to play a role in immune evasion (Guan et al., 2012).

P7 is a viroporin that forms hexamers with ion channel capacity. So far, its molecular function has not been clarified, but it is important for virus assembly and release (Moradpour and Penin, 2013).

NS2 is a cysteine protease that is necessary to cleave NS3 at the NS2/NS3 junction. Additionally, the N-terminal part of NS3 is needed for the NS2 autoprotease activity. Besides, NS2 seems to be required for HCV assembly (Moradpour and Penin, 2013).

NS3 has a serine protease and NTPase/RNA helicase function. It builds a complex with its co-factor NS4A. NS3-NS4A is found at the ER membrane and to a lesser extent at the mitochondria and at mitochondria-associated membranes. In addition to the viral polyprotein NS3-NS4A has been described to cleave several enzymes that are involved in innate immunity (Moradpour and Penin, 2013). NS4A can also bind to NS5A, which is required for the phosphorylation of NS5A (Asabe et al., 1997).

NS4B is known to be an initiator of the membranous web formation, it can bind viral RNA and it plays a role in viral assembly. The oligomerization of NS4B seems to be required for the formation of the membranous web. In addition, NS4B has been shown to be palmitoylated (Moradpour and Penin, 2013).

NS5A has been described to be a regulator of viral RNA replication and virus assembly. It is suggested that the different domains of NS5A fulfill separate roles and either function in RNA replication or assembly. NS5A is highly phosphorylated and exists in two variants, the basal and the hyper-phosphorylated form. However, the precise role of these two variants is not clear (Ross-Thriepland and Harris, 2015). One important NS5A interaction partner is phosphatidylinositol 4-kinase III alpha (PI4KIII α) (Moradpour and Penin, 2013). PI4KIII α is important for the membranous web formation and has been shown to modulate the phosphorylation of NS5A (Reiss et al., 2013). NS5A is highly abundant in the RNA replication complexes and can additionally localize to lipid droplets (Moradpour and Penin, 2013).

NS5B is the RNA-dependent RNA polymerase. This enzyme synthesizes a negative RNA strand from the positive RNA strand and uses this negative RNA strand as template for the subsequent synthesis of a positive RNA strand. It lacks a proofreading function and therefore

causes the diversity of the HCV genomes (Moradpour and Penin, 2013; Neumann-Haefelin and Thimme, 2013).

1.2.3. Viral RNA replication

The HCV replication complex consists of membrane vesicles that minimally contain the non-structural proteins NS3/4A–NS5B and the viral RNA (Figure 5 A). One replication site has been suggested to harbor several copies of positive strand RNA but only one copy of negative strand RNA. It is believed that the vesicles contain pores to facilitate the influx of nucleotides and the exit of the positive RNA strand for assembly (Lohmann, 2013). The membrane rearrangements are termed the membranous web, a structure of double (DMVs) and multi-membrane vesicles (MMVs) (Figure 5 B). Those structures are ER-derived, were found to be detergent resistant, and are assumed to protect the viral RNA against detection and degradation. The resistance is due to the presence of lipid rafts in the membrane DMVs and MMVs (Aizaki et al., 2004; Gao et al., 2004; Romero-Brey et al., 2012; Shi et al., 2003). The expression of NS4B is sufficient to induce the formation of membrane rearrangements

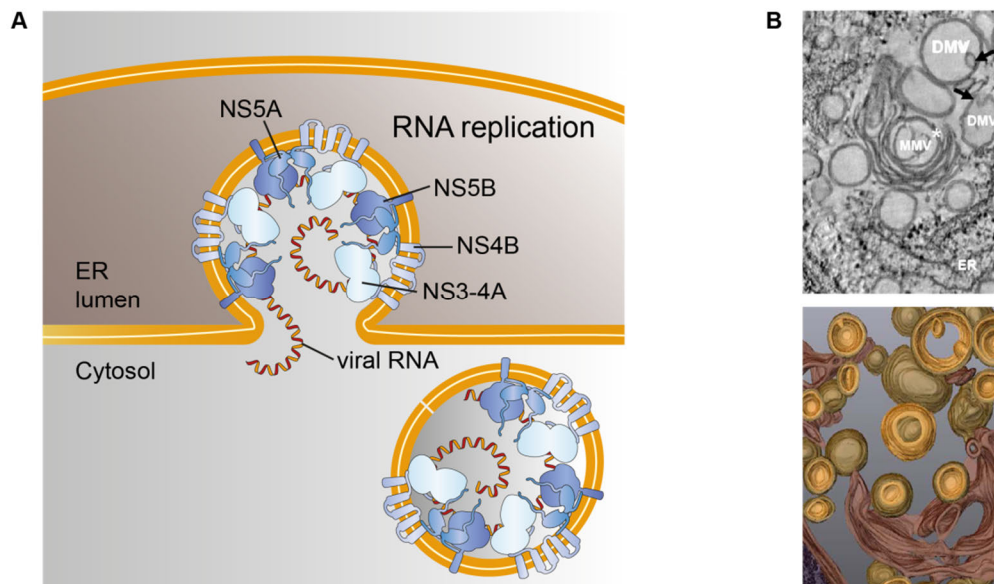


Figure 5: Viral RNA replication sites.

HCV RNA replicates in the membranous web. A) Scheme of an HCV replication site in endoplasmic reticulum (ER) invaginations comprising the viral proteins and the viral RNA. B) Electron microscopy image and a tomography of the membranous web showing ER-derived multi- (MMV) and double-membrane vesicles (DMV). Scale bar 100 nm. Brown: ER; ocher: membranous web. A) Modified from (Lindenbach and Rice, 2013); B) Taken from (Romero-Brey et al., 2012).

and therefore it was believed that NS4B is the initiator of the membranous web formation. Meanwhile it has been shown that the proteins NS3/4A, NS5A, and NS5B are also capable of inducing membrane rearrangements. Nevertheless, the expression of single proteins resulted in an aberrant membranous web indicating that several viral proteins have to act together to form this structure (Romero-Brey et al., 2012). In addition to the viral proteins NS3–NS5B, host proteins have been identified to play a role in viral replication, like the phosphatidylinositol-4-kinase III alpha (PI4KIII α) (Lohmann, 2013).

1.2.4. Viral assembly and release

Lipid droplets are described as sites for viral assembly (Figure 6). Core contains a hydrophobic domain that is required for its localization to lipid droplets and for viral particle production (Shavinskaya et al., 2007). Furthermore, the trafficking of core to lipid droplets is dependent on host factors like diacylglycerol acyltransferase 1 (DGAT1) (Herker et al., 2010). In addition to core, NS5A has been shown to localize to lipid droplets and to be required for viral assembly. A mutation in NS5A resulted in a blockade of early assembly steps (Zayas et al., 2016). Further important NS proteins for assembly are p7, NS2, NS3-4A,

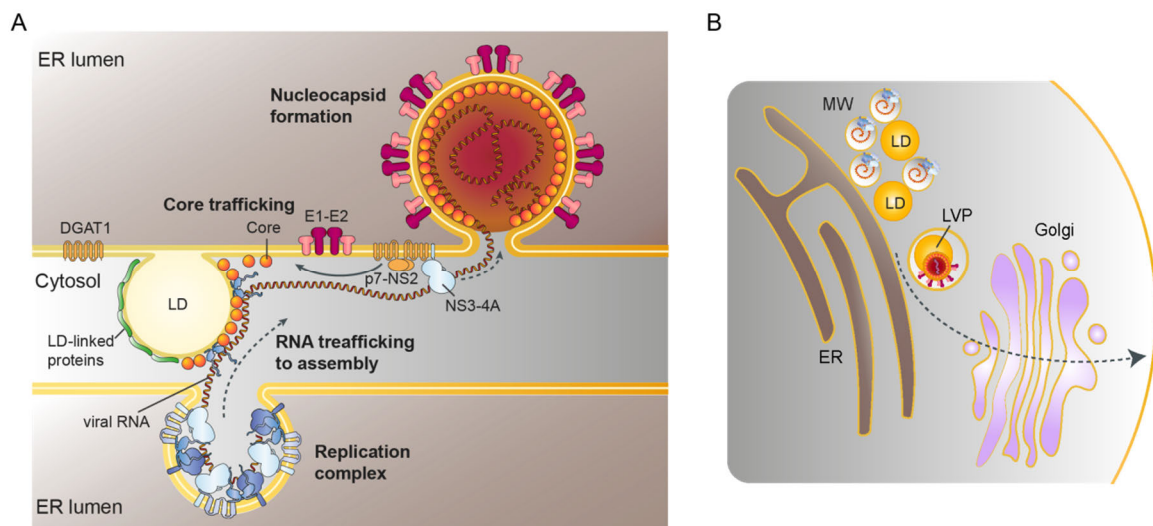


Figure 6: HCV assembly and release.

A) HCV assembly takes place at lipid droplets (LDs) in close proximity to RNA replication sites. The viral RNA, as well as core and the envelope proteins are recruited to the assembly site where the viral particle buds into the endoplasmic reticulum (ER) lumen. B) The secretory pathway is one possibility for HCV to exit the cell and to attach to lipoproteins. MW, membranous web; LVP, lipoviroparticle. Modified from (Lindenbach and Rice, 2013).

and NS5B. It is supposed that the interaction of NS2 with p7 is required to move NS proteins and core containing lipid droplets to the assembly site. The RNA is suggested to be encapsidated with the assistance of the RNA helicase function of NS3-NS4A. As mentioned before, the envelope proteins E1 and E2 form a heterodimer at the luminal site of the ER. The current model suggests that this heterodimer moves to the assembly site, where the viral particle buds into the ER and associates to lipoproteins (Lindenbach and Rice, 2013). The lipoprotein secretion pathway is the supposed route for viral exit. This is supported by different experiments that block the lipoprotein secretion pathway. For example, the inhibition of the microsomal transfer protein (MTTP), as well as the knockdown of ApoB or ApoE reduced viral particle production (Chang et al., 2007; Gastaminza et al., 2008). Further evidence are the post-translational modifications of the envelope proteins: those modifications are known to occur in the Golgi and lipoproteins pass through the Golgi during their secretion (Lindenbach and Rice, 2013). However, the exact mechanism is still unclear. Recent studies imply alternative mechanisms either by a route that involves the *trans*-Golgi network, but are unrelated to the VLDL secretion, or even a secretory mechanism without passing the Golgi (Bayer et al., 2016; Mankouri et al., 2016).

1.3. Lipid metabolism

The basic definition of lipids is that they are molecules, which are poorly soluble in water, but highly soluble in organic solvents, like chloroform or ether. They are important as structural elements of the cell, as they form membranes. In addition to their structural function, they act as a reservoir for energy and can function in signal transduction (van Meer et al., 2008). Lipids comprise different subclasses such as fatty acids, eicosanoids, glycerolipids, phospholipids, sphingolipids, sterols, prenols, fat-soluble vitamins, and waxes (Fahy et al., 2009).

1.3.1. Fatty acids

Fatty acids (FAs) are components of lipids like triglycerides (TAGs), cholesteryl esters (CEs), and phospholipids (PLs). The degree of desaturation and the length of membrane lipid acyl chains influences the membrane fluidity. Fatty acids are used for the acylation of proteins, which is important for protein function or can serve as a membrane anchor. Another feature is the production of energy by fatty acid degradation. Furthermore, they can act as cofactors for transcription factors (Rustan and Devron, 2005).

Fatty acids consist of a hydrocarbon chain with a carboxyl group at one terminus and a methyl group at the other (Figure 7). They are classified according to their degree of desaturation, which is the number of double bonds in the hydrocarbon chain. Saturated fatty acids (SFAs) contain no double bond, monounsaturated fatty acids (MUFAs) contain one double bond, and polyunsaturated fatty acids (PUFAs) contain at least two double bonds. Carbon atoms are counted from the methyl group and the location of the double bond is indicated by n . Alternatively, the carbon atoms are counted from the carboxyl terminus and the position is depicted by Δ (Ridgway ed., 2015).

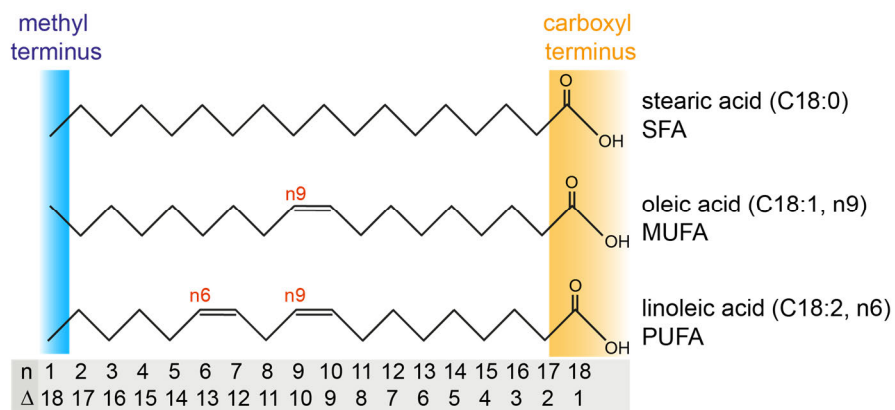


Figure 7: Fatty acid structure.

Scheme of representative saturated fatty acids (SFA), monounsaturated fatty acids (MUFA), and polyunsaturated fatty acids (PUFAs). The carbon atoms are counted from the methyl terminus (blue) depicted by n , or from the carboxyl terminus (yellow) depicted by Δ (Ridgway ed., 2015).

The majority of fatty acids is provided by the diet, but some tissues, like the liver, are capable of producing fatty acids on their own in a process termed *de novo* lipogenesis. The degradation of glucose yields pyruvate, which can be converted into acetyl-CoA. To produce fatty acids acetyl-CoA is extended into palmitic acid (C16:0) and to a lesser extent into myristic acid (C14:0) or stearic acid (C18:0). However, the essential fatty acids linoleic acid (LA, 18:2 n6) and α -linolenic acid (ALA, 18:3 n3) cannot be synthesized by *de novo* lipogenesis in humans and need to be taken up from the diet. The amount *de novo* lipogenesis contributes to the total fatty acid content depends on the diet: The lower the fat content and the higher the amount of carbohydrates, the higher the proportion of *de novo* lipogenesis (Ridgway ed., 2015). Both, fatty acids obtained by *de novo* lipogenesis and from nutrition are further processed by elongases and desaturases (Figure 8, Figure 9). For elongation the fatty acid is activated by the transfer of a CoA moiety, which results in

acyl-CoA. The elongation of fatty acids by two carbons contains four consecutive enzymatically catalyzed steps. The first step, the reaction of acyl-CoA with malonyl-CoA, is rate limiting and the responsible enzymes are the so-called elongases (ELOVLs). Seven elongases, ELOVL1-7, are known in humans and although there is a certain substrate specificity, ELOVLs are not exclusively reacting with one fatty acid and are found on several sections in the elongation and desaturation pathways. Fatty acid elongation primarily occurs at the ER, but can also take place in mitochondria and peroxisomes as a reversal to β -oxidation (Naganuma et al., 2011; Ridgway ed., 2015).

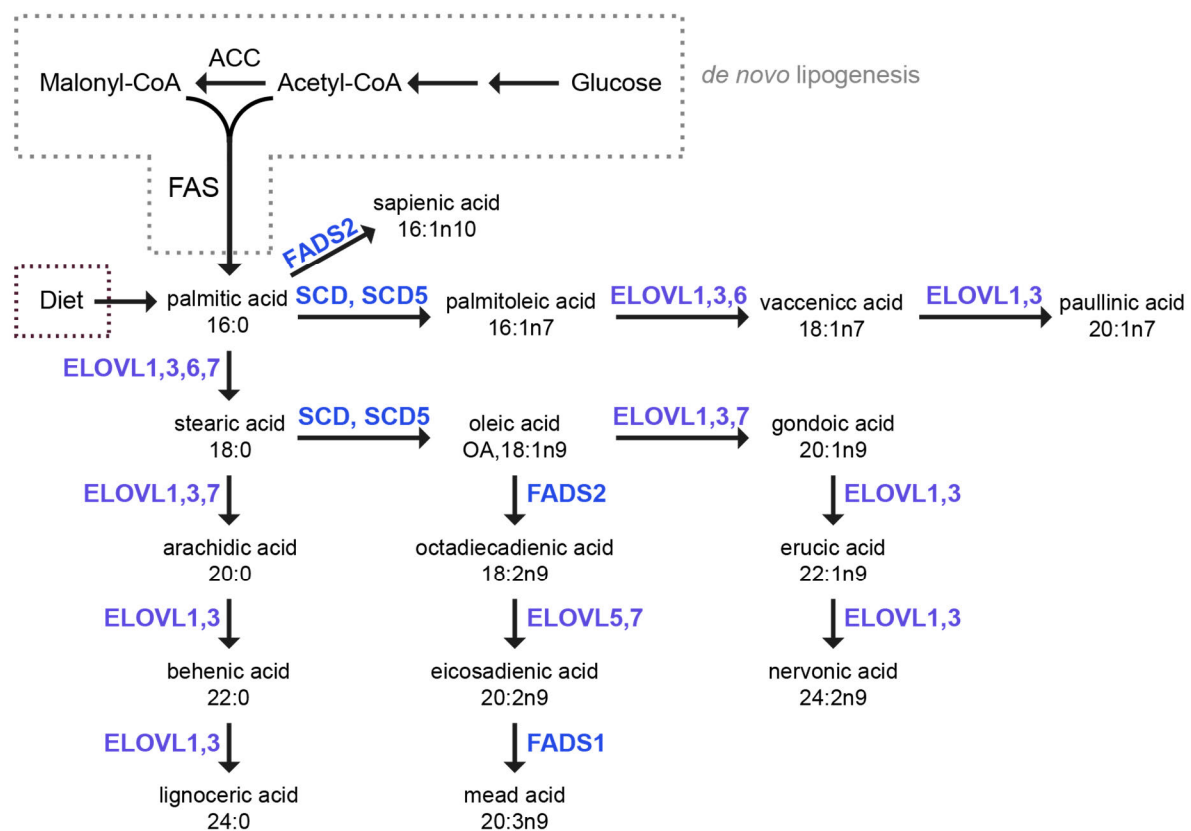


Figure 8: Fatty acid elongation and desaturation.

Fatty acids derived from *de novo* lipogenesis or from the diet are further processed by elongases (purple) and desaturases (blue). Elongases elongate the fatty acid by two carbon atoms and desaturases introduce double bonds. ACC, acetyl-CoA carboxylase; FAS, fatty acid synthase; ELOVL, fatty acid elongase; SCD, stearoyl-CoA desaturase; FADS, fatty acid desaturase (Naganuma et al., 2011; Ridgway ed., 2015).

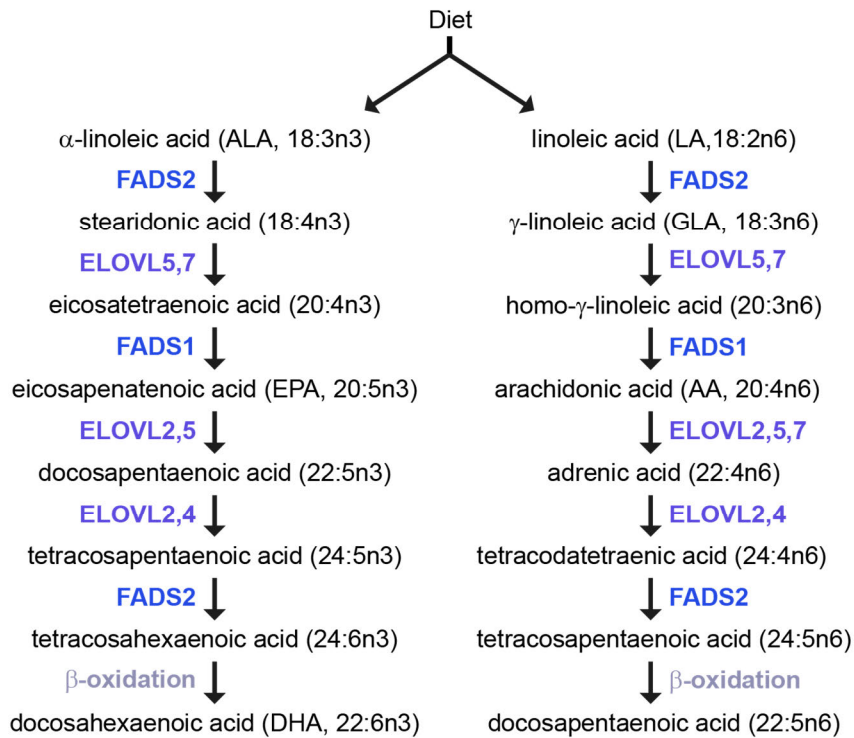


Figure 9: Polyunsaturated fatty acid synthesis pathway.

The essential fatty acids α -linolenic acid (ALA) and linoleic acid (LA) are further processed by elongases (purple) and desaturases (blue). The last step is a chain shortening by β -oxidation. ELOVL, fatty acid elongase; FADS, fatty acid desaturase (Naganuma et al., 2011; Ridgway ed., 2015).

The induction of double bonds into fatty acids is catalyzed by desaturases. In contrast to elongases, the desaturases have higher substrate specificity. Several desaturases are known in humans, like the stearoyl-CoA desaturases (SCD, Δ 9-desaturase) with its two isoforms SCD1 and SCD5, the Δ 6-desaturase (FADS2) and the Δ 5-desaturase (FADS1). SCDs catalyze the synthesis of monounsaturated fatty acids, by desaturating palmitic acid (16:0) or stearic acid (18:0) to palmitoleic acid (16:1n7) or oleic acid (OA, 18:1n9), respectively. FADS2 and FADS1 further convert oleic acid to mead acid (20:3, n9) and in addition FADS2 desaturates palmitic acid to sapienic acid (16:1n10) (Figure 8). Furthermore, FADS1 and FADS2 are important desaturases of n3- and n6-polyunsaturated fatty acid synthesis pathway (Figure 9). This synthesis starts with the essential fatty acids linoleic acid (LA, 18:2n6) and α -linolenic acid (ALA, 18:3n3). FADS2 is responsible for the synthesis of γ -linolenic acid (GLA, 18:3n6) and stearidonic acid (18:4n3) from LA and ALA, respectively. After elongation by ELOVL5, FADS1 desaturates homo- γ -linolenic acid (20:3n6) and

eicosatetraenoic acid (20:4n3) to arachidonic acid (AA, 20:4n6) and eicosapentaenoic acid (EPA, 20:5n3). This is followed by two subsequent elongation steps by ELOVL2, ELOVL5 or ELOVL4. The last desaturation step to tetracosahexaenoic acid (24:6n3) and tetracosapentaenoic acid (24:5n6) is catalyzed by FADS2. Each is then converted to docosahexaenoic acid (DHA, 22:6n3) and docosapentaenoic acid (22:5n6) by β -oxidation. To provide energy fatty acids have to be degraded. The degradation of lipids is termed β -oxidation (Figure 10). This process contains four consecutive enzymatic reactions and in each β -oxidation cycle, the fatty acyl-chain is shortened by two carbon atoms that are released as acetyl-CoA. In addition, in each cycle one NADH and one FADH₂ are produced. Acetyl-CoA enters the citric acid cycle and the acyl-CoA re-enters the β -oxidation process. β -Oxidation is mainly localized in the mitochondria, but can also occur in peroxisomes. During β -oxidation the liver is capable of producing ketone-bodies that are exported to other tissues as source of energy (Houten and Wanders, 2010).

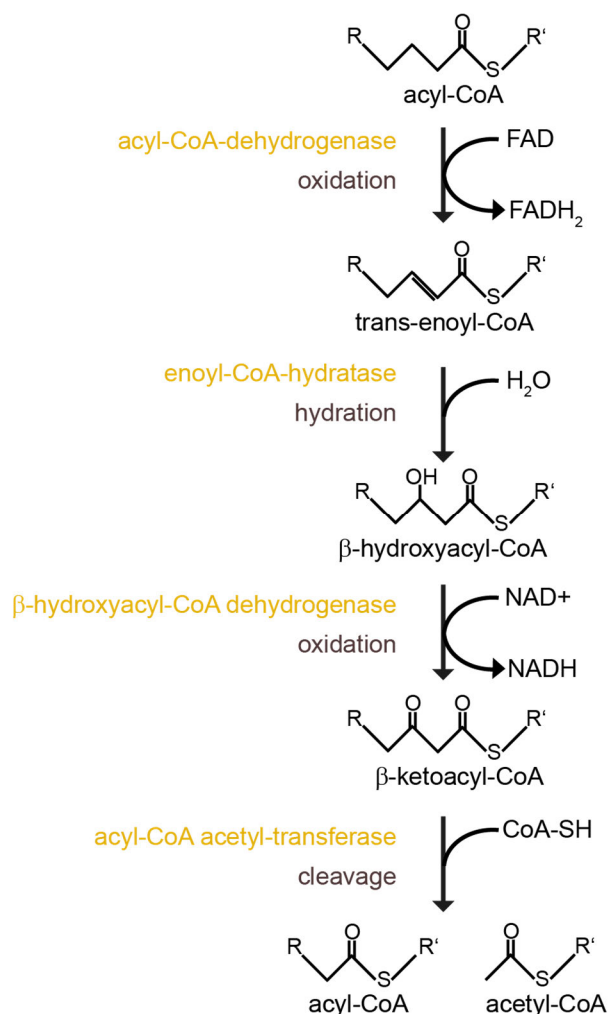


Figure 10: β -oxidation.

Fatty acids are degraded by β -oxidation. Therefore, the activated fatty acid (acyl-CoA) processed by consecutive enzymatically catalyzed steps, that results in acetyl-CoA and the shortened acyl-CoA. Yellow: enzymes; brown: reaction (Da Poian A.T.; Ridgway ed., 2015).

Fatty acids are released into the blood from circulating lipoproteins (see 1.3.5.) or from white adipose tissue. There the fatty acids are bound to albumin for better solubility. How the cellular uptake of fatty acids occurs is still not completely understood. One proposed model was the diffusion of protonated fatty acids through the plasma membrane. Now it is believed that a protein-mediated uptake is more common. One receptor that was found to be responsible for fatty acid uptake is the cluster of differentiation 36 (CD36), which belongs to the scavenger B receptor family (Ridgway ed., 2015; Schwenk et al., 2010).

1.3.2. Glycerolipids

Glycerolipids consist of a glycerol backbone esterified with fatty acids (Figure 11). Monoglycerides (MAG) contain one, diglycerides (DAG) contain two, and triglycerides contain three fatty acyl-chains. Triglycerides are very important in terms of energy storage (Ruggles et al., 2013).

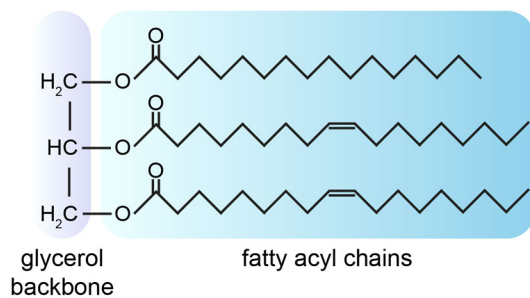


Figure 11: Triglyceride.

Scheme of a triglyceride (TAG) containing three fatty acyl chains that are esterified to the glycerol backbone (Ridgway ed., 2015).

Triglycerides can be synthesized by two different ways: One is the glycerol-3-phosphate pathway, which begins with the production of lyso-phosphatidic acid (LPA, 1-acylglycerol-3-phosphate) by addition of a fatty acyl chain to glycerol-3-phosphate. In the next step lyso-phosphatidic acid is coupled with a second fatty acyl chain to form phosphatidic acid (PA), a basic phospholipid (see 1.3.3.). The phosphatidic acid phosphatase dephosphorylates phosphatidic acid to diglyceride (DAG). Afterwards the diglyceride acyltransferases (DGAT1 and DGAT2) catalyze the last addition of a fatty acyl chain to form triglycerides (Ridgway ed., 2015).

The other pathway uses monoglyceride as a substrate and rather functions in the small intestine (Takeuchi and Reue, 2009). Here, the monoglyceride acyltransferase (MGAT) transfers a fatty acyl chain to monoglyceride to form diglyceride, which is then further converted to triglyceride by DGAT (Shi and Cheng, 2009).

1.3.3. Membrane lipids

Lipids are crucial as the major part of cellular membranes. Membrane lipids are divided into phospholipids (PL), sphingolipids (SL), and sterols (Figure 12).

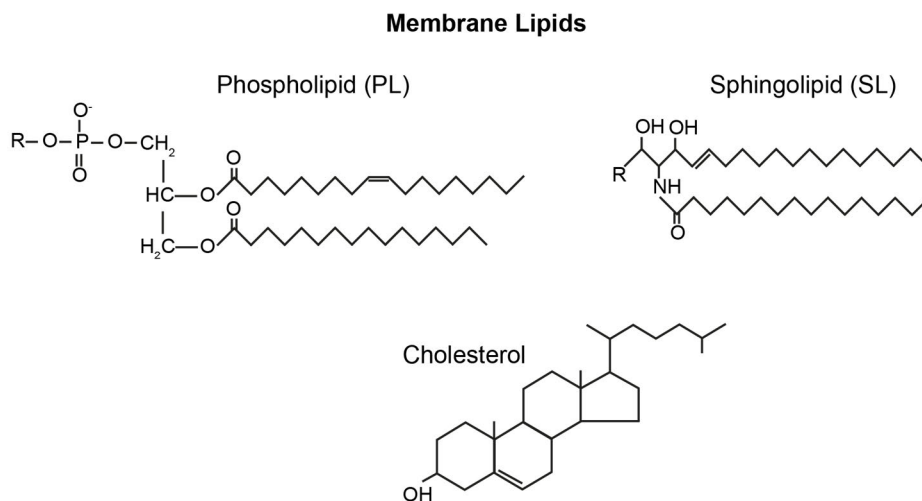


Figure 12: Membrane lipids.

Scheme of the different lipid species phospholipids (PL), sphingolipids (SL), and cholesterol (Ridgway ed., 2015).

50–60% of cellular membranes are built by phospholipids and over 50% of those phospholipids are phosphatidylcholine (PC) (van Meer et al., 2008). Phospholipids contain two fatty acyl chains that are esterified at the sn-1 and sn-2 hydroxyl groups of a glycerol backbone and form the hydrophobic part of a phospholipid. The sn-3 position of the glycerol is esterified with a hydrophilic head group. The basic head group is a phosphate, which forms phosphatidic acid. The attachment of choline, ethanolamine, serine, glycerol or inositol to the phosphate of phosphatidic acid forms a variety of phospholipids and gives them their corresponding name (Stryer ed. and Tymoczko ed., 2003).

The first step in the phospholipid synthesis is the production of phosphatidic acid, as described in the triglyceride synthesis pathway (see 1.3.2.). Afterwards, phosphatidic acid can undergo different routes either for the production of phosphatidylcholine (PC) and phosphatidylethanolamine (PE) or for the production of phosphatidylglycerol (PG) and phosphatidylinositol (PI) (Figure 13). The production of phosphatidylcholine and phosphatidylethanolamine occurs by the Kennedy-Pathway that contains two branches, one via cytidin-5'-diphosphoethanolamin (CDP-Etn) and one via cytidin-5'-diphosphocholin (CDP-Cho). Choline and ethanolamine are taken up by the cells and are phosphorylated.

Afterwards, phosphocholine (p-Cho) and phosphoethanolamin (p-Etn) are converted to CDP-Cho or CDP-Etn. This step is rate limiting in the phosphatidylcholine synthesis and the enzyme activity is regulated by the membrane composition (Ridgway ed., 2015). In the last step the p-Cho or p-Etn is transferred from CDP-Cho or CDP-Etn to the sn-3 position of diglyceride to form phosphatidylcholine or phosphatidylethanolamine, respectively. In addition, in hepatocytes 30% of phosphatidylcholine is synthesized by a catalyzed transfer of methyl groups to phosphatidylethanolamine. Phosphatidylcholine and phosphatidylethanolamine can be further converted to phosphatidylserine (PS) by a serine substitution of the head group (Ridgway ed., 2015).

Another class of lipids that is found in the membranes are sphingolipids (SLs), which account for around 30% of membrane lipids. Sphingolipids consist of a sphingosine or sphingalanin (long chain base) backbone that is coupled to one fatty acyl residue to form ceramide, the basic building block of sphingolipids (Figure 12). According to the head group at the C1 atom of the ceramide, sphingolipids are classified as sphingomyelins (head group is a phosphorylcholine) and glycosphingolipids (head group is a glucose or galactose). The first and rate limiting step is the synthesis of 3-ketosphinganine from serine and fatty acyl-CoA. Next, the 3-ketosphinganine is converted into sphinganine and further to dihydroceramide. Dehydroceramide is desaturated to ceramide (Figure 13). All of these steps are catalyzed by enzymes that may have certain specificity for fatty acids. For example, dependent on the isoform of the enzyme serine palmitoyl transferase (SPT), palmitoyl-CoA, stearoyl-CoA, or myristoyl-CoA are preferentially used for the production of 3-ketosphinganine. Another example is the enzyme class of ceramide synthases (CerS). In the liver the isoform CerS2 is expressed and predominantly uses C22-C24 acyl-chains for the N-acylation of sphinganine (Ridgway ed., 2015).

Concerning the lipid class of sterols cholesterol is the most prominent member (Figure 12). Cholesterol is an important membrane component and can influence the biophysical properties of membranes. Cholesterols together with sphingolipids form lipid rafts, the detergent resistant areas of membranes (Pike, 2003). Cholesterol is taken up by nutrition and is additionally synthesized in the body. In the first step of cholesterol synthesis, acetyl-CoA is converted to acetoacetyl-CoA and further to HMG-CoA (Figure 13). The HMG-CoA-reductase (HMGCR) uses HMG-CoA to produce mevalonic acid in a rate-limiting step. This is further converted via several steps into lanosterol and finally cholesterol. Cholesterol synthesis mainly occurs in the intestine and skin and cholesterol is transported to most cell types via the lipoprotein LDL (see 1.3.5). Therefore, *de novo* cholesterol synthesis is controlled by exogenous LDL availability and is highly regulated by a negative feedback mechanism, where the HMGCR plays an important role. Regulation on transcriptional level is mediated by the transcription factors sterol regulatory element-binding proteins (SREBPs). In

presence of sufficient cholesterol in the membrane, SREBP is retained at the ER, but upon reduced cholesterol levels it translocates into the nucleus, where it binds to sterol regulatory elements (SREs) in the promoter. Enzymes from the *de novo* synthesis pathway contain two SREs in their promoter, while the LDLR promoter contains only one SRE, which results in a faster expression of LDLR and an uptake of exogenous LDL. Further regulatory mechanisms are the proteasomal degradation and post-transcriptional modifications of HMGCR (Ridgway ed., 2015).

For transport and storage cholesterol is esterified with fatty acids as cholesteryl ester (CE). The main fatty acids used for esterification are C16:0, C18:1 and C18:2 (Todoroki et al., 2000).

1.3.4. Localization of lipid synthesis

The most important compartment of lipid synthesis is the ER, where the majority of phospholipids, triglycerides, cholesterol, and precursors for further lipids are synthesized. In addition to the ER, the mitochondria and the Golgi contribute to lipid biosynthesis. The main focus of lipid synthesis in the Golgi is on sphingolipids and complex glycosphingolipids (GSLs). The mitochondria produce cardiolipin (CL) and are the only compartment containing these lipids. Both, mitochondria and the Golgi are capable of decarboxylating phosphatidylserine to phosphatidylethanolamine and the Golgi contains enzymes catalyzing the final step in phosphatidylcholine synthesis (Figure 7) (Holthuis and Menon, 2014; van Meer et al., 2008).

The lipid composition of cellular organelles differs and is already indicated by its lipid synthesis pathways. But not all lipids remain at their site of synthesis as there is a broad transport between organelles (Holthuis and Menon, 2014). For example, sterols, like cholesterol, are produced at the ER, but the ER contains only a low amount since they are transported into other compartments like the Golgi or the plasma membrane. Ceramides are also produced at the ER, but are then transported to the Golgi for sphingolipid synthesis. The ER membrane has a loose packaging due to the low amount of cholesterol and the abundance of unsaturated fatty acyl chains in its phospholipids. In contrast, the plasma membrane contains a higher amount of sphingolipids and sterols and more saturated phospholipids, which contributes to its stability. Areas in the membrane that accumulate sterols and sphingolipids are termed lipid rafts, which is a structure important for membrane signaling and trafficking (Holthuis and Menon, 2014; Lingwood and Simons, 2010).

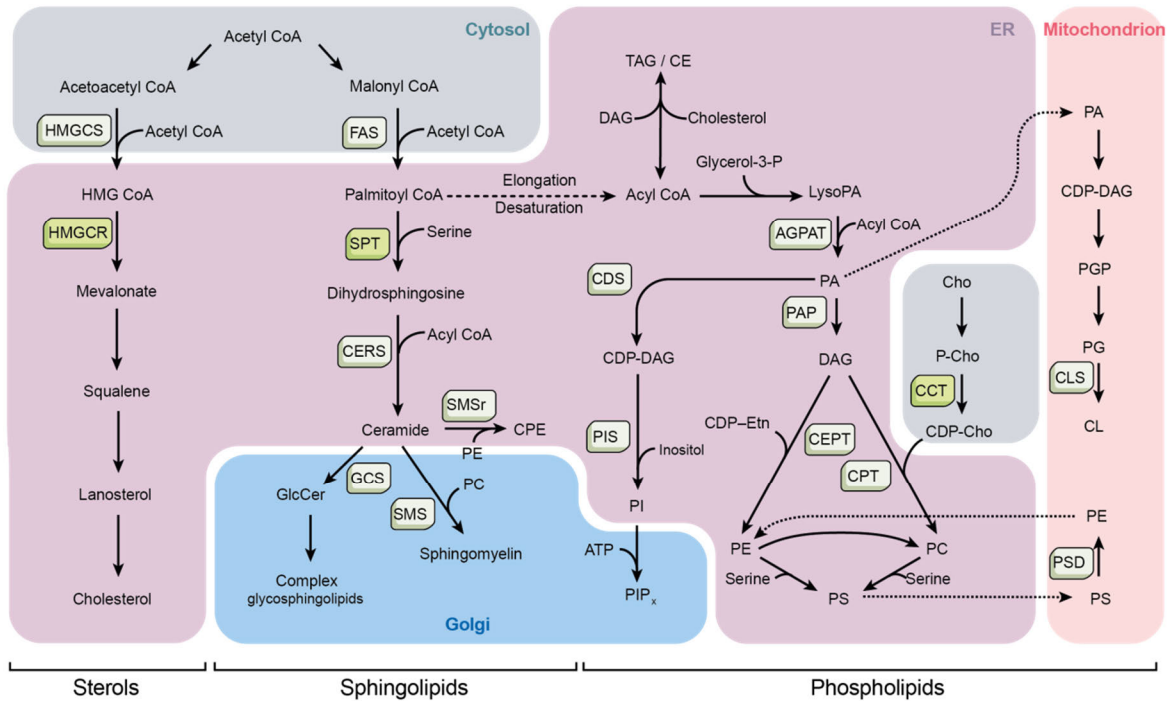


Figure 13: Lipid synthesis pathways.

Subcellular compartmentalization of the different lipid synthesis pathways. Grey: cytosol; purple: endoplasmic reticulum (ER); rose: mitochondria; blue: Golgi; AGPAT, 1-acylglycerol-3-phosphate-O-acyltransferase; CCT, CTP:phosphocholine cytidyltransferase; CDP-Cho, cytidinediphosphate choline; CDP-DAG, cytidine diphosphate diacylglycerol; CDP-Etn, cytidine diphosphate ethanolamine; CDS, cytidine diphosphate diacylglycerol; CEPT, choline/ethanolaminephosphotransferase; CERS, ceramide synthase; Cho, choline; CL, cardiolipin; CLS, cardiolipin synthase; CPE, ceramide phosphoethanolamine; CPT, cholinephosphotransferase; DAG, diglyceride; FAS, fatty acid synthase; GCS, glucosylceramide synthase; HMGCS, hydroxymethylglutaryl coenzyme A (CoA) synthase; HMGCR, 3-hydroxy-3-methylglutaryl-CoA reductase; PA, phosphatidic acid; PAP, phosphatidic acid phosphatase; P-Cho, phosphocholine; PG, phosphatidylglycerol; PGP, phosphatidylglycerolphosphate; PIP, phosphoinositide; PC, phosphatidylcholine; PE, phosphatidylethanolamine; PIS, phosphatidylinositol synthase; PS, phosphatidylserine; SMS, sphingomyelin synthase; SMSr, sphingomyelin synthase-related enzyme; SPT, serine palmitoyltransferase; TAG, triglyceride; CE, cholesteryl ester. Taken from (Holthuis and Menon, 2014).

Lipids have different shapes: cylindrical (phosphatidylcholine, phosphatidylserine), conical (diglyceride, phosphatidylethanolamine, phosphatidic acid, cholesterol, fatty acids), or inverted conical (phosphatidylinositol, lyso-phosphatidic acid, lyso-phosphatidylethanolamine, monoglyceride). Therefore, the lipid composition can determine the membrane shape. It is important for a cellular membrane to keep a certain lipid composition and several sensor mechanisms are in place for its maintenance (Holthuis and Menon, 2014).

1.3.5. Lipid transport is performed by lipoproteins

Lipoproteins transport cholesterol and triglycerides between tissues through the blood stream. The core of a lipoprotein consists of triglycerides and cholesteryl ester and is surrounded by a phospholipid monolayer that contains cholesterol and is associated with apolipoproteins. Lipoproteins differ in their size, density, lipid composition, and the associated apolipoproteins (Figure 14).

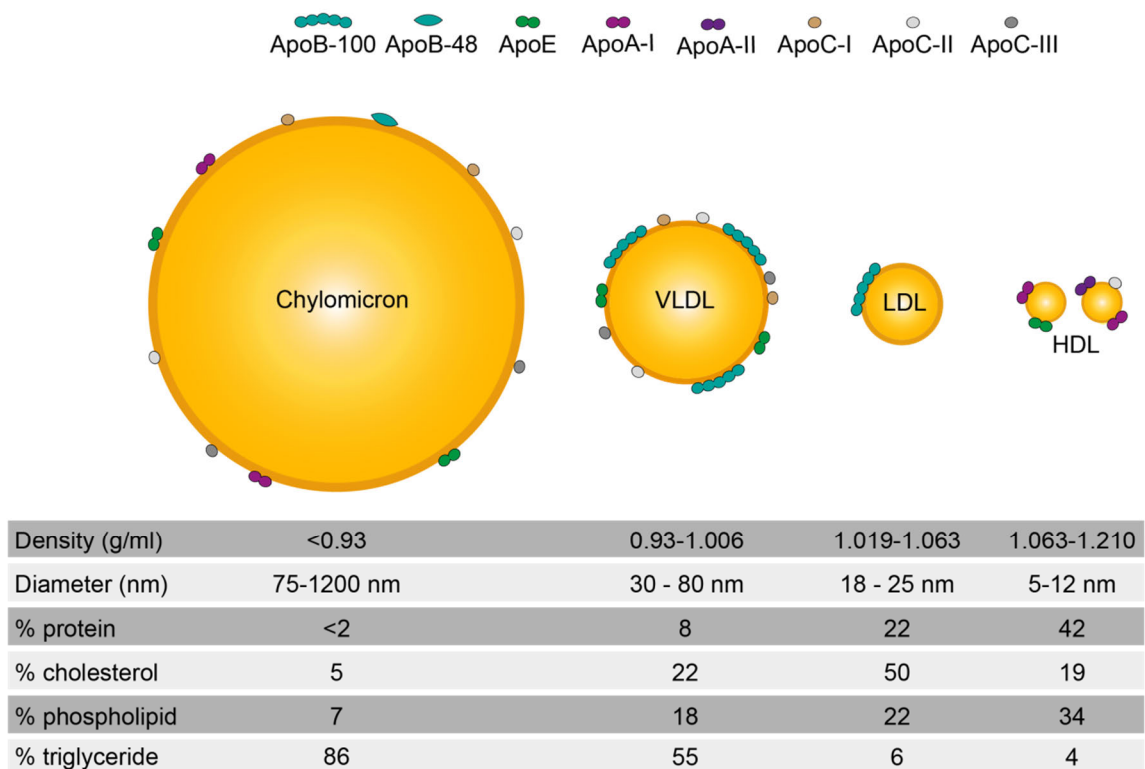


Figure 14: Lipoproteins.

Lipoproteins sorted according to their density: chylomicrons, very-low-density-lipoproteins (VLDLs), low-density-lipoproteins (LDLs), and high-density-lipoproteins (HDLs) (Löffler ed., 2014).

Chylomicrons show the lowest density, followed by very-low density lipoproteins (VLDL), low-density lipoproteins (LDL), and high-density lipoproteins (HDL). The higher density is based on the higher protein to lipid ratio.

Chylomicrons (CM) have a density of <0.93 g/ml and contain ApoB (truncated isoform ApoB-48), ApoE, ApoA-I, ApoC-I, ApoC-II, and ApoC-III (Löffler ed., 2014). They are produced in the intestine and transport triglycerides and cholesteryl ester that are taken up from the diet. Lipoprotein lipases hydrolyze triglycerides and release free fatty acids that serve as an energy source. The hydrolysis of triglycerides results in a cholesteryl ester-rich chylomicron remnant, which is taken up by the liver via LDLR (Cooper, 1997; Stryer ed. and Tymoczko ed., 2003). The liver supplies triglycerides and cholesterol to other tissues via VLDLs. In contrast to chylomicrons from the intestine, VLDLs contain triglycerides derived from *de novo* synthesis. VLDLs have a density of 0.93 – 1.006 g/ml and are associated with ApoB (isoform ApoB-100), ApoE, ApoC-I, ApoC-II, and ApoC-III (Löffler ed., 2014). It is still not fully understood how the synthesis of VLDL in the liver occurs. One model suggests that triglyceride recruitment begins with the translocation and folding of ApoB into the ER lumen. The recruitment of triglycerides to the site where ApoB is bound to the membrane causes a bud formation (Mitsche et al., 2014). An earlier model proposed that ApoB and the microsomal triglyceride transfer protein (MTTP) form a pocket for lipid binding that facilitates the formation of a primordial lipid particle (Dashti et al., 2002). It is further suggested that the lipidation proceeds in two steps, but whether this occurs in the ER or the Golgi is still not clear (Ridgway ed., 2015; Tiwari and Siddiqi, 2012). After their formation, VLDLs are transported to the Golgi in VLDL transport vesicles (VTV). In the lumen of the Golgi the particle undergoes further processing, like glycosylation and phosphorylation of the ApoB protein, and it seems that ApoA-I and ApoE are associated to the VLDL in the Golgi. Additionally, further lipidation of the VLDL can take place in the Golgi. Afterwards, the VLDL is transported from the *trans*-Golgi network in vesicles that fuse with the plasma membrane and release the VLDL (Hossain et al., 2014). After their secretion, lipases hydrolyze triglycerides which first results in cholesterol rich intermediate-density-lipoproteins and after further triglyceride depletion in LDLs. LDLs have a density of 1.019 – 1.063 g/ml and contain only a single ApoB (isoform ApoB-100). They play a crucial role in the delivery of cholesterol through the bloodstream (Löffler ed., 2014; Stryer ed. and Tymoczko ed., 2003).

HDLs have a density of 1.063 – 1.210 g/ml and the most abundant apolipoprotein is ApoA-I followed by ApoA-II. Additionally, they contain members of the ApoE and ApoC protein families. The function of HDL is the incorporation of cholesterol in the periphery, which is then transported back to the liver to be secreted as bile. Afterwards poorly lipidated HDLs can recycle back to their pathway (Löffler ed., 2014; Ridgway ed., 2015).

Lipoprotein uptake occurs via clathrin-dependent receptor-mediated endocytosis. Different receptors are known to play a role, such as the LDL-receptor family (for example LDLR and VLDLR) and the scavenger-receptor family (for example SR-BI, CD36) (Ridgway ed., 2015).

1.3.6. Lipid storage takes place in lipid droplets

Free fatty acids are toxic to the cells, a process termed lipotoxicity. In cells this is prevented by incorporation of excess fatty acids in neutral lipids, mainly diglycerides, triglycerides and cholesteryl ester, which are stored in lipid droplets (Herms et al., 2013). Fatty acids that are released from the lipid droplets can be degraded by β -oxidation to provide energy, they can be used as signaling molecules, or for the synthesis of triglycerides and membrane lipids (Smirnova et al., 2006; Walther and Farese, 2012). As neutral lipids are not soluble in the cytosol, lipid droplets form a hydrophobic core that is surrounded by a phospholipid monolayer (Figure 15). All cells have the capacity to form lipid droplets, but they differ in amount and size. For example, adipocytes mainly have a single lipid droplet with a size of up to 100 μm , while other cell types have smaller lipid droplets of 100–200 nm (Walther and Farese, 2012). Lipid droplets are associated with proteins of the PAT family. The family is named after its members: perilipin, adipophilin (ADRP), and tail-interacting protein 47 (TIP47). Meanwhile, two additional family members were identified: S3-12 and oxidative tissue-enriched PAT protein (OXPAT). These proteins protect lipid droplets from degradation and play a role in the regulation of lipolysis (Brasaemle, 2007).

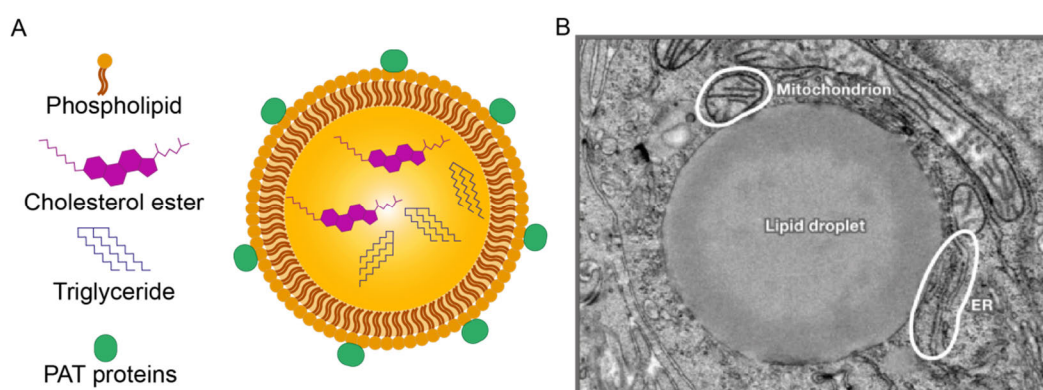


Figure 15: Lipid droplets.

A) Scheme of a lipid droplet: hydrophobic core of neutral lipids surrounded by a phospholipid monolayer and associated with PAT proteins (Farese and Walther, 2009). B) Image of a lipid droplet recorded by electron microscopy. Taken from (Farese and Walther, 2009).

How lipid droplets are generated is still not clear. The current model suggests that enzymes like acyl-cholesterol-acyltransferases (ACAT-1, ACAT-2) or diglyceride-acyltransferases (DGAT-1 and DGAT-2) synthesize neutral lipids that accumulate between the ER membrane leaflets. Whether neutral lipid synthesis is distributed along the ER and neutral lipids diffuse to formation spots or the enzymes localize to the sites of lipid droplet formation for neutral lipid synthesis is unclear. After a certain amount of neutral lipids has accumulated between the leaflets, the lipid droplet starts to bud from the ER (Wilfling et al., 2014). Not all lipid droplets keep their size after formation. Enzymes of the triglyceride synthesis pathway localize on lipid droplets and expand the lipid core by newly synthesized triglycerides. In turn, other enzymes are capable of depleting lipids from the lipid droplet to reduce them in size. Lipid droplets have the ability to fuse, a mechanism termed coalescence. This can be caused by the depletion of phosphatidylcholines from the lipid droplet membrane or by introduction of lipids with a negative curvature (Ridgway ed., 2015). Furthermore, lipid droplets are capable of transferring lipids to neighboring lipid droplets which is called ripening (Listenberger et al., 2003).

1.4. HCV causes an alteration in the lipid composition of the host cell

The HCV life cycle reveals several relations to lipids: it uses lipid droplets as assembly sites, relies on the secretion and entry routes of the lipoproteins, as well as the lipoprotein association to form a lipovirion. HCV also influences the lipid metabolism of the host cell. The first hint was the observation of steatosis, a lipid accumulation in the liver, in HCV-infected patients (Rubbia-Brandt et al., 2000). Later on, it was shown that the viral core protein of GT1b is capable of inducing steatosis in mice and an accumulation of lipid droplets in cell culture. This lipid droplet accumulation is dependent on DGAT1, an enzyme catalyzing the triglyceride synthesis and being a host-factor for HCV (Harris et al., 2011; Moriya et al., 1997). Meanwhile, lipidomic and metabolomic studies gave further insights into alterations in the lipid turnover caused by HCV. A time course analysis of early infection has revealed that several lipids of different lipid species like phospholipids, triglycerides, cholesteryl ester, and sphingomyelins are reduced over time. This reduction correlates with an increased viral titer, suggesting a role of certain lipids in particle production. Another option for the decline is their processing into another related lipid class, as it has been shown for the reduction of SM (d18/24:1) and the increase of Cer (d18/24:1) (Diamond et al., 2010). Furthermore, HCV infection may switch the PC synthesis route from the CDP-choline-pathway to the conversion of phosphatidylethanolamine to phosphatidylcholine (Roe et al., 2011). Besides changes in the lipid composition, effects on enzymes of lipid synthesis pathways have also been studied. These studies have revealed a dependence of the viral replication on the functionality of

different enzymes. Lipogenic enzymes, like FASN, are upregulated during HCV infection and in turn an inhibition of FASN causes a reduction in viral replication, showing the importance of *de novo* lipogenesis for HCV infection (Diamond et al., 2010; Narayanan et al., 2016; Yang et al., 2008). In addition, HCV causes the activation SREBP, a transcription factor regulating the expression of many enzymes involved in the synthesis of cholesterol, fatty acids, triglycerides, and phosphatidylcholines (Eberle et al., 2004; Waris et al., 2007). HCV infection also increases the level of cholesterol and sphingosine, components of lipid rafts (Roe et al., 2011). For both lipid species it was shown that synthesis inhibition resulted in an inhibition of viral replication (Amemiya et al., 2008). Furthermore, fatty acid synthesis does also play a role in viral replication. SCD catalyzes the production of the monounsaturated fatty acids palmitoleic acid and oleic acid from the saturated fatty acids palmitic acid and stearic acid, respectively. An inhibition of SCD causes a disruption of the membranous web and subsequently a reduction in viral replication (Lyn et al., 2014). Moreover, direct interactions of viral proteins with certain enzymes were uncovered. NS5A is capable to bind and activate PI4KIII α , an enzyme catalyzing the synthesis of phosphatidyl-inositol 4 phosphate (PI4P). Its activity is needed for viral replication, since PI4P accumulates on HCV replication sites (Reiss et al., 2011).

These are some examples that clearly show the connection between the HCV replication and the host lipid metabolism.

1.5. Aim of the project

HCV and the host cell lipid metabolism are intertwined: The HCV particle is associated with lipoproteins and uses several entry factors known for lipoprotein uptake. Further, HCV causes strong membrane rearrangements to support its RNA replication (Herker and Ott, 2011). Lipidomic studies have identified the dysregulation of several lipid species at early time points post infection (Diamond et al., 2010; Roe et al., 2011). However, differences may occur between an early and an established HCV infection regarding the cellular lipid composition. Therefore, the first goal of this study was to generate lipid profiles from Huh7.5 cells after a prolonged infection in comparison to uninfected Huh7.5 cells.

Vice versa, it was of interest how manipulation of the lipid homeostasis affects the HCV life cycle. HCV replicon studies have identified saturated- and monounsaturated fatty acids as beneficial for viral RNA replication, while polyunsaturated fatty acid supplementation decreased viral RNA replication (Kapadia and Chisari, 2005). So far it was unclear which influence these fatty acids have on a fully replicating virus. Thus, the second goal of this project was to study the viral RNA replication and virus production upon lipid supplementation in a fully infectious HCV system. The third focus of this study was set on

fatty acid remodeling enzymes. Fatty acids are remodeled by several elongases and desaturases (Ridgway ed., 2015). It has already been shown that the inhibition of the $\Delta 9$ -desaturase SCD impairs HCV replication (Lyn et al., 2014). Hence, knockdown experiments were performed to study the role of different elongases and desaturases in the HCV life cycle.

2. Results

2.1. HCV infection shifts the lipid profile of the host cell

HCV is known to interfere with the host lipid metabolism (Herker and Ott, 2011). Therefore, this study focused on HCV-infection mediated alterations in the host lipid composition. Lipidomics provided detailed lipid profiles of infected and uninfected cells. In this approach neutral lipids, triglycerides and cholesterol ester, and membrane lipids, phosphatidylcholines and sphingomyelins, were under investigation.

2.1.1. Preparation of whole cell extracts for mass spectrometry

Huh7.5 cells were infected with the HCV reporter strain Jc1^{Flag-E2 NS5AB-EGFP} 6–10 days prior lipid extraction (Figure 16 A). The percentage of HCV-infected cells was determined by flow cytometry. The HCV infection rate was over 79% in all three independent experiments (Exp.1–3) (Figure 16 B). A high infection rate is required to avoid confounding effects from the uninfected cells. In addition, the HCV infection was quantified by the determination of the HCV copy number by RT-qPCR in samples of the HCV-infected cells from each independent experiment (Figure 16 C). In each independent experiment the cells were split into three to five technical replicates for lipid extraction and mass spectrometry. The lipid extraction method according to acidified Bligh & Dyer enabled the isolation of lipids from the organic phase and proteins from the aqueous phase (Weerheim et al., 2002). The organic phase was then subjected to shotgun mass spectrometry and proteins were analyzed by SDS-PAGE followed by Coomassie staining or western blotting (Schwudke et al., 2011).

The expression of the HCV core protein was analyzed by western blotting in each experiment to additionally confirm equal viral infection. All Jc1^{Flag-E2 NS5AB-EGFP}-infected samples revealed a similar expression of core, while uninfected Huh7.5 cells remained negative. α -Tubulin expression was analyzed as a loading control (Figure 17 A). To evaluate whether the protein extraction after Bligh & Dyer produced similar protein yields, equal volumes of protein lysate were analyzed by SDS-PAGE followed by Coomassie staining. This approach revealed equal amounts of protein in all samples of each experiment (Figure 17 B).

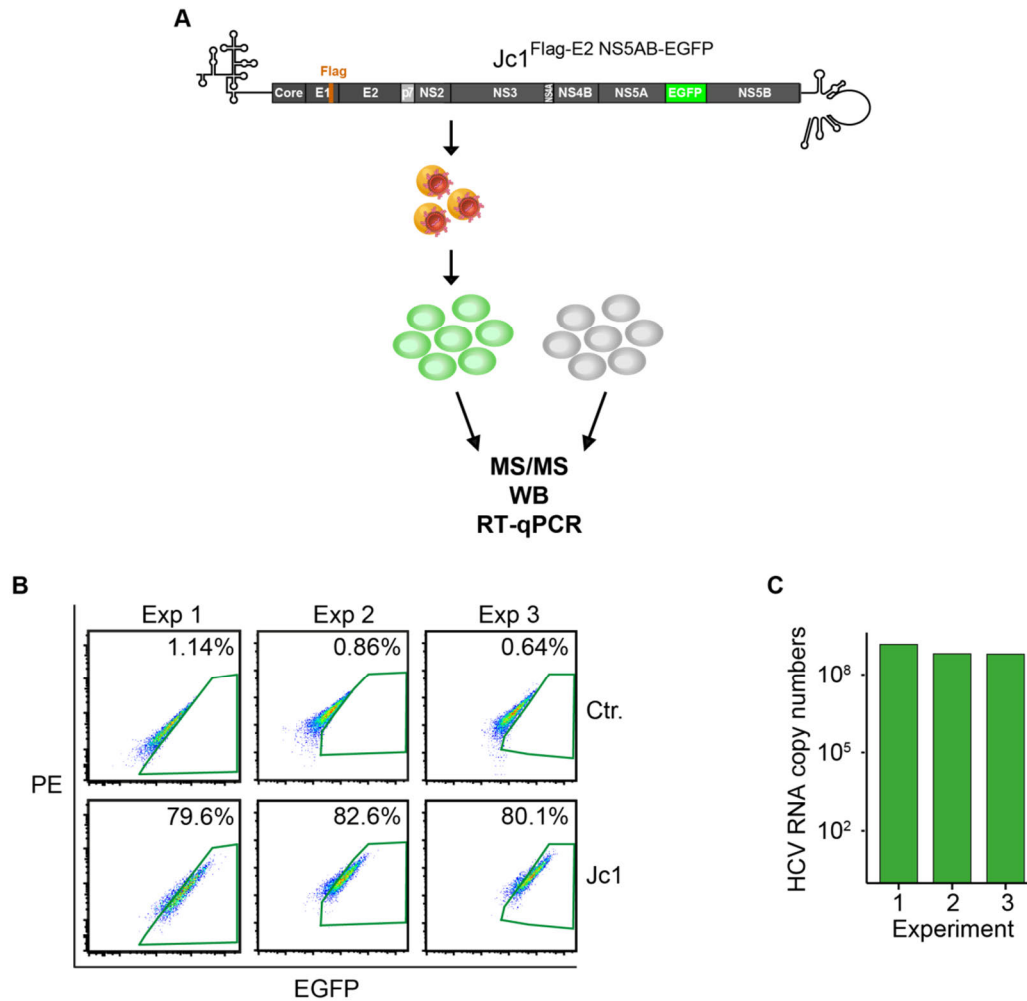


Figure 16: Experimental setup and flow cytometry analysis of HCV-infected and control cells for lipidomics.

A) The Jc1^{Flag-E2 NS5AB-EGFP} reporter virus carries an EGFP between a duplicated NS5A and NS5B cleavage site to monitor the amount of Jc1^{Flag-E2 NS5AB-EGFP}-infected cells by flow cytometry (Webster et al., 2013). Huh7.5 cells were infected with an MOI of 0.03–0.5 of Jc1^{Flag-E2 NS5AB-EGFP} and cultivated for 6–10 days. The infection rate was verified by flow cytometry. Uninfected Huh7.5 (ctr.) and HCV-infected Huh7.5 (Jc1^{Flag-E2 NS5AB-EGFP}) cells were harvested and subjected to lipid extraction. Lipids were analyzed by tandem mass spectrometry (MS/MS) and proteins by SDS-PAGE followed by Coomassie staining and western blotting (WB). Mass spectrometry was performed by Matthias Krajewski and Dominik Schwudke. B) Flow cytometry analysis of uninfected Huh7.5 (ctr.) and HCV-infected Huh7.5 (Jc1^{Flag-E2 NS5AB-EGFP}) cells to determine the percentage of HCV-infected cells. C) HCV RNA copy numbers were determined for each experiment (Exp.1–3) by RT qPCR detecting Jc1 and usage of an HCV cDNA standard curve. Results are shown for all three independent experiments (Exp. 1–3). PE: empty channel used for gating.

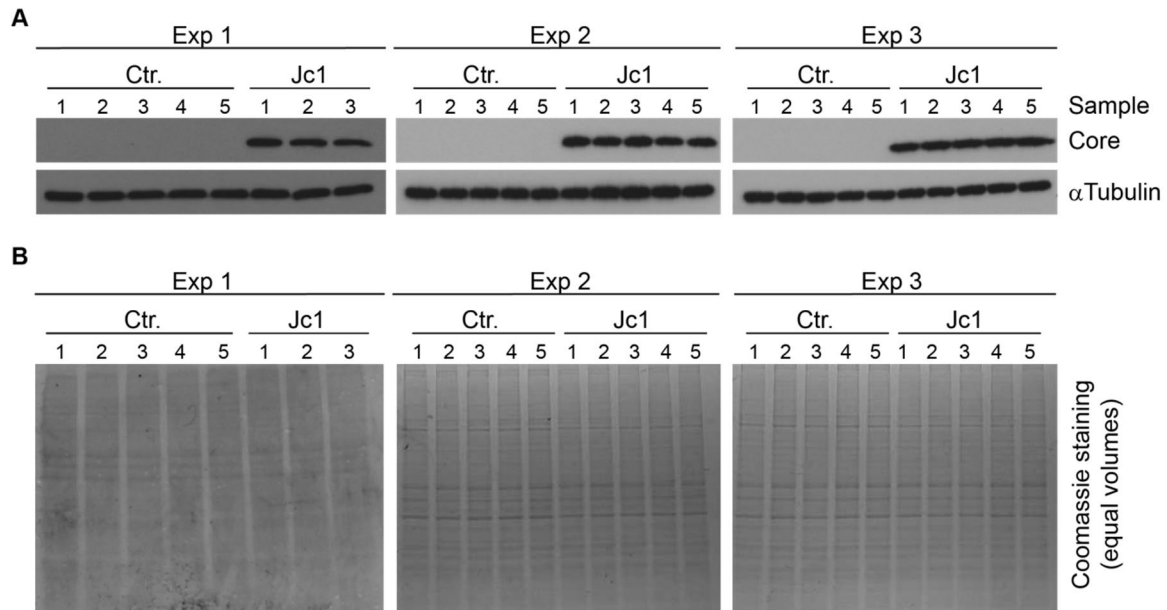


Figure 17: Western blot analysis of proteins from Bligh & Dyer extraction (whole cell extracts).

A) Equal amounts of proteins (25 μ g) were loaded to an SDS-PAGE and analyzed by western blotting with antibodies directed against core and α -tubulin. B) Coomassie staining of an SDS-PAGE loaded with equal volumes (1 μ l) of protein lysate. Three independent experiments (Exp. 1–3) were performed with three to five technical replicates.

2.1.2. HCV-infected cells contain a higher portion of membrane lipids compared to neutral lipids

The crude lipid samples were subjected to electrospray ionization tandem mass spectrometry (shotgun lipidomics) and datasets were analyzed with lipid explorer (Herzog et al., 2011; Schwudke et al., 2011). The measurement in the positive ion mode enabled the analysis of the following lipid classes: sphingomyelins (SMs), phosphatidylcholines (PCs), triglycerides (TAG), and cholesteryl ester (CE). First, the abundance of the different lipid classes was calculated. Sphingomyelins accounted for 2% of all detected lipids in uninfected cells but only for 1% in HCV-infected cells. The proportion of phosphatidylcholine was 41% in uninfected cells and increased to 50% in HCV-infected cells. The relative levels of triglycerides were reduced after HCV infection from 56% to 48%, while the cholesteryl ester abundance remained unchanged (Figure 18 A). It is known that HCV causes membrane rearrangements and, therefore, the ratio of neutral lipids (triglycerides and cholesteryl ester) to membrane lipids (phosphatidylcholine and sphingomyelin) was assessed. This ratio decreased in HCV-infected cells (Jc1^{Flag-E2 NS5AB-EGFP}) compared to uninfected control cells, demonstrating that HCV infection changes the lipid profile towards a higher proportion of membrane lipids (Figure 18 B).

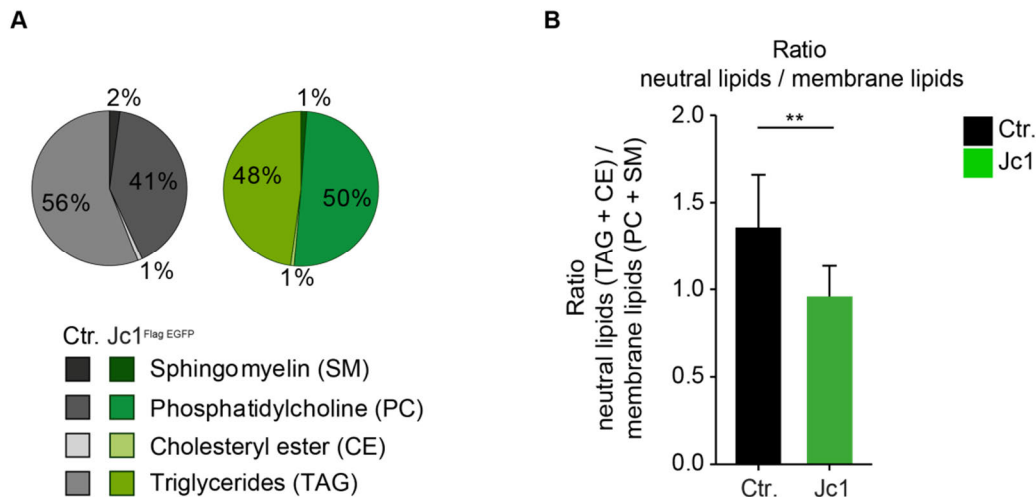


Figure 18: HCV infection alters the relative abundance of lipid classes.

A) Triglycerides, cholesteryl ester, phosphatidylcholines, and sphingomyelins in whole cell extracts of HCV-infected or uninfected Huh7.5 cells were analyzed by mass spectrometry. Proportions of the different lipid classes detected in uninfected Huh7.5 cells (grey) or Jc1^{Flag-E2 NS5AB-EGFP}-infected Huh7.5 cells (green) are depicted in the pie chart. B) The ratio of neutral lipids (triglycerides and cholesteryl ester) to membrane lipids (phosphatidylcholines and sphingomyelins) was calculated in uninfected Huh7.5 (ctr., black) and Jc1^{Flag-E2 NS5AB-EGFP}-infected (Jc1, green) Huh7.5 cells (mean \pm SD; n = 3; * p < 0.05; ** p < 0.01).

2.1.3. HCV-infected cells contain a higher relative abundance of lipids with longer fatty acyl chains

Each lipid class includes several lipid species. The lipid species name, exemplary for the triglyceride TAG[52:4], is composed as follows: the lipid class (triglycerides/TAG), the summed fatty acyl chain carbon number (52 carbon atoms) and the total amount of double bonds in the fatty acyl chains (4 double bonds).

The next analysis focused on detailed profiles of the different lipid classes. For each lipid species the amount in mol% was calculated. The most abundant lipid species in uninfected samples was defined as 100%. This lipid species served for normalization of all lipid species in the corresponding lipid class (Figure 19). The comparison of the relative abundance in triglycerides showed that triglycerides with shorter fatty acyl chains from TAG[44:0] to TAG[52:4] were more abundant in uninfected cells. Triglycerides with longer fatty acyl chains from TAG[52:3] to TAG[58:1] had a higher abundance in HCV-infected cells. Phosphatidylcholines revealed a similar shift at PC[34:0]. This shift was dependent on the

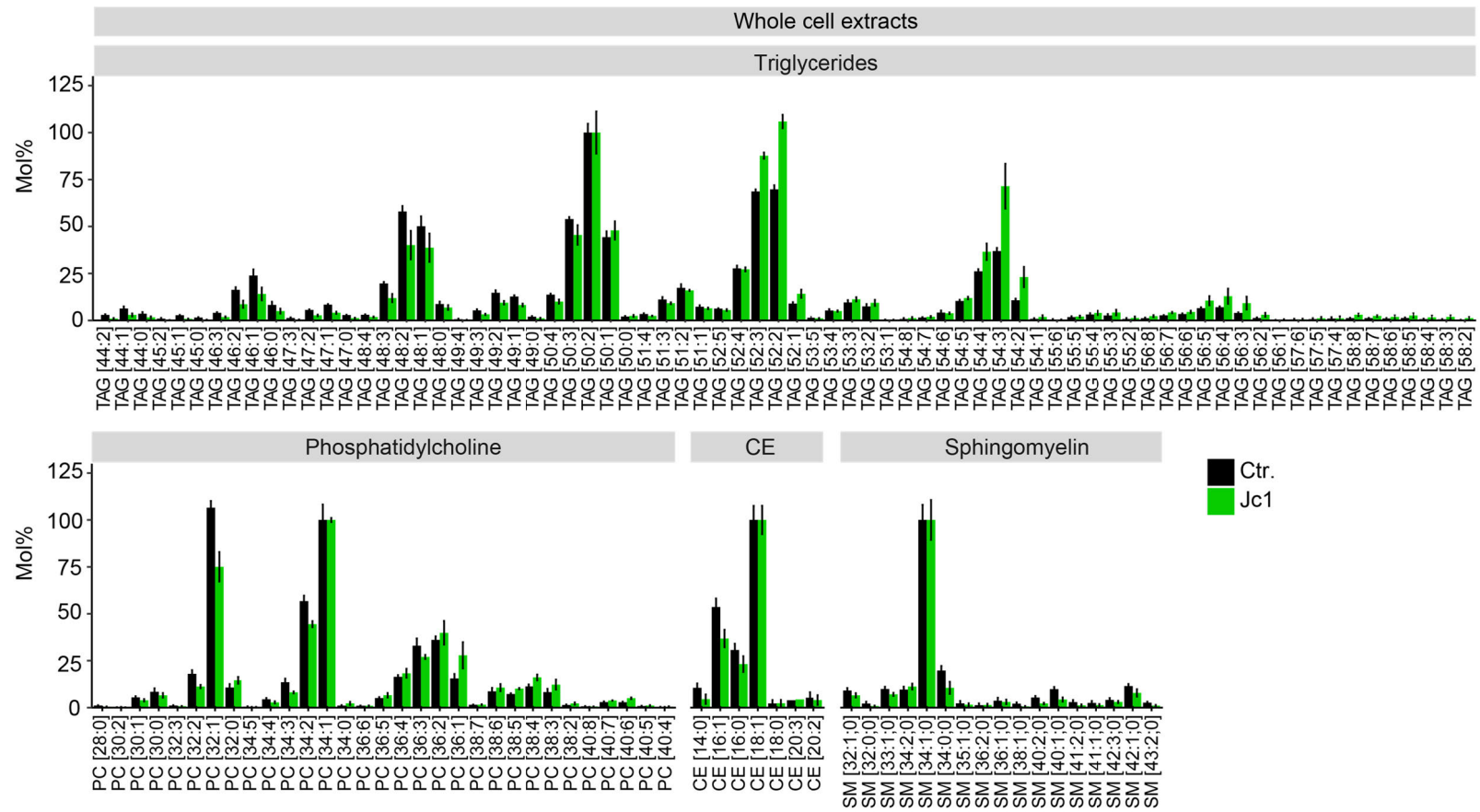


Figure 19: Lipid profile of whole cell extracts from uninfected and HCV-infected cells.

Lipid profiles of uninfected (ctr., black) and Jc1^{Flag-E2} NS5AB-EGFP-infected Huh7.5 cells (Jc1, green) were measured by shotgun mass spectrometry. Shown are lipid profiles of triglycerides (TAG), phosphatidylcholines (PC), cholesteryl ester (CE), and sphingomyelins (SM). Mol% were calculated for each sample and each lipid species. Within each lipid class the average mol% of a lipid that was most abundant in uninfected Huh7.5 cells was used for normalization (mean \pm SD; n = 3).

fatty acyl chain length, but mainly independent on the degree of desaturation. Sphingomyelins behaved in a different manner with a higher relative abundance in uninfected cells for all sphingomyelins, except SM[34:1,0], which served for normalization. Analysis of cholesteryl ester revealed that CE[14:0] to CE[16:0] were more abundant in uninfected cells, while levels of CE[18:1] to CE[20:2] were similar in HCV-infected and uninfected samples (Figure 19).

2.1.4. The absolute amount of polyunsaturated fatty acids is increased upon HCV infection

Many lipid classes contain fatty acids as fatty acyl chains. Fatty acyl chains are introduced by the esterification of fatty acids to the lipid backbone (Ridgway ed., 2015). Previous studies of unesterified fatty acids (free fatty acids, FFAs) in HCV-infected and uninfected cells have described the capability of HCV to change the amount of different free fatty acids (Douglas et al., 2016; Roe et al., 2011). Therefore, the question arises whether the higher abundance of lipid species with longer fatty acyl chains is connected to the amount of certain free fatty acids in HCV-infected cells. The free fatty acids in lipid extracts from Jc1^{Flag-E2 NS5AB-EGFP}-infected and uninfected Huh7.5 cells were analyzed by LC-MS/MS. Arachidonic acid (AA, C20:4n6), eicosapentaenoic acid (EPA, C20:5n3), and docosahexaenoic acid (DHA, C22:6n3) were significantly more abundant upon HCV infection (Figure 20). Shorter free fatty acids were not evaluated due to technical reasons.

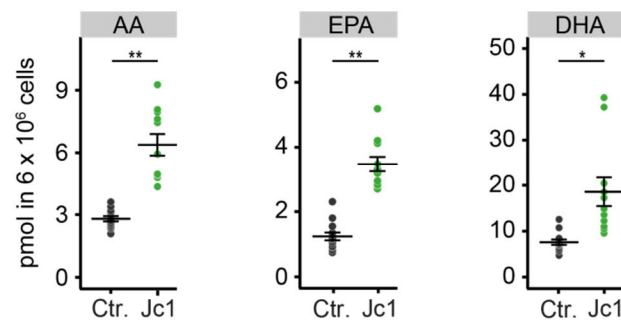


Figure 20: Analysis of free fatty acids.

Lipid fractions were subjected to liquid chromatography-tandem mass spectrometry (LC-MS/MS). The amount of arachidonic acid (AA), eicosapentaenoic acid (EPA), and docosahexaenoic acid (DHA) was analyzed in whole cell extracts of uninfected (ctr., black) or Jc1^{Flag-E2 NS5AB-EGFP} infected (Jc1, green) Huh7.5 cells (mean ± SD, n = 3; Mann-Whitney-U-Test, *p < 0.05, **p < 0.01).

2.2. Metabolomic screen of HCV-infected Huh7.5 cells

In addition to the lipidomic analysis, a targeted metabolomics study was performed. Therefore, Huh7.5 cells were infected with Jc1^{NS5AB-EGFP} for 5 days and flow cytometry analysis revealed 69% HCV-positive cells. Uninfected and HCV-infected samples were subjected to chloroform/methanol/water extraction, which enabled the precipitation of proteins but kept water-soluble metabolites in the liquid phase. The absolute amounts of metabolites were analyzed by flow injection analysis-tandem mass spectrometry (FIA-MS/MS) or liquid chromatography-tandem mass spectrometry (LC-MS/MS) by BIOCRATES Life Sciences. The data includes the results of the absolute quantification of phosphatidylcholines, sphingomyelins, carnitines, and amines (Figure 21, Figure 22).

2.2.1. HCV infection changes the phosphatidylcholine composition and decreases sphingomyelins

Phosphatidylcholines are separated into those containing two acyl chains (PC) and those containing one acyl and one alkyl chain (PCae). Overall, PCs were more abundant than PCaes. In the case of phosphatidylcholine, the results of the detailed analysis were similar to the observation previously made in the lipidomic approach. The level of several phosphatidylcholine species with shorter fatty acyl chains was reduced upon infection with Jc1^{NS5AB-EGFP} (Figure 21). These were, for example, PC[30:0], PC[32:1], PC[34:2], PC[34:1], and the slightly reduced PC[36:3]. Phosphatidylcholines containing longer fatty acyl chains were mainly increased upon Jc1^{NS5AB-EGFP} infection. This was observed for PC[36:1], PC[36:4], PC[36:5], and several lipid species with 38 or more carbon atoms in sum. An exception was PC[32:0], which belongs to the phosphatidylcholines with shorter fatty acyl chains but was enriched upon HCV infection. Regarding the PCaes this trend was less prominent but overall the majority of lipid species containing 36 or less acyl chain carbon atoms decreased in HCV-infected cells. The most abundant PCae was PCae[34:1] and it showed the strongest reduction. However, no PCae was clearly increased upon infection with HCV.

Similarly the amount of all sphingomyelin (SM) and hydroxysphingomyelin (SM(OH)) species decreased by 30–40% upon HCV infection (Figure 21).

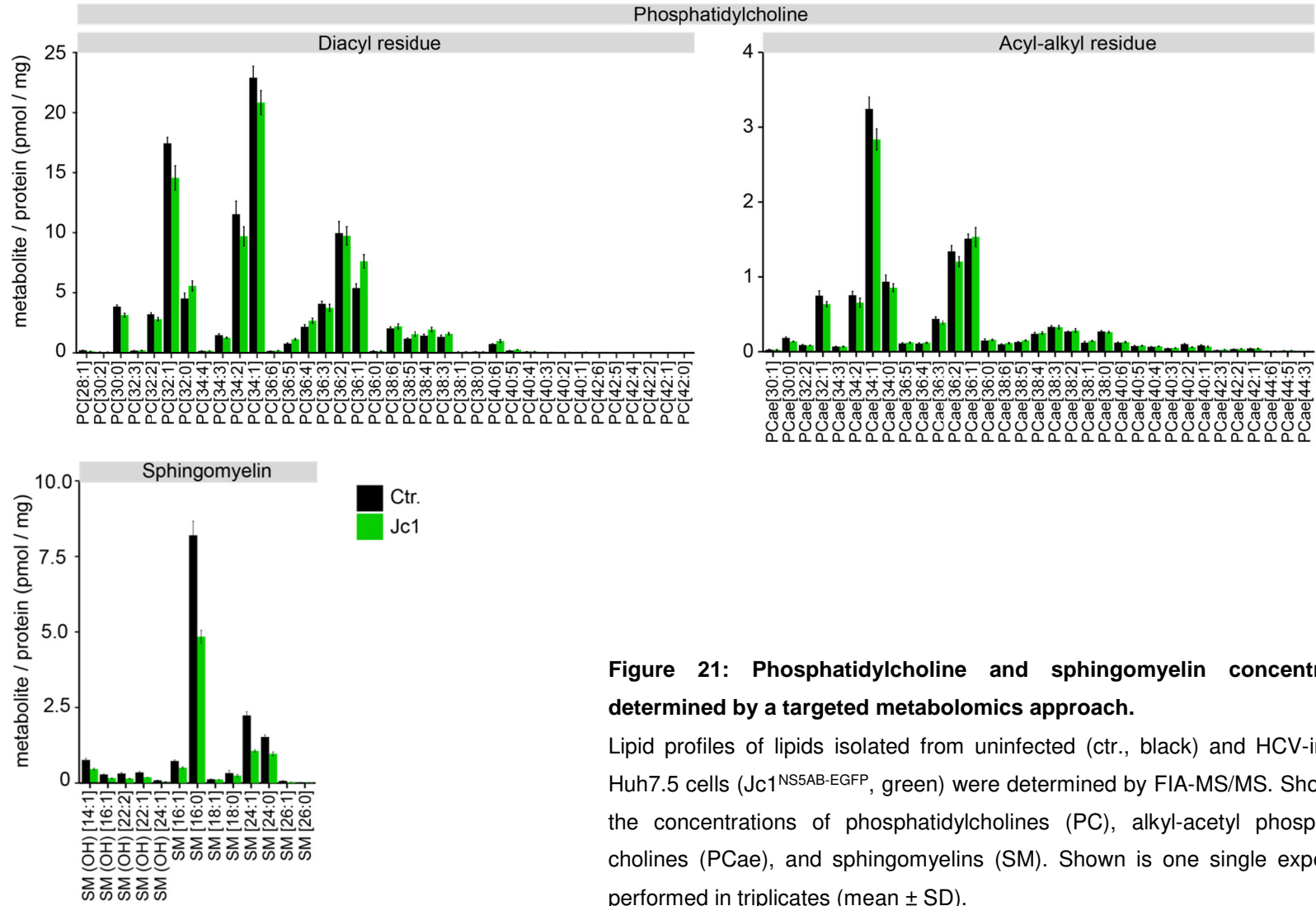


Figure 21: Phosphatidylcholine and sphingomyelin concentrations determined by a targeted metabolomics approach.

Lipid profiles of lipids isolated from uninfected (ctr., black) and HCV-infected Huh7.5 cells (Jc1^{NS5AB-EGFP}, green) were determined by FIA-MS/MS. Shown are the concentrations of phosphatidylcholines (PC), alkyl-acetyl phosphatidylcholines (PCae), and sphingomyelins (SM). Shown is one single experiment performed in triplicates (mean \pm SD).

2.2.2. Analysis of amino acids and biogenic amines

The metabolomic approach additionally included the analysis of amino acids, biogenic amines, and carnitines (Figure 22).

HCV infection increased the amount of most amino acids. Only a few amino acids were decreased, such as alanine (Ala), proline (Pro), and, to a lesser extent, aspartic acid (Asp), serine (Ser), and threonine (Thr). Glutamic acid (Glu) was present in a high amount and equal in both HCV-infected and uninfected samples (Figure 22 A).

Biogenic amines are nitrogen-containing compounds that are derived from amino acids. α -aminoadipic acid (α -AAA) is an intermediate of lysine catabolism, while creatinine is a product of the arginine catabolic pathway (Higashino et al., 1967; Michal ed., 1999). In addition to creatinine synthesis, the arginine catabolism produces a metabolite that is further converted to spermidine via putrecine and spermine (Michal ed., 1999). Trans-4-hydroxyproline (T4-OH-proline) arises from the hydroxylation of the amino acid proline (Michal ed., 1999). α -AAA, putrecine, spermidine, and spermine as well as T4-OH-proline were reduced upon HCV infection. Only creatinine remained unchanged (Figure 22 B).

Another metabolite, propionylcarnitine, was reduced in HCV-infected cells (Figure 22 C). Propionylcarnitine is a derivative of carnitine and results from the esterification of carnitine with propionyl-CoA. Propionyl-CoA is a product of the amino acid metabolism or results from the β -oxidation of odd-chain fatty acids and its downstream products are fed into the citric acid cycle (Michal ed., 1999; Ridgway ed., 2015; Stryer ed. and Tymoczko ed., 2003).

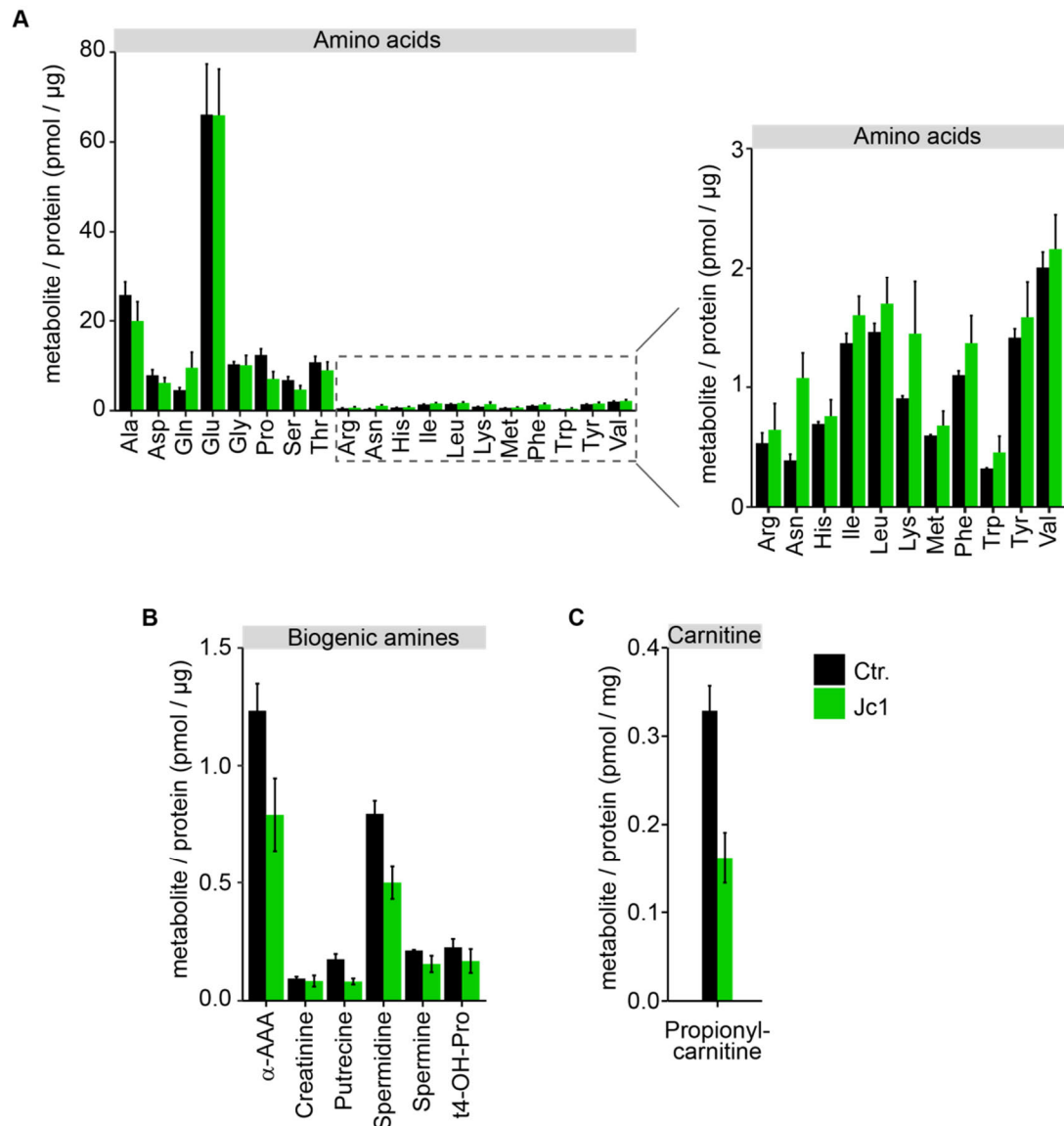


Figure 22: Intracellular levels of amino acids, biogenic amines, and carnitines determined by targeted metabolomics.

Profiles of metabolites isolated from uninfected (ctr., black) and HCV-infected Huh7.5 cells (Jc1, green) were evaluated by FIA-MS/MS (carnitines) or LC-MS/MS (amino acids and biogenic amines). Shown are the concentrations of amino acids, biogenic amines and propionylcarnitine. Ala, alanine; Asp, aspartate; Gln, glutamine; Glu, glutamate; Gly, glycine; Pro, proline; Ser, serine; Thr, threonine; Arg, arginine; Asn, asparagine; His, histidine; Ile, isoleucine; Leu, leucine; Lys, lysine; Met, methionine; Phe, phenylalanine; Trp, tryptophan; Tyr, tyrosine; Val, valine; α -AAA, α -aminoadipic acid; t4-OH-Pro, trans-4-hydroxyproline. Shown is one single experiment performed in triplicates (mean \pm SD).

2.3. Free cholesterol accumulates in the perinuclear region upon HCV infection

Free cholesterol (unesterified cholesterol) is part of lipid rafts. Lipid rafts have been described to contribute to membranous web stability and thereby playing a role in viral replication (Aizaki et al., 2004). Free cholesterol was not measurable in the lipidomic or metabolomic approach. Thus, free cholesterol was studied in HCV-infected and uninfected cells by microscopy (Figure 23). Huh7-Lunet cells were transduced with RFP-NLS-IPS, a reporter to monitor HCV infection. The reporter translocates from the mitochondria into the nucleus after it is cleaved by the viral protease NS3-4A (Jones et al., 2010).

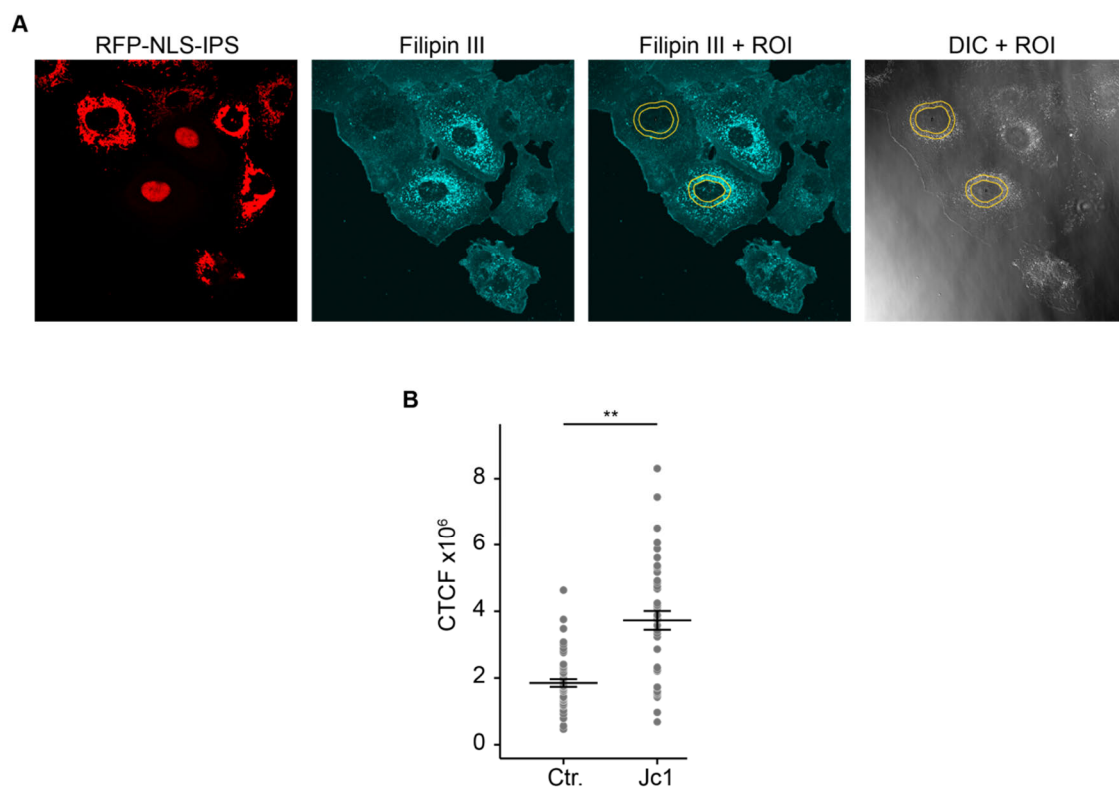


Figure 23 Staining of free cholesterol in HCV-infected cells.

A) Huh7-Lunet cells were transduced with RFP-NLS-IPS to monitor HCV infection by the translocation of RFP into the nucleus. Cells were analyzed 5 days post infection, when staining for free cholesterol with Filipin III was performed. To determine the fluorescent signal in the perinuclear region a region of interest (ROI) was set around the nucleus using the differential interference contrast (DIC) image. The Filipin III signal in this ROI was analyzed with Fiji. B) Filipin III corrected total cell fluorescence (CTCF) in uninfected (ctr.) and Jc1^{Flag-E2} infected Huh7.5 cells (Jc1) (mean \pm SEM; n \geq 42; * p < 0.05; ** p < 0.01).

Stably transduced Huh7-Lunet cells were infected with Jc1^{Flag-E2} for 5 days and stained for free cholesterol with Filipin III. A brighter fluorescent signal appeared around the nucleus of HCV-infected cells (Figure 23 A). For the quantification of the perinuclear region, a region of interest (ROI) was set around the nucleus and the fluorescence intensity was measured (Figure 23 A). HCV-infected cells exhibited a significant increase of the Filipin III signal in the ROI, indicating an increased amount of free cholesterol in the perinuclear region (Figure 23 B).

2.4. HCV infection alters the lipid profile but not the morphology of lipid droplets

Lipid droplets, the lipid storage organelles, play an important role in the HCV life cycle as virion assembly platforms (Lindenbach and Rice, 2013). Furthermore, it has been shown that the full replicating virus or single viral proteins can manipulate lipid droplets by changing their proteome or by slowing down their turnover (Harris et al., 2011; Rosch et al., 2016). Therefore, the question arises whether lipidomic changes occur in lipid droplets in a similar manner as in whole cell extracts or whether their lipid profile is regulated in a different manner.

2.4.1. HCV infection has no impact on lipid droplet morphology in Huh7.5 cells

The first approach of the lipid droplet analysis investigated the impact of HCV on lipid droplet morphology. It has been described that the area occupied by lipid droplets is increased in HCV-infected cells (Akil et al., 2016; Li et al., 2013). Triglycerides represent the major lipid classes contained in the lipid droplet hydrophobic core of hepatic cells (Herms et al., 2013). An increase in the lipid droplet volume suggests an increase in the amount of triglycerides. Therefore, the total amount of triglycerides was assessed in HCV-infected and uninfected cells. Huh7.5 cells were infected with Jc1^{NS5AB-EGFP} for 6–12 days and revealed an infection rate of at least 66%. HCV-infection had no significant impact on the amount of triglycerides (Figure 24).

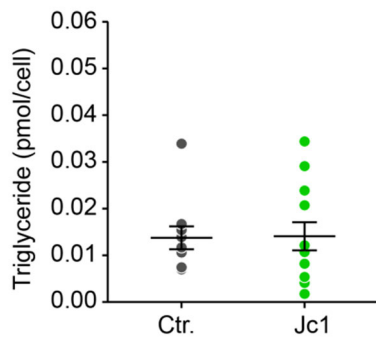


Figure 24: Amount of triglycerides in infected and uninfected Huh7.5 cells.

Lipid extraction of uninfected (ctr., black) or Jc1^{NS5AB-EGFP}-infected (Jc1, green) Huh7.5 cells was performed at 6–12 days post infection according to Bligh & Dyer. Triglycerides were measured using the infinity triglyceride kit (Thermo Fisher). The amount of triglycerides was calculated as pmol per cell (mean \pm SEM; $n = 4$; * $p < 0.05$, ** $p < 0.01$).

So far, most studies have described the area occupied by lipid droplets without determining the single lipid droplet volumes and analyzed cells in different wells and not neighboring cells under the same culture conditions. Therefore, lipid droplet volumes and the number of lipid droplets were analyzed by confocal microscopy. Huh7.5 cells carrying the HCV reporter RFP-NLS-IPS were infected with the viral strain Jc1^{Flag-E2} for 5–6 days and seeded for microscopy. The samples were stained with Hoechst and BODIPY 493/503 to detect the nucleus and the lipid droplets, respectively. Stacks were recorded with the Nikon C2plus confocal microscope and 3D images were generated and evaluated with Imaris (Figure 25 A). The infection of Huh7.5 cells with Jc1^{Flag-E2} revealed no significant impact on lipid droplet volumes, as well as on the number of lipid droplets and the total lipid droplet volume (Figure 25 B).

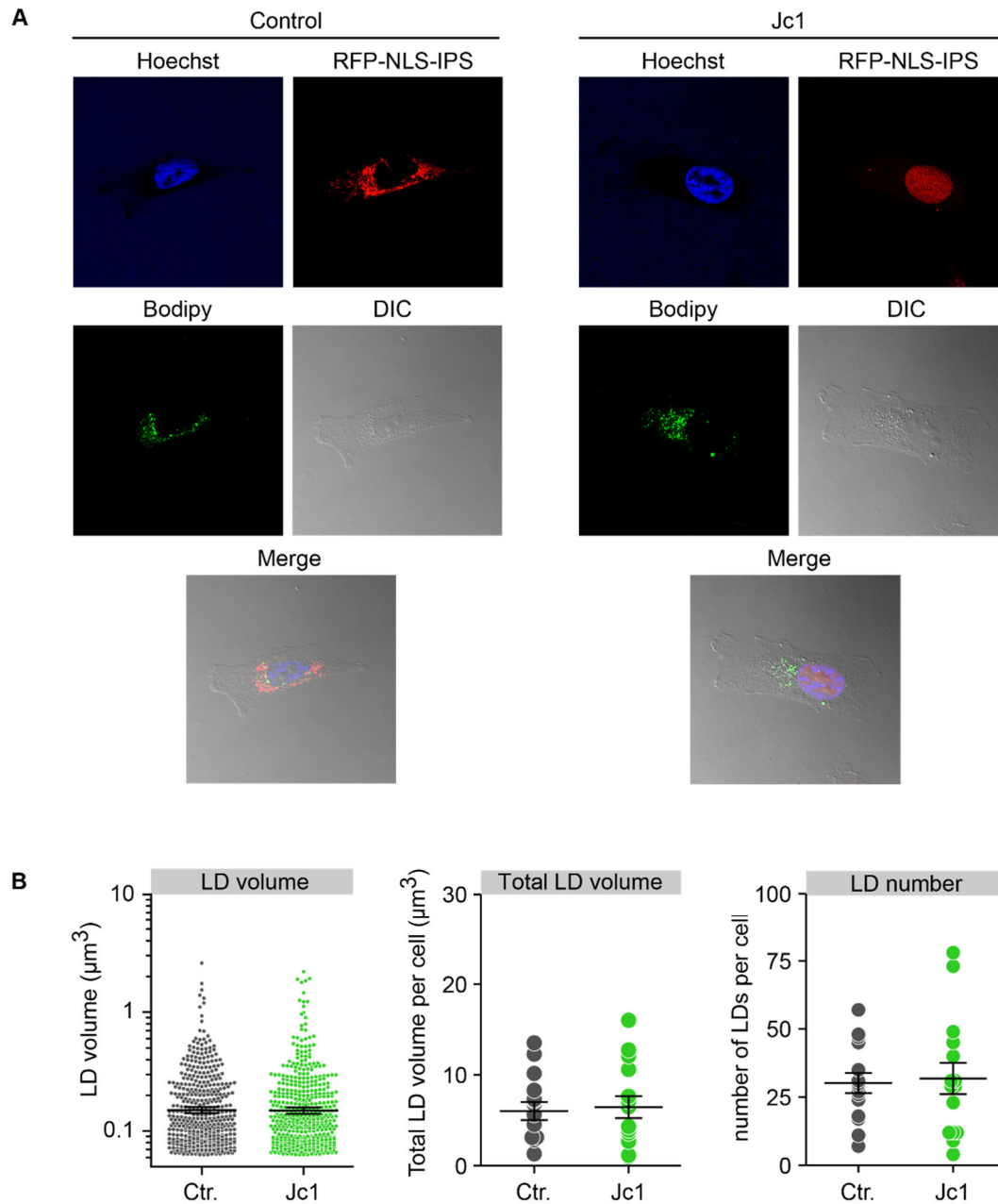


Figure 25: Volumetric analysis of lipid droplets.

A) Exemplary images of uninfected (ctr., black) or Jc1^{Flag-E2-infected} (Jc1, green) Huh7.5 cells. Huh7.5 cells were stably transduced with RFP-NLS-IPS to identify HCV-infected cells by the RFP signal in the nucleus. Cells were stained with Hoechst for the nucleus and with BODIPY 493/503 for lipid droplets. Recordings were performed on a Nikon C2plus confocal microscope. Stacks were recorded from the cells and a 3D reconstruction was performed with Imaris. B) Volume analysis of average lipid droplet (LD) volume, number of lipid droplets per cell, and total lipid droplet volumes per cell. 3D reconstruction and volumetric analysis were done using Imaris (average lipid droplet volumes: geometric mean \pm 95% CI, number of lipid droplets per cell and total volume per cell: mean \pm SEM; n = 9–20; * p < 0.05, ** p < 0.01).

2.4.2. Preparation of lipid droplet extracts for mass spectrometry

HCV infection had no impact on the lipid droplet morphology. However, the question remained if the lipid profile is altered regarding the abundance of different lipid species. Therefore, Huh7.5 cells were infected with Jc1^{Flag-E2 NS5AB-EGFP} for 7–17 days before the cells were subjected to lipid droplet isolation followed by lipid and protein extraction according to acidified Bligh & Dyer (Figure 26 A). The percentage of infected cells was determined by flow cytometry and infection rates were over 83% in all three independent experiments (Exp. 1–3) (Figure 26 B). The lipids were analyzed by shotgun mass spectrometry and proteins were analyzed by SDS-PAGE for Coomassie and silver gel staining, as well as western blotting (Schwudke et al., 2011). Cells were homogenized in hypotonic lysis buffer and after removal from the nuclei by centrifugations the lysate was termed post-nuclear supernatant (PNS). The post-nuclear supernatants were subjected to ultracentrifugation to separate lipid droplets from remaining cell debris. All extraction steps were performed with samples lacking cells to generate a background control for lipidomic analysis (☞). Equal protein amounts of post-nuclear supernatant samples or equal volumes of lipid droplet protein lysates were subjected to SDS-PAGE. The HCV core protein localizes to lipid droplets in HCV-infected cells (Boulant et al., 2006). Thus, core serves as a marker for infection that can be used in post-nuclear supernatants and lipid droplets fraction. Core was present in all post-nuclear supernatant and lipid droplet samples from HCV-infected cells, while no bands were observed in the uninfected controls (Figure 27 A). The presence of the lipid droplet binding protein ADRP confirmed almost equal loading of all lanes. Furthermore, the samples were analyzed for the comparability of the protein yields by subjecting equal sample volumes onto SDS-PAGE for Coomassie or silver staining (Figure 27 B). The Coomassie staining of the post-nuclear supernatants revealed equal protein yields, indicating that equal amounts of samples were subjected to lipid droplet isolation. Silver staining of isolated lipid droplets indicated slightly lower protein amounts in samples from HCV-infected cells compared to uninfected cells (Figure 27 B). All background controls (☞) remained empty illustrating that no contamination with proteins occurred during the experiment.

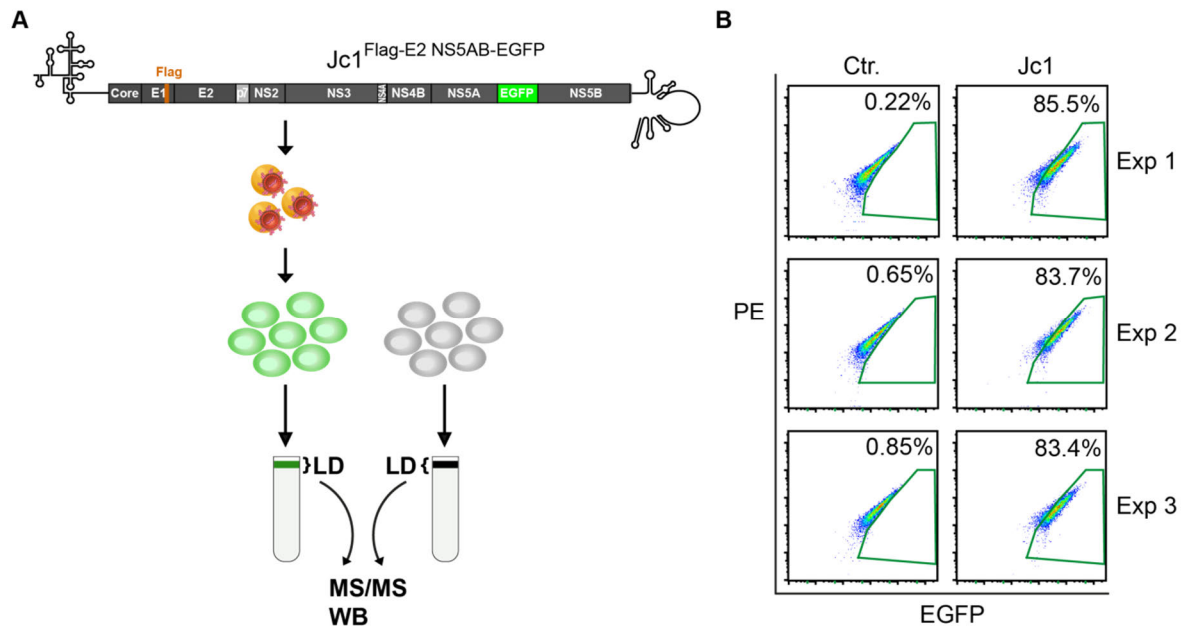


Figure 26: Experimental setup and flow cytometry analysis for lipidomics of isolated lipid droplets.

A) Huh7.5 cells were infected with an MOI of 0.1–0.3 of the HCV reporter virus Jc1^{Flag-E2 NS5AB-EGFP} and cultivated for 7–17 days. The infection rate was monitored by flow cytometry. Uninfected Huh7.5 (grey/black) and Jc1^{Flag-E2 NS5AB-EGFP}-infected (green) Huh7.5 cells were subjected to lipid droplet (LD) isolation followed by lipid extraction. Lipids were analyzed by tandem mass spectrometry (MS/MS) and proteins by Coomassie and silver gel staining, as well as western blotting (WB). Mass spectrometry was performed by Matthias Krajewski, Verena Scholz, and Dominik Schwudke.

B) Uninfected Huh7.5 (ctr.) and Jc1^{Flag-E2 NS5AB-EGFP}-infected Huh7.5 (Jc1) cells were analyzed by flow cytometry to determine the percentage of infected cells. Shown are all three independent experiments (Exp. 1–3). PE: empty channel used for gating.

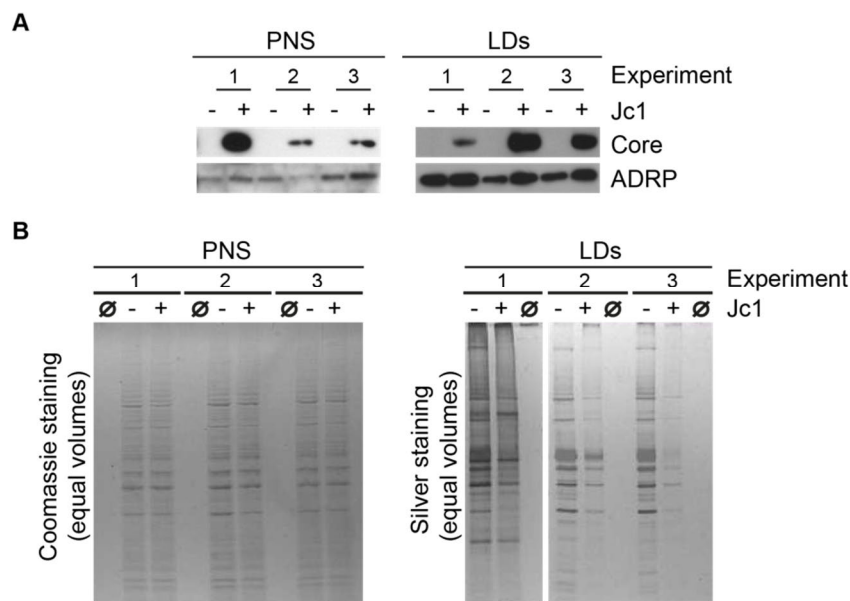


Figure 27: Western blot analysis of proteins obtained from Bligh & Dyer extraction (lipid droplets).

A) Post-nuclear supernatants (PNS) and lipid droplet fractions were analyzed for the expression of core and ADRP. For PNS samples equal amounts of proteins (10 µg) and for lipid droplets equal volumes were loaded (15 µl for Exp. 1 and 20 µl for Exp. 2 and Exp. 3). B) Equal volumes of PNS (1 µl) and lipid droplet lysates (10 µl for Exp. 1 and 5 µl for Exp. 2 and Exp. 3) were analyzed by Coomassie and silver gel staining, respectively. Results are shown for all three independent experiments.

2.4.3. Lipids with longer fatty acyl chains have a higher abundance in lipid droplets isolated from HCV-infected cells

In lipid droplet extracts the amount of triglycerides, diglycerides, phosphatidylcholines, and cholesteryl ester were determined. The profiles of triglycerides, diglycerides, and phosphatidylcholines revealed a higher abundance of lipids with longer fatty acyl chains due to HCV infection. The shift occurred at DAG[36:3], TAG[52:3], and PC[36:2], respectively. Cholesteryl ester with a shorter chain length have a higher abundance in uninfected cells, whereas CE[18:1] and subsequent cholesteryl esters with increasing fatty acyl chain lengths were equally abundant in both samples (Figure 28).

Three lipid classes (triglycerides, phosphatidylcholines, and cholesteryl esters) were measured in both, lipid droplets and whole cell extracts. The number of lipid species differed between the two samples. However, comparing the lipid species that were quantifiable in whole cell extracts and lipid droplets revealed that the profiles are highly similar.

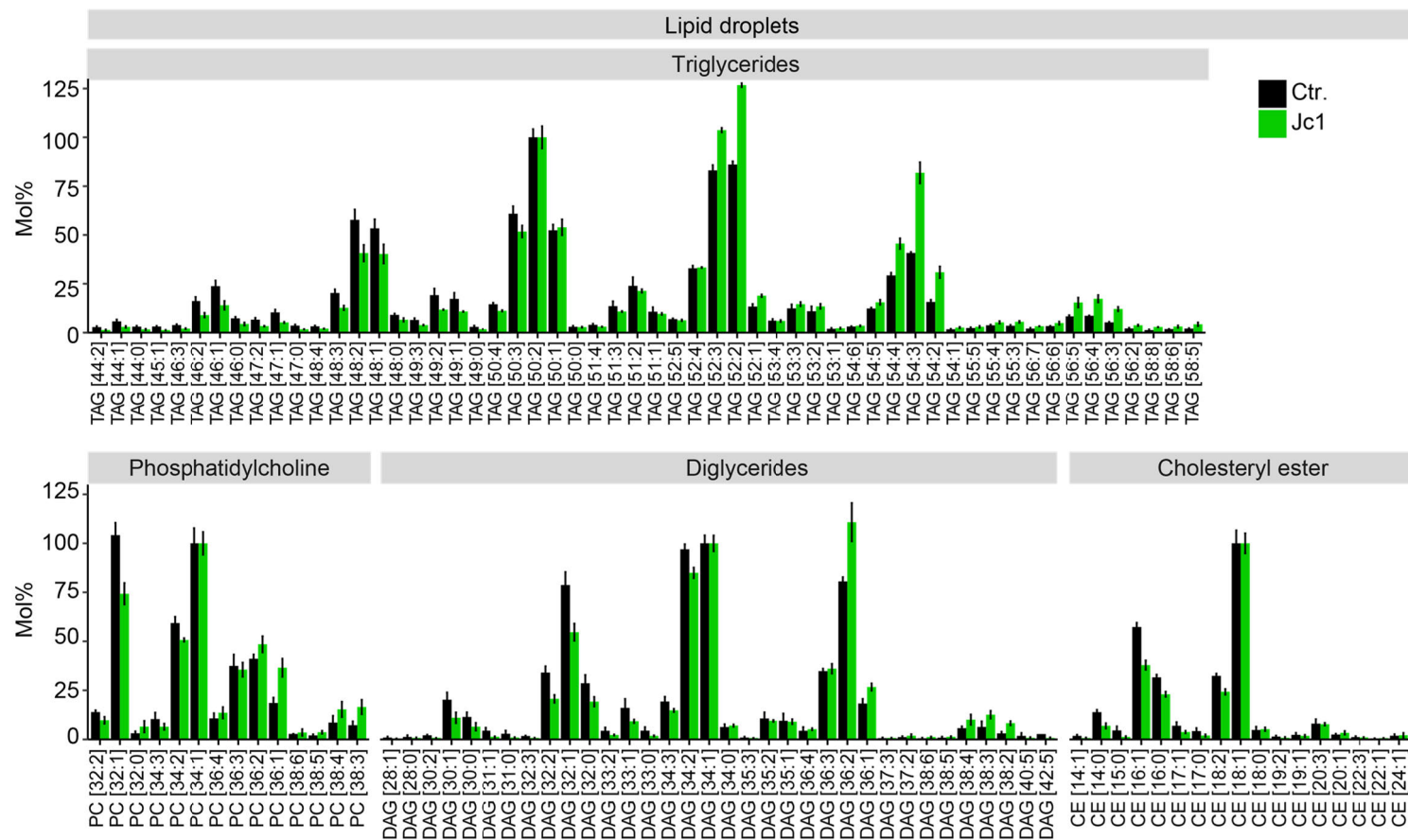


Figure 28: Lipid profile of lipid droplets from uninfected and HCV-infected cells.

Lipid profiles of lipid droplets isolated from uninfected (ctr., black) and Jc1^{Flag-E2 NS5AB-EGFP}-infected Huh7.5 cells (Jc1, green) were determined by shotgun mass spectrometry. Shown are lipid profiles of triglycerides, phosphatidylcholines, diglycerides, and cholesteryl ester. Mol% were calculated for each lipid species. Within each lipid class the average mol% of a lipid that was most abundant in uninfected Huh7.5 cells was used for normalization (mean \pm SD; n = 3).

2.5. Different lipid species have diverse effects on HCV replication

So far, the experiments clearly showed that an HCV infection changes the host cell lipid composition. This raises the question whether HCV replication is influenced by exogenous supplementation of different lipid classes or species.

2.5.1. Cholesterol has a dose- and time-dependent impact on HCV infection

The importance of a functional cholesterol synthesis for the HCV RNA replication has been investigated in earlier studies, for example, the inhibition of viral RNA replication by statins (Ye et al., 2003). This study showed an increase of free cholesterol in the perinuclear region of HCV-infected cells (Figure 23). The cholesterol synthesis underlies a strong feedback mechanism and, therefore, the question arises if the treatment with cholesterol affects the viral life cycle in a dose-dependent manner (DeBose-Boyd, 2008). Supplementation of 100 μ M cholesterol for 3 days or 5 days did not affect cell viability (Figure 29 B). Huh7.5 were electroporated with Jc1^{NS5AB-Fluc} and treated with 10 μ M, 50 μ M, and 100 μ M cholesterol for 3 and 5 days. At both time points, the cells were lysed to analyze viral RNA replication and their supernatants were transferred to naïve Huh7.5 cells to analyze virus production (Figure 29 A). Viral RNA replication was not impaired in a significant manner with any concentration at both time points (Figure 29 C). In contrast, cholesterol supplementation had opposing effects on virus production depending on treatment length and dose. On 3 days post treatment virus production decreased in a dose dependent manner, with the highest dose causing the strongest reduction. The virus production increased after the 5 day treatment with the low 10 μ M and 50 μ M concentration, while 100 μ M of cholesterol had no effect.

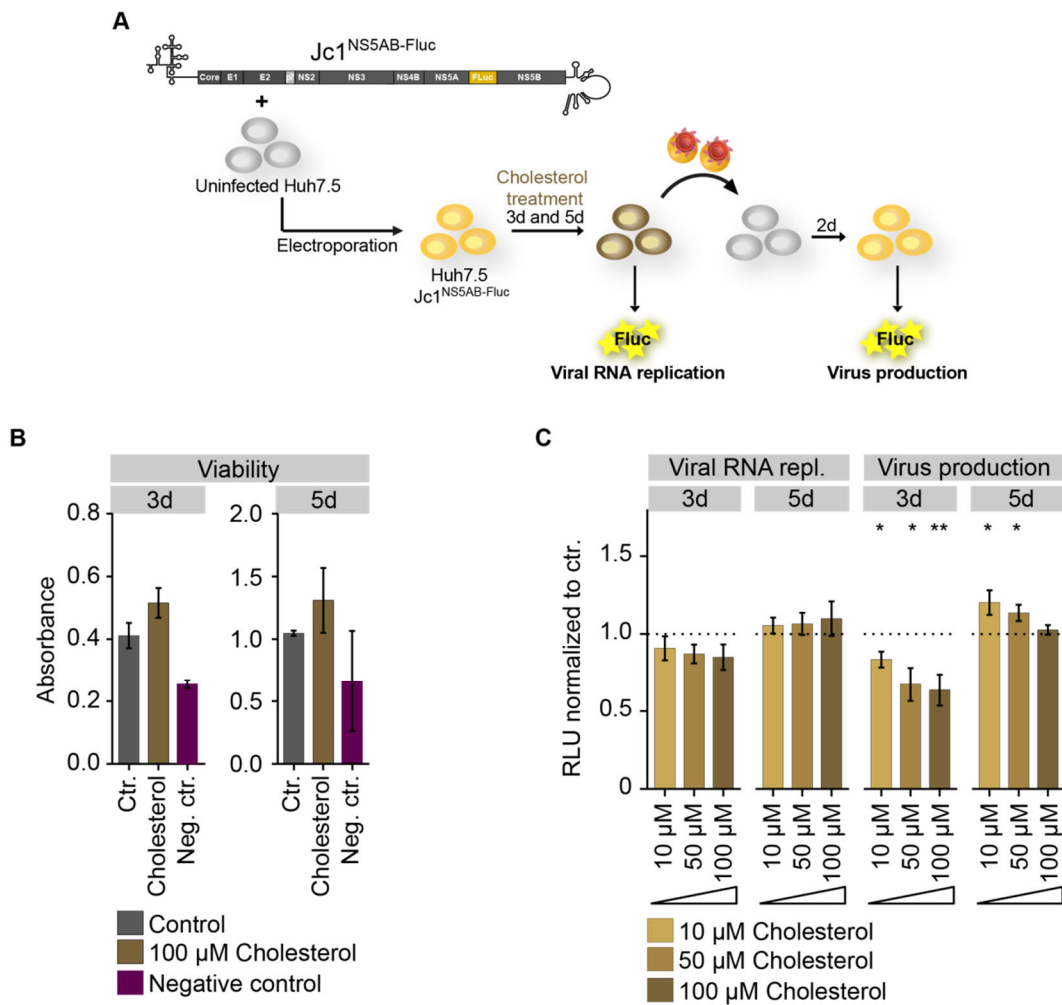


Figure 29: Luciferase assay to study the impact of cholesterol on the viral life cycle.

A) Huh7.5 cells were electroporated with Jc1^{NS5AB-Fluc} and 4 h after electroporation cells were treated with different cholesterol concentrations for 3 and 5 days. At both time points cells were lysed to study viral replication. To study virus production the supernatants were transferred to uninfected Huh7.5 cells, medium was changed 3 h after infection and cells were incubated for 2 days before cells were lysed. B) Cell viability was studied in uninfected Huh7.5 cells at 3 and 5 days after the treatment with 100 μM cholesterol, mock-control (ctr.) or 0.1 M H₂O₂ as negative control (Neg. ctr.) (mean ± SEM; n = 2). The cell viability was measured with a CellTiter 96 AQueous One Solution assay (Promega) by measuring the absorbance at 490 nm. C) Huh7.5 cells were electroporated with Jc1^{NS5AB-Fluc} and treated with different concentrations of cholesterol for 3 and 5 days. At both time points samples were taken to analyze viral replication and were additionally transferred to uninfected Huh7.5 cells to study virus production (mean ± SEM; n = 8; * p < 0.05, ** p < 0.01).

2.5.2. The triglyceride level is altered upon fatty acid treatment in HCV-infected and uninfected cells in a similar manner

As mentioned above, triglycerides are composed of three fatty acids esterified to glycerol (Figure 11) (Herms et al., 2013). They are stored in lipid droplets and can serve for the production of membrane lipids (Ducharme and Bickel, 2008). The overall level of triglycerides was not changed in HCV-infected cells, but the lipid profile of triglycerides was affected by the infection. In the lipidomics analysis HCV infection affected the total chain lengths of the fatty acids in triglycerides. Due to this finding the ability of fatty acids with different chain length and degree of desaturation to induce the triglyceride formation was investigated. Moreover, the incorporation into triglycerides was compared between HCV-infected and uninfected cells to elucidate potential preferences regarding the incorporation of fatty acid species. Jc1^{NS5AB-EGFP}-infected Huh7.5 cells used for these experiments were at least 66% positive for HCV infection at 6–12 days post infection. HCV-infected and naïve Huh7.5 cells were treated with 100 μ M fatty acids for 1 day and the amount of triglycerides was determined biochemically after lipid extraction. The mock-controls (Ctr.) harbored a triglyceride amount of 0.013 pmol/cell in uninfected cells and 0.016 pmol/cell in HCV-infected cells (Figure 30). The saturated fatty acid lauric acid (C12:0) caused a slight and not significant increase of the triglyceride level. The amount of triglycerides further increased

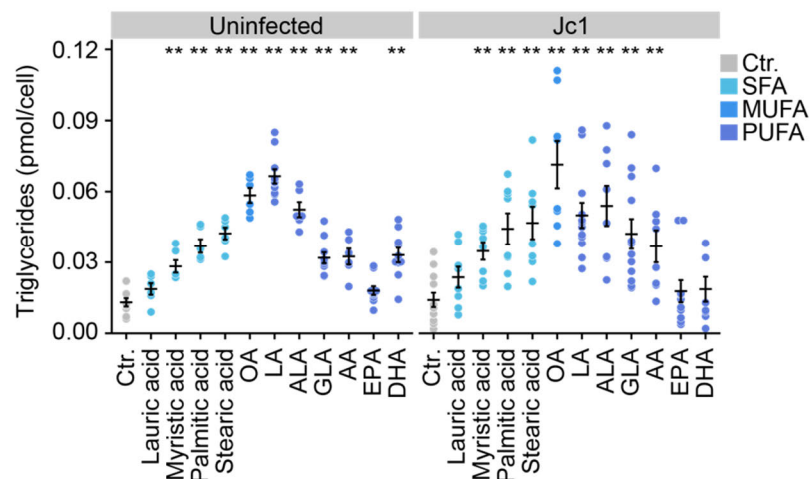


Figure 30: Triglyceride levels after fatty acid treatment.

Uninfected or Jc1^{NS5AB-EGFP}-infected Huh7.5 cells were treated with 100 μ M fatty acid for 1 day. Lipids were extracted after Bligh & Dyer and triglycerides were measured using the infinity triglyceride kit (Thermo Fisher). The amount of triglycerides was calculated as pmol per cell (mean \pm SEM; $n \geq 3$; * $p < 0.05$, ** $p < 0.01$). Ctr., mock-control; OA, oleic acid; LA, linoleic acid; ALA, α -linolenic acid; GLA, γ -linolenic acid; AA, arachidonic acid; EPA, eicosapentaenoic acid; DHA, docosahexaenoic acid.

concomitant with the fatty acid chains, as shown for myristic acid (C14:0), palmitic acid (C16:0), and stearic acid (C18:0). Oleic acid (OA, C18:1n9) has the same chain length as stearic acid but carries one double bond. Supplementation of oleic acid increased the amount of triglycerides to 0.058 pmol/cell in uninfected and to 0.071 pmol/cell in HCV-infected cells. Oleic acid caused the highest increase in triglycerides in HCV-infected cells, while linoleic acid (LA, C18:2n6) caused the highest increase in uninfected cells. The amount of triglycerides started to decrease again as chain length and the degree of desaturation further increased, as depicted for α -linolenic acid (ALA, 18:3n3), γ -linolenic acid (GLA 18:3n6), and arachidonic acid (AA, 20:4n6). Cells treated with eicosapentaenoic acid (EPA, 20:5n3) had a triglyceride level of 0.018 pmol/cell in uninfected and 0.019 pmol/cell in HCV-infected cells, which is only slightly above the mock-controls (ctr.). In contrast, docosahexaenoic acid (DHA, 22:6n3) significantly increased the triglyceride level in uninfected cells and, to a lesser extent, in HCV-infected cells. Overall, the triglyceride levels after the treatment with fatty acids were dependent on the chain length and desaturation. The triglyceride levels were almost identical for most fatty acids in HCV-infected and uninfected cells. Slight differences were observed for oleic acid, linoleic acid, and docosahexaenoic acid.

2.5.3. Fatty acids have diverse effects on HCV replication depending on fatty acyl chain length and desaturation

Next, the impact of these fatty acids on the viral life cycle was assessed. First, the cell viability was tested after 100 μ M fatty acid treatment for 3 and 5 days (Figure 31). Cell viability was confirmed after a 5 day treatment for all fatty acids, except of stearic acid, arachidonic acid, and docosahexaenoic acid (Figure 31 A). For those, different concentrations were evaluated in the cell viability assay and for further experiments reduced to 10 μ M for stearic acid and docosahexaenoic acid. Although toxicity of arachidonic acid was not obvious in this approach the concentration was reduced to 50 μ M for further experiments (Figure 31 B).

Jc1^{NS5AB-Fluc}-electroporated Huh7.5 cells were treated with fatty acids for 3 days or 5 days. At the indicated time points the cells were lysed to analyze viral RNA replication and their supernatants were used to infect naïve Huh7.5 cells to analyze virus production. The analysis was performed with a luciferase assay (Figure 32 A). Lauric acid treatment caused a significant increase in viral replication at 3 days post treatment and a significant increase in virus production at 5 days post treatment (Figure 32 B). Myristic and palmitic acid had no effect on viral replication but decreased virus production at 3 days post treatment or both time points post treatment. Stearic acid caused no effect at 3 days post treatment but decreased viral RNA replication and virus production significantly at the second time point.

The monounsaturated fatty acid oleic acid and the polyunsaturated fatty acids decreased viral RNA replication and, consequently, reduced virus production at both time points. In this setup the supplementation of DHA had no effect on the viral life cycle (Figure 32 B).

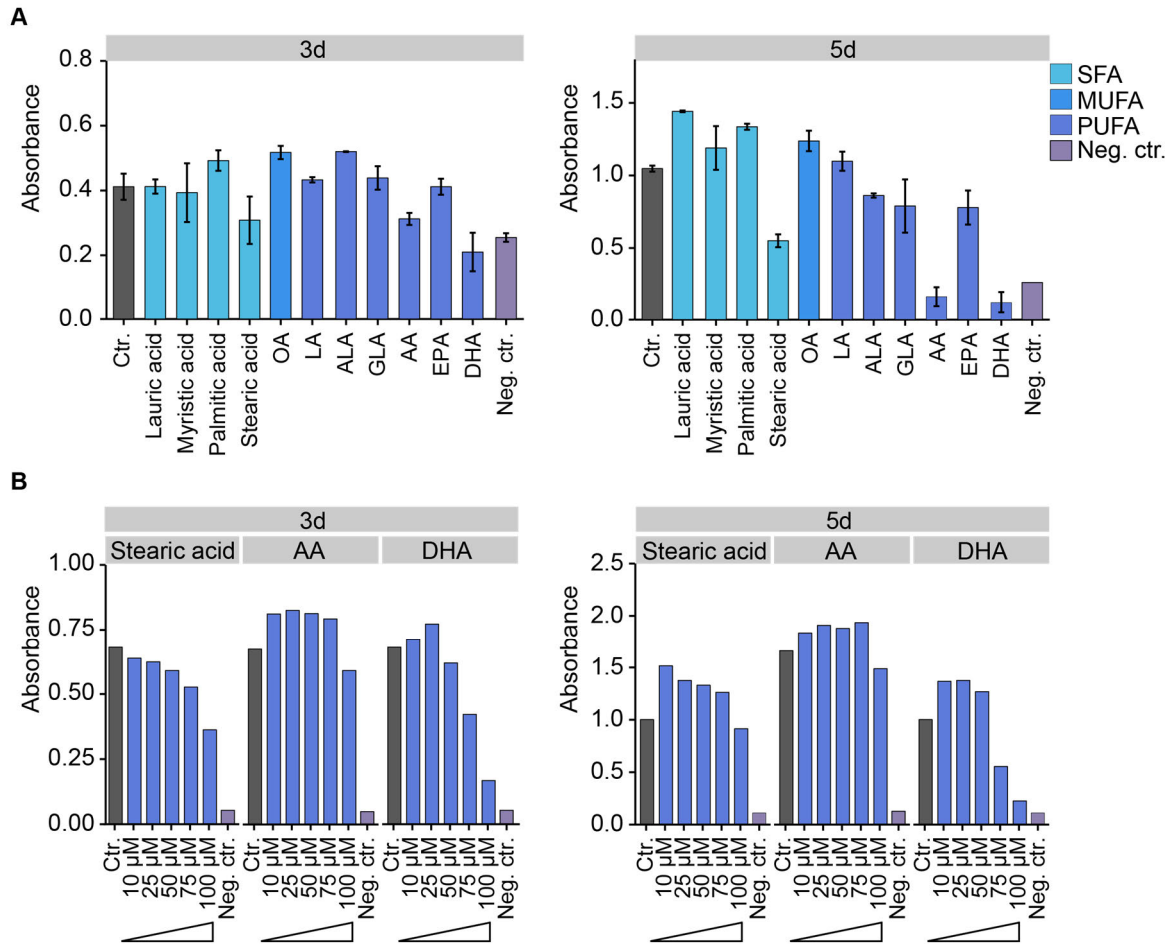


Figure 31: Cell viability after fatty acid treatment.

A) Huh7.5 cells were treated with 100 μM for 3 and 5 days and cell viability was analyzed with a CellTiter 96 AQueous One Solution assay (Promega) by measuring the absorbance at 490 nm. As negative control (neg. ctr.) cells were treated with 0.1 M H_2O_2 (mean \pm SEM; $n = 2$). B) Huh7.5 cells were treated with different concentrations of stearic acid, arachidonic acid, and docosahexaenoic acid for 3 and 5 days and analyzed as in A) ($n = 1$). Ctrl., mock-control; OA, oleic acid; LA, linoleic acid; ALA, α -linolenic acid; GLA, γ -linolenic acid; AA, arachidonic acid; EPA, eicosapentaenoic acid; DHA, docosahexaenoic acid; SFA, saturated fatty acid; MUFA, monounsaturated fatty acid; PUFA, polyunsaturated fatty acid.

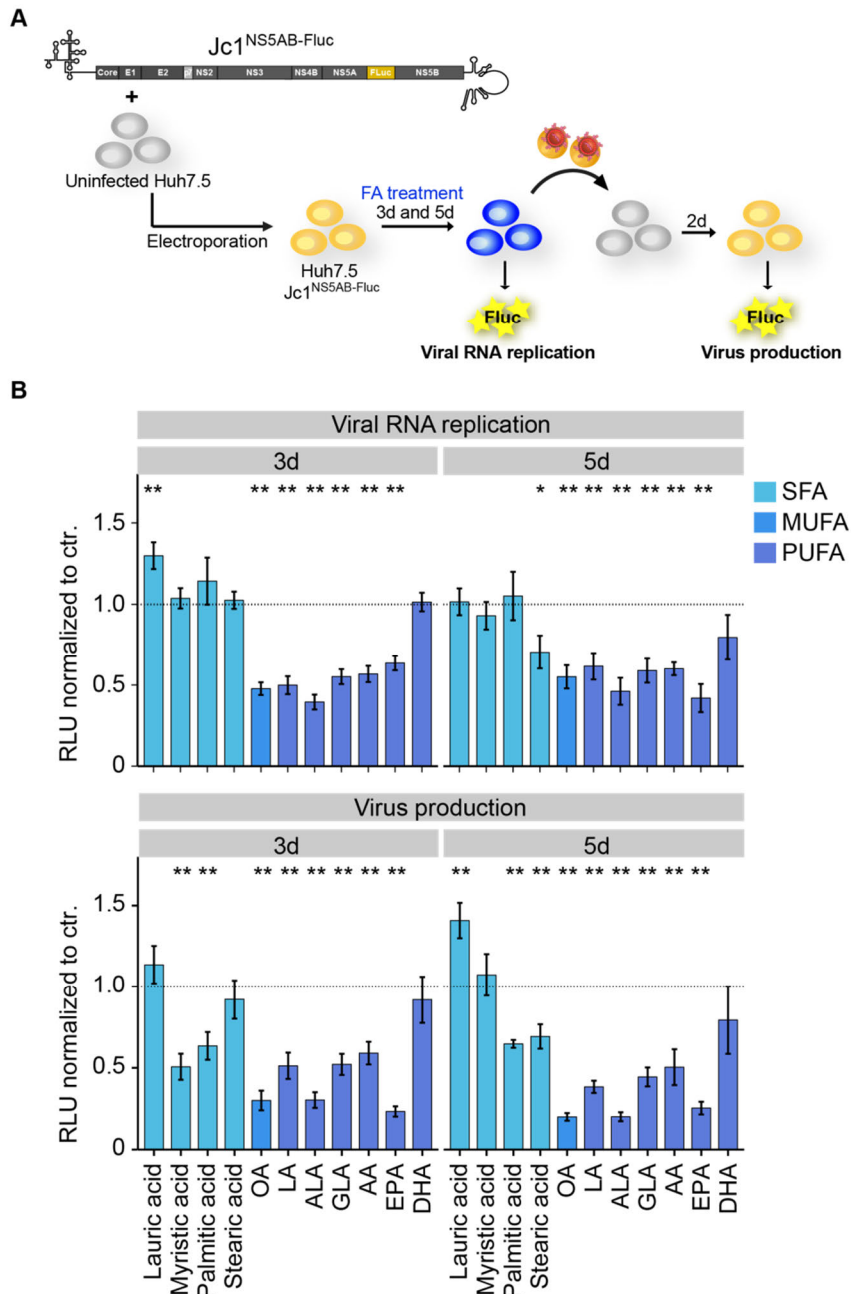


Figure 32: Analysis of viral replication after fatty acid treatment.

A) Huh7.5 cells were electroporated with Jc1^{NS5AB-Fluc} and 4 h after electroporation the cells were treated with fatty acids for 3 and 5 days (d). At both time points the cells were lysed to study viral replication. To study virus production the supernatants were transferred to uninfected Huh7.5 cells, the medium was changed 3 h after infection and cells were incubated for 2 days before cell lysis. B) The luciferase assay was carried out with 100 μ M fatty acid, except for arachidonic acid which was used in a concentration of 50 μ M and stearic acid and docosahexaenoic acid which were used in a concentration of 10 μ M. Results are shown as relative light units (RLU) normalized to mock-control (albumin-control), as fatty acids are complexed to albumin for cellular uptake ($n \geq 6$; mean \pm SEM; * $p < 0.05$, ** $p < 0.01$). OA, oleic acid; LA, linoleic acid; ALA, α -linolenic acid; GLA, γ -linolenic acid; AA, arachidonic acid; EPA, eicosapentaenoic acid; DHA, docosahexaenoic acid; SFA, saturated fatty acid; MUFA, monounsaturated fatty acid; PUFA, polyunsaturated fatty acid.

2.5.4. Lauric acid has no impact on HCV particle density

Lauric acid was the only fatty acid that increased virus production in the luciferase assay. This observation might be caused by a shift in the virus particle density, as particles with a lower density have a higher infectivity (Hijikata et al., 1993). Therefore, Huh7.5 cells were infected with Jc1^{NS5AB-EGFP} or Jc1^{p7-Gluc-2A} for 4–16 days and treated with 100 μ M lauric acid or mock-treated for 5 days. After subjecting the supernatants to density gradient ultracentrifugation, the fractions were analyzed for HCV RNA copy numbers and infectivity (Figure 33 A). Both parameters revealed a similar density distribution of particles produced by lauric acid treated cells and mock-control cells (Figure 33 B).

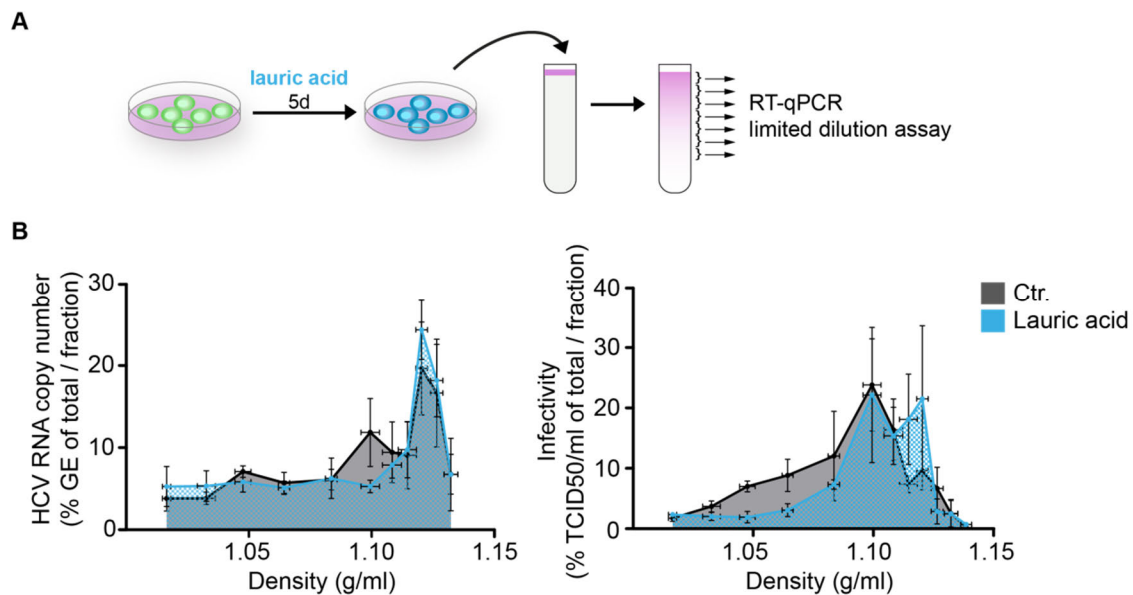


Figure 33: Density distribution of viral particles after lauric acid treatment.

A) Huh7.5 Jc1^{NS5AB-EGFP} or Jc1^{p7-Gluc-2A}-infected cells at 4–16 days post infection were treated with 100 μ M lauric acid or as mock-control (ctr.) for 5 days. Supernatants were subjected to an iodixanol density gradient ultracentrifugation and fractions were analyzed for the viral titer (TCID50/ml) and HCV RNA copy numbers. RNA copy numbers were determined by RT-qPCR and viral titer by limited dilution assay. B) Shown are the distributions of HCV RNA copy number and the viral titer (TCID50/ml) according to the density of the fraction (mean \pm SD; n = 4).

2.5.5. Polyunsaturated fatty acids cause alterations of the membranous web in HCV-infected cells

Mono- and polyunsaturated fatty acids caused a decrease in viral RNA replication (Figure 32). HCV RNA replication takes place in the membranous web, a structure consisting of double- (DMVs) and multi-membrane vesicles (MMVs) (Romero-Brey et al., 2012). Changes in the fatty acid composition by mono- and polyunsaturated fatty acid supplementation may cause an alteration of these membrane structures. To test this, Huh7.5 cells were infected with Jc1^{NS5AB-EGFP} and treated with oleic acid, linoleic acid, and α -linolenic acid for 3 days, fixed and subjected to transmission electron microscopy (TEM). The control cells nicely formed double- and multi-membrane vesicles upon Jc1^{NS5AB-EGFP}-infection (Figure 34).

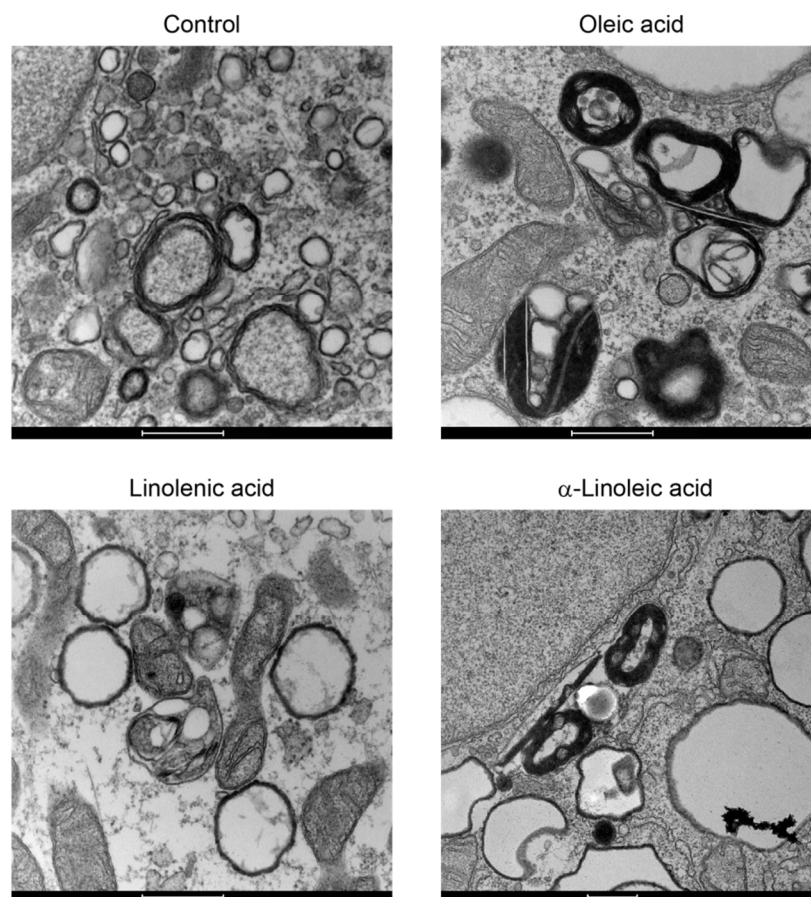


Figure 34: Transmission electron microscopy was used to study the membranous web after fatty acid treatment.

Huh7.5 cells were stably transduced with RFP-NLS-IPS to monitor viral infection and infected with Jc1^{NS5AB-EGFP} for 2 days. Afterwards cells were seeded into IBIDI dishes and treated with oleic acid, linoleic acid, α -linolenic acid, or albumin as control (Ctr.) for 3 days. The cells were analyzed by transmission electron microscopy (performed by Valerie Mordhorst). Scale bars 500 nm.

Cells treated with oleic acid still harbored membrane vesicles, but those were surrounded by a large amount of membranes. After the treatment with linoleic acid, the cells revealed no membranous web, as shown in the control sample, but displayed unusual membrane structures. Additionally, after α -linolenic acid treatment the membranous web did not form correctly and multi-membrane vesicles with a high amount of membranes occurred.

2.6. Fatty acid elongation and desaturation is necessary for viral replication

As described above, HCV infection elevated the amount of the polyunsaturated fatty acids arachidonic acid, eicosapentaenoic acid, and docosahexaenoic acid. Furthermore, a higher abundance of lipid species with longer fatty acyl chains was observed in HCV-infected cells (see 2.1.3.). These observations could be caused by an increase in fatty acid elongation and desaturation. Fatty acid elongation and desaturation occur in alternating steps. Elongases extend the fatty acid chain by two carbon atoms, while desaturases introduce double bonds (Ridgway ed., 2015).

2.6.1. Fatty acid elongases and desaturases are differentially expressed in HCV-infected cells

Fatty acid elongation and desaturation are controlled by the mRNA expression levels of the elongases and desaturases (Wang et al., 2006). To test if HCV infection alters the expression levels, RNA samples extracted in parallel to the lipidomic experiment were subjected to RT-qPCR and analyzed for the expression of all known desaturases and elongases. First, the dCT was determined in the uninfected control cells to evaluate the expression level of the different enzymes in hepatoma cells (Figure 35 A). Elongases and desaturases differed in their expression level. *SCD* is highly expressed, followed by *FADS2*. The lowest expressed enzymes are *ELOVL3*, *ELOVL4*, and *FADS6*.

Next, the differences in the mRNA expression upon HCV infection were calculated using the $2^{-\Delta\Delta CT}$ method (Figure 35 B). The elongases *ELOVL4*, *ELOVL7*, and desaturases *SCD5*, *FADS3*, and *FADS6* were increased upon HCV infection. This increase was only significant in the case of *FADS6*. In contrast, the expression of *ELOVL2* and *ELOVL3* was significantly reduced. The expression of all other elongases and desaturases remained unchanged.

The lyso-phosphatidylcholine acyltransferase 3 (*LPCAT3*) is an acyltransferase that plays a role in phosphatidylcholine synthesis by transferring preferentially unsaturated fatty acyl chains to lysophosphatidylcholine (LPC) (Zhao et al., 2008). In this analysis, *LPCAT3* mRNA expression seemed to be slightly but not significantly reduced in HCV-infected cells.

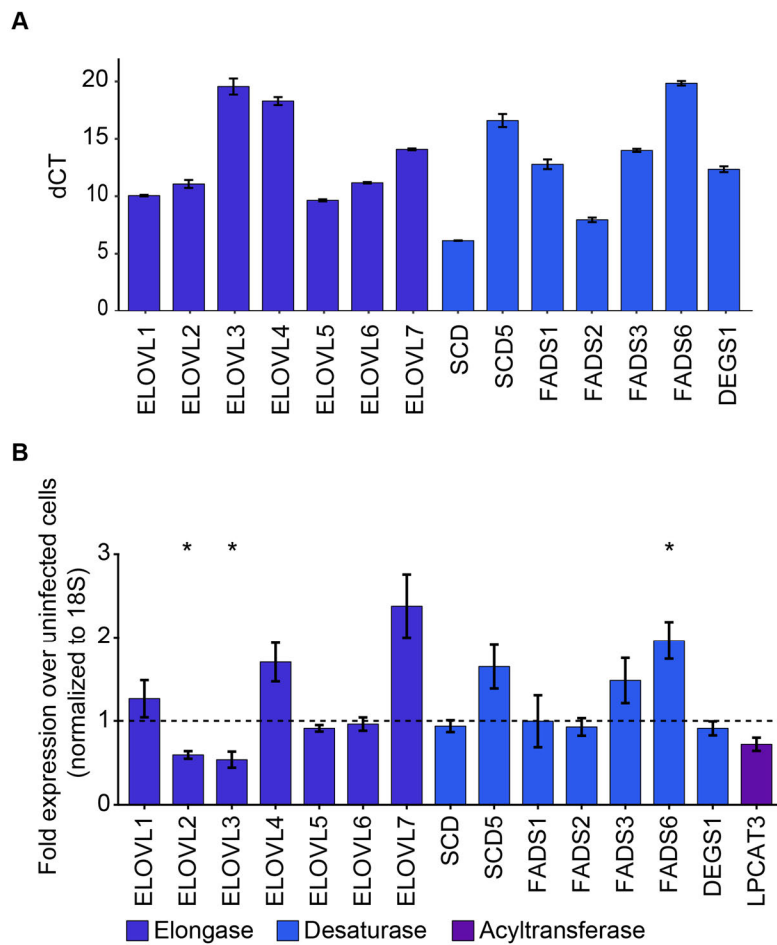


Figure 35: HCV infection changes the expression of enzymes involved in fatty acid elongation and desaturation and lipid remodeling.

RNA samples were generated in parallel to whole cell samples from the lipidomic analysis. A) Shown are dCT levels of elongases and desaturases in uninfected Huh7.5 cells. dCT values were calculated by subtracting the 18S rRNA CT values from the corresponding enzyme CT values (mean \pm SEM; n = 3). B) RT-qPCR analysis of desaturases, elongases, and the LPCAT3 acyltransferase in uninfected and Jc1^{Flag-E2 NS5AB-EGFP}-infected Huh7.5 cells. Shown is the fold expression of Jc1^{Flag-E2 NS5AB-EGFP}-infected over uninfected cells normalized to 18S rRNA (mean \pm SEM; n = 3; * p < 0.05). RT-qPCR data partially contributed by Christina Scherer and Pavel Truschow.

2.6.2. Knockdown of elongases and desaturases has diverging effects on the HCV life cycle

A potential role of elongases and desaturases in the HCV life cycle was further investigated with knockdown experiments. Therefore, shRNAs targeting various elongases (ELOVL2, ELOVL4, ELOVL5, ELOVL6, and ELOVL7) and desaturases (SCD, SCD5, FADS2, FADS3, and FADS6) were cloned into a lentiviral vector to perform stable transduction of Huh7.5 cells. Knockdown-efficiency and survival of the cells after transduction have been demonstrated previously (Scherer, unpublished data). ELOVL1, ELOVL3, FADS1 and DEGS1 could not further be evaluated due to impaired cell viability or an insufficient knockdown (Scherer, unpublished data). Huh7.5 cells were transduced with lentiviral constructs prior to infection with Jc1^{p7-Gluc-2A}. The *Gaussia* luciferase (Gluc) activity was measured at 1, 3, and 5 days post infection reflecting viral replication (rep). At 3 and 5 days post infection the supernatant of infected cells was transferred to naïve cells to analyze the virus production (pro) (Figure 36 A). Viral replication and virus production were not affected by shELOVL5, shSCD, and shFADS3. In contrast, a reduction of viral replication was significant for shELOVL2, shELOVL4, shELOVL6, shELOVL7, and shFADS6 at all time points. Despite a reduced viral replication, the virus production was not affected by shELOVL2, shELOVL4, shELOVL7, and shFADS6. The only enhancement on virus production was observed upon knockdown of ELOVL6, but the independent experiments exhibited strong variations. shSCD5 significantly reduced viral replication at the first two time points, but had no significant effect on virus production, although it seems to be slightly reduced at 3 days post infection. Furthermore, shFADS2 caused a significant decrease in viral replication after 1 day post infection, but had no effect on 3 and 5 days post infection. Interestingly, knockdown of FADS2 significantly decreased virus production at 5 days post infection (Figure 36 B).

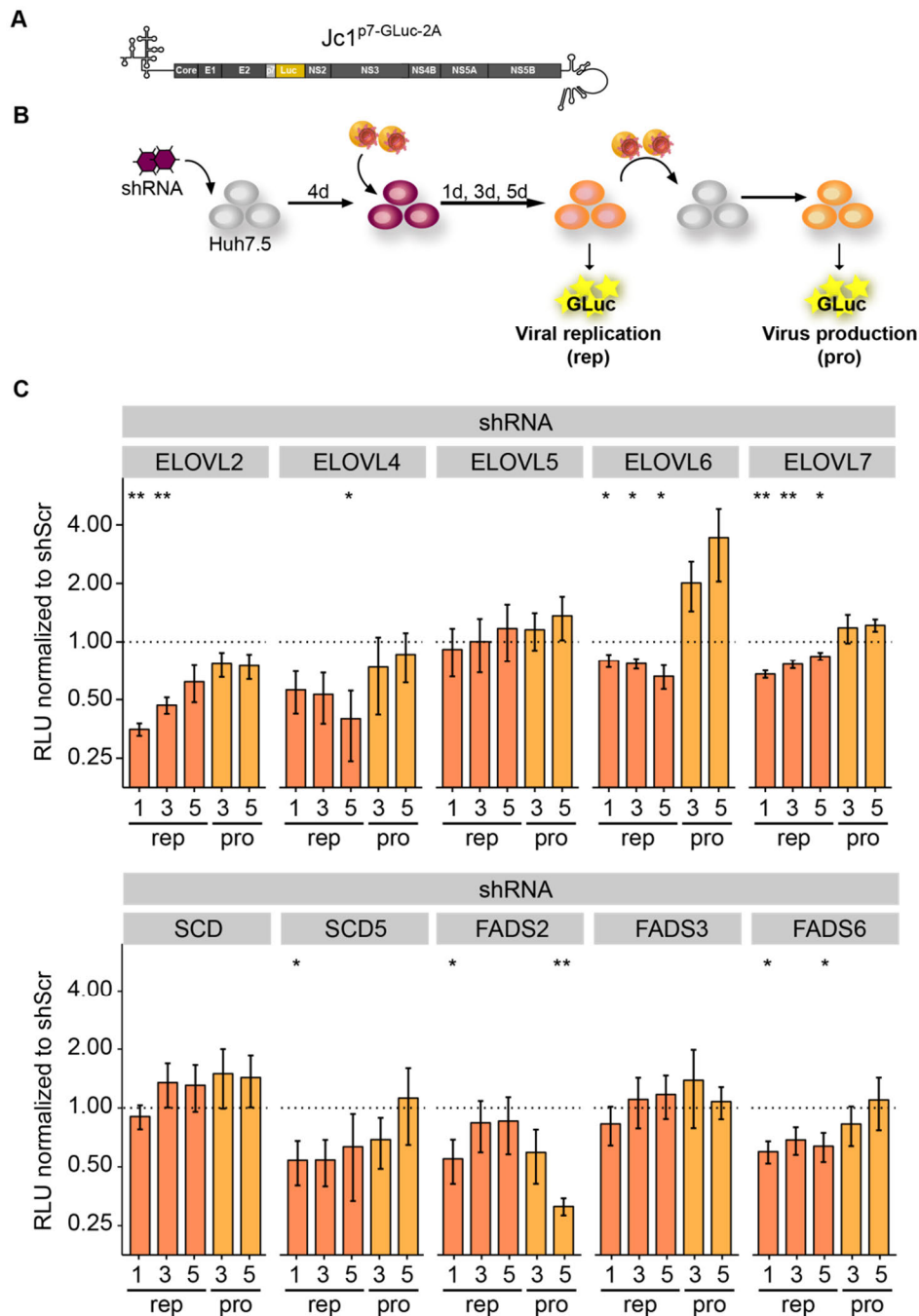


Figure 36: HCV replication after knockdown of different elongases and desaturases.

A) Luciferase assays were performed with Jc1^{p7-Gluc-2A}, a reporter virus carrying the *Gaussia* luciferase after the p7 cleavage site followed by a 2A sequence (Marukian et al., 2008). B) Huh7.5 cells were transduced with lentivirus containing shRNA constructs to target elongases and desaturases. 4 days after transduction cells were infected with Jc1^{p7-Gluc-2A} with an MOI of 0.5 and samples were taken at 1, 3, and 5 days post infection to measure viral replication (rep). At 3 and 5 days post infection, the supernatants of infected cells were transferred to naïve Huh7.5 cells and 2 days afterwards samples were taken to analyze virus production (pro). C) Shown are RLU normalized to scramble control (shScr) (mean \pm SEM; n = 4; * p < 0.05, ** p < 0.01). Experiment was performed by Christina Scherer.

2.7. FADS2 inhibition impairs HCV replication

FADS2 encodes for the $\Delta 6$ -desaturase *FADS2*, the enzyme catalyzing the first step of the n3- and n6-polyunsaturated fatty acid synthesis pathway. Furthermore, *FADS2* desaturates palmitic acid and oleic acid (Ridgway ed., 2015). Only the knockdown of *FADS2* caused a decrease in virus production, suggesting a role in the late steps of the viral life cycle, which are not well understood to date. The specific *FADS2* inhibitor SC-26196 enabled the analysis of putative dose-dependent effects.

2.7.1. SC-26196 has no impact on cell viability and *FADS2* expression

First, the effect of SC-26196 treatment on cell viability and gene expression was assessed. Experiments were carried out for a maximum of 5 days treatment and even the highest SC-26196 concentration (4 μM) did not affect cell viability (Figure 37 A). It is known that metabolic pathways can underlie feedback control mechanisms (Stryer ed. and Tymoczko ed., 2003). Thus, it was evaluated whether the cell compensates the reduced *FADS2* activity upon SC-26196 treatment with an increased expression of *FADS2*. Therefore, Huh7.5 cells were treated with 0.1 μM or 4 μM SC-26196 for 1 day or 3 days, and RNA was extracted and subjected to RT-qPCR. The treatment with SC-26196 only had a minor impact on the *FADS2* mRNA expression (Figure 37 B).

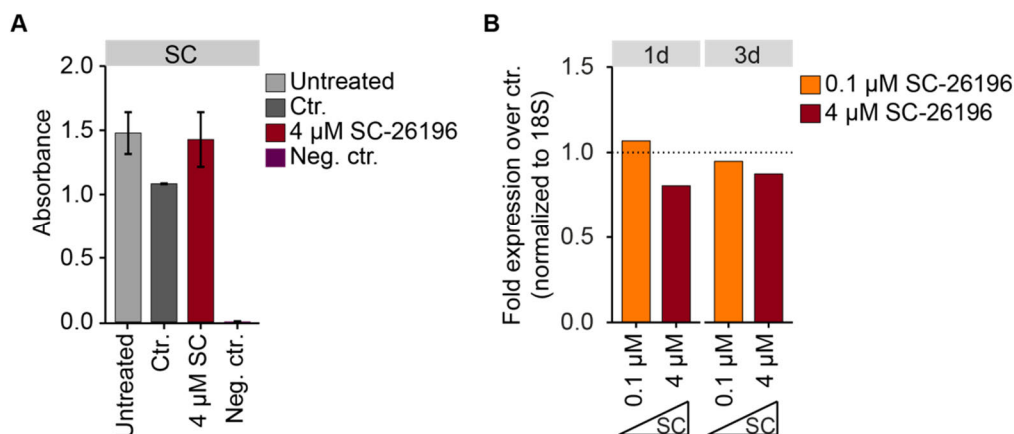


Figure 37: Viability assay and *FADS2* expression after SC-26196 treatment.

A) Cell viability was assessed with the CellTiter 96 AQueous One Solution assay (Promega) cell viability assay. Huh7.5 cells were untreated, treated as mock-control (ctr.), 4 μM SC-26196, or 5% DMSO (neg. ctr.) for 5 days (mean \pm SEM; n = 2). B) Huh7.5 cells were treated with 0.1 μM or 4 μM SC-26196 for 1 and 3 days and RNA was isolated and subjected to RT-qPCR. Shown is the fold expression of SC-26196-treated cells over mock-control normalized to 18S rRNA (n = 1).

2.7.2. FADS2 inhibition has diverging dose- and time-dependent effects on HCV infection

First, the impact of FADS2 inhibition with SC-26196 on early steps of the HCV life cycle, including entry and early replication, was assessed. This was studied by a pretreatment of Huh7.5 cells with different SC-26196 concentrations for 3 days or 1 day prior to infection with Jc1^{p7-Gluc-2A}. The *Gussia* luciferase activity was analyzed at 1 day post infection (Figure 38 A+B). The 0.1 μ M, 2 μ M, and 4 μ M SC-26196 concentrations exhibited diverging effects at the two different time points. FADS2 had no effect on virus replication after a 3 day pretreatment with 0.1 μ M and 2 μ M SC-26196. However, the highest SC-26196 concentration (4 μ M) slightly impaired HCV replication when cells were pretreated for 3 days. In contrast, the pretreatment for 1 day with 0.1 μ M and 2 μ M SC-26196 increased virus replication significantly, although to a lesser extent with the 2 μ M concentration. The 1 day pretreatment with 4 μ M SC-26196 slightly reduced viral replication, although not in a significant manner (Figure 38 B). These results indicate that short-term treatment with low concentration of the FADS2 inhibitor is proviral while longer treatment with higher concentrations is antiviral.

The effect on viral replication and virus production was further studied in a persistent infection in Huh7.5 cells infected with Jc1^{p7-Gluc-2A} for 8–18 days prior the experiment. The infected cells were treated with different SC-26196 concentrations for 1 day, 3 days, and 5 days. At the indicated time points, supernatants were used to infect naïve Huh7.5 cells to analyze virus production. Viral replication was affected by none of the treatment conditions. However, virus production was reduced with 4 μ M SC-26196 at 3 and 5 days post treatment and with 2 μ M SC-26196 at 5 days post treatment. The 0.1 μ M SC-26196 concentration had no effect on virus production (Figure 38 B).

A third approach was performed to analyze if the lower doses might cause an effect when Huh7.5 cells were treated shortly after electroporation with Jc1^{NS5AB-Fluc} RNA. This approach reflects an unestablished viral replication without confounding effects of virus entry. Treatment was started 4 h after electroporation and carried out for 3 and 5 days. In addition, virus production was analyzed at both time points (Figure 39 A). Here, viral replication was slightly reduced and this reduction was only significant after a 5 day treatment with 0.1 μ M SC-26196. Virus production was reduced for all treatment conditions, but not significantly due to the variations between the replicates (Figure 39 B).

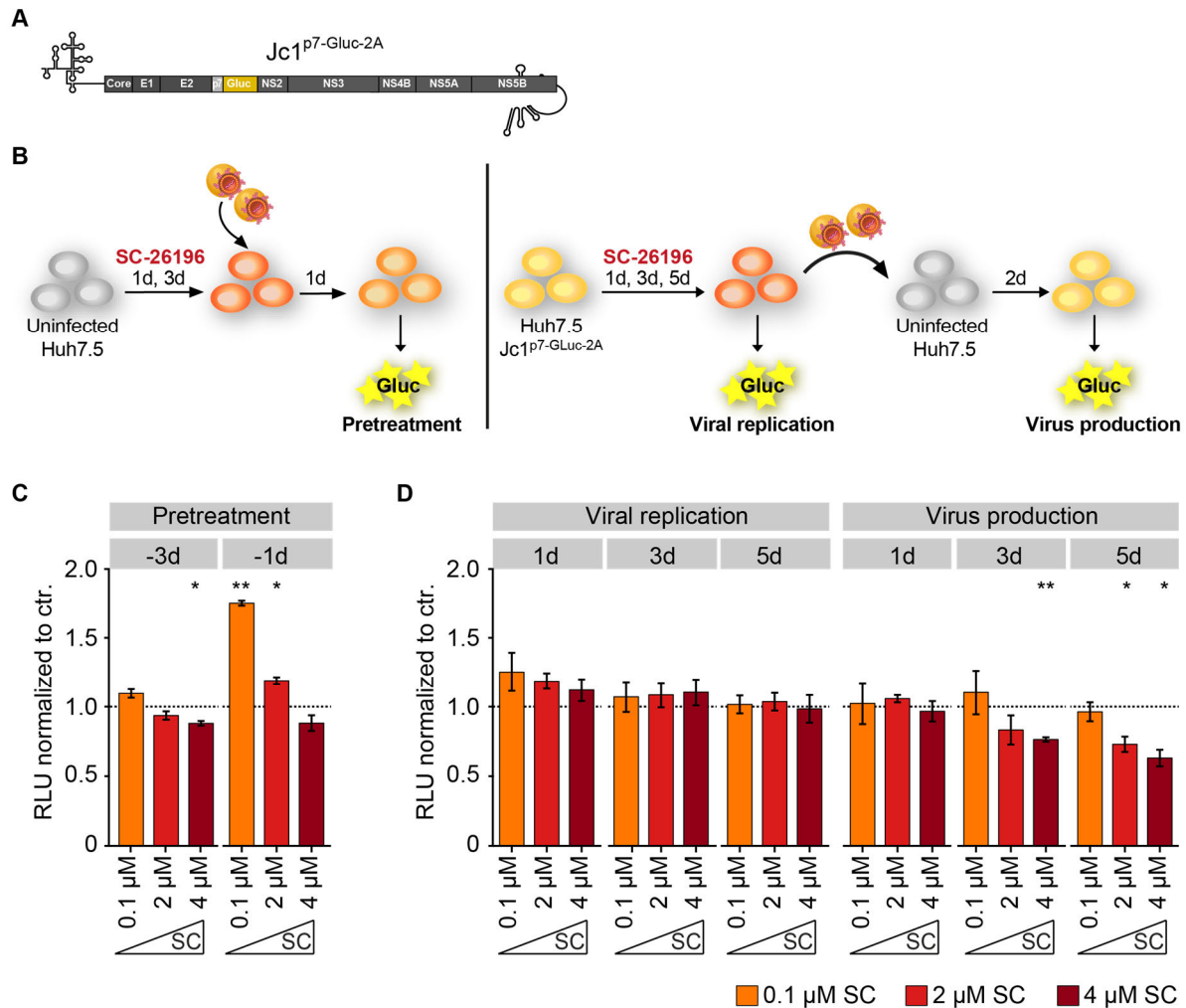


Figure 38: Evaluation of SC-26196 treatment on the HCV life cycle.

A) Luciferase assays were performed with Jc1^{p7-Gluc-2A}, a reporter virus carrying the *Gaussia* luciferase after the p7 cleavage site followed by a T2A sequence (Marukian et al., 2008). B) Huh7.5 cells were pretreated with different concentrations of SC-26196 for 1 or 3 days and infected with an MOI of 1 (1 day time point) or MOI of 0.5 (3 day time point) Jc1^{p7-Gluc-2A}. Samples were taken 1 day after infection. Viral replication and virus production were studied in Jc1^{p7-Gluc-2A}-infected Huh7.5 cells at 8–18 days post infection. Cells were treated with different concentrations of SC-26196 for 1 day, 3 days, and 5 days. Samples were taken at each time point reflecting viral replication, while supernatants were additionally transferred to uninfected Huh7.5 cells to study virus production. Results for C) pretreatment and D) viral replication and virus production are shown as relative light units (RLU) normalized to mock-control (mean ± SEM; n = 3–4; * p < 0.05, ** p < 0.01).

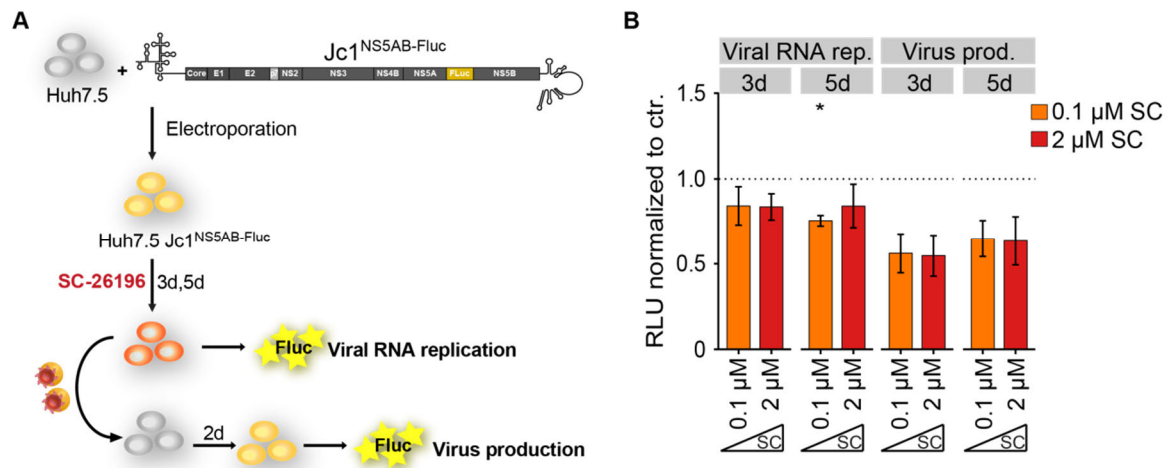


Figure 39: Analysis of HCV replication after early SC-26196 treatment.

A) Huh7.5 cells were electroporated with Jc1^{NS5AB-Fluc} and 4 h after electroporation the SC-26196 treatment was started and carried out for 3 and 5 days. At both time points samples were lysed to study viral RNA replication (viral RNA rep.) and supernatants transferred to naïve Huh7.5 cells to study virus production (virus prod.). B) Depicted are relative light units (RLU) normalized to mock-control (mean \pm SEM; n = 3; * p < 0.05).

2.7.3. FADS2 inhibition increases the surface expression of SR-BI

The previous observations have raised the question whether the increase in viral replication after the 1 day pretreatment with 0.1 μM SC-26196 was due to an increased virus entry. For this purpose, the cell surface expression of the HCV entry factors LDLR, CD81, and SR-BI after the SC-26196 treatment was analyzed. Huh7.5 cells were treated with 0.1 μM or 4 μM SC-26196 for 1 day and stained for the above-mentioned surface proteins and measured by flow cytometry (Figure 40 A). Both concentrations significantly increased the surface expression of SR-BI whereas no effect on CD81 and LDLR was observed (Figure 40 B).

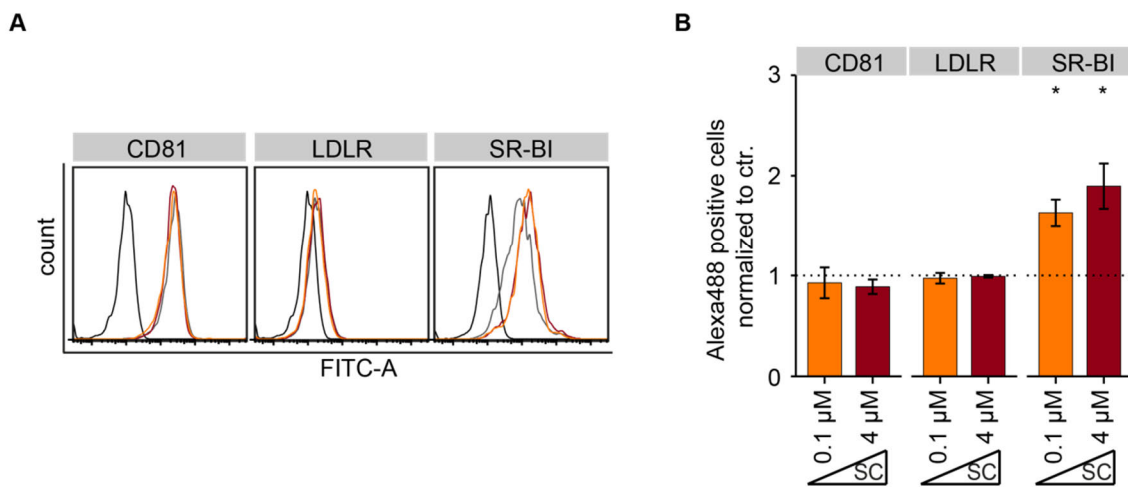


Figure 40: Surface expression of HCV entry factors after SC-26196 treatment.

Huh7.5 cells were treated with 0.1 μM or 4 μM SC-26196 for 1 day and stained for CD81, LDLR and SR-BI. Measurement was performed with flow cytometry. A) Exemplary histogram for CD81, LDLR and SR-BI. B) Results are shown as mean fluorescence fold over secondary antibody control and normalized to mock-control (mean \pm SEM; $n = 3-4$; * $p < 0.05$).

2.7.4. FADS2 inhibition has no impact on viral particle density

Next, it was assessed why treatment with 4 μM SC-26196 negatively affected later steps of the HCV life cycle. As noted above, 4 μM SC-26196 reduced virus production after 3 and 5 days treatment of HCV-infected cells. Impaired virus production can reflect a reduced virus particle production or an alteration in infectivity of the virus particle. The possibility of an altered infectivity was addressed in the following experiment. It has been shown previously that lipovirions of a higher density have a lower infectivity (Hijikata et al., 1993). To test whether the treatment with SC-26196 causes an alteration in the lipovirion density, Huh7.5 cells were infected with Jc1 and treated with 4 μM SC-26196 or DMSO as mock-control for 5 days. Supernatants were harvested, subjected to gradient ultracentrifugation,

and the viral RNA copy numbers and TCID₅₀/ml were determined per fraction (Figure 41 A). The RNA copy numbers peak at a similar density in SC-26196- and mock-treated cells. The peak of the SC-26196 samples compared to the controls is slightly smaller at 1.12 g/ml, while the peak at densities below 1.05 g/ml is slightly higher. However, as seen in the measurements of the TCID₅₀/ml, the RNA at densities below 1.05 is only minimally infectious. The infectivity distribution, measured as TCID₅₀/ml per fraction, revealed no striking differences between the SC-26196-treated sample and the mock-control. Only the infectivity at the lowest densities was higher in the SC-treated sample compared to the mock-control, but with strong variances (Figure 41 B).

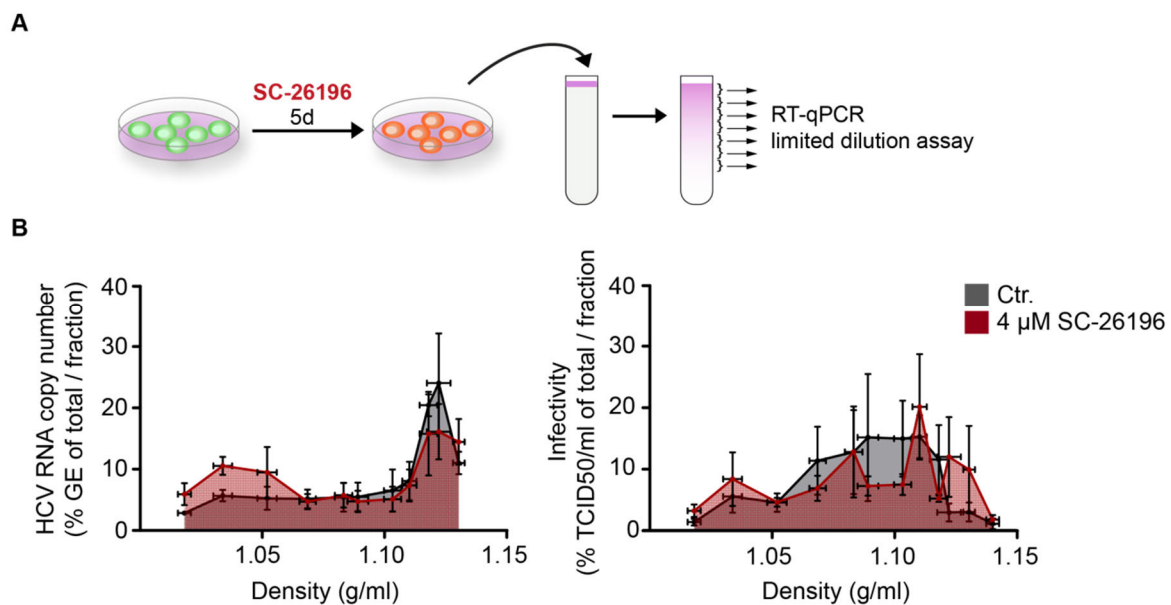


Figure 41: Analysis of viral particle density after SC-26196 treatment.

A) Huh7.5 Jc1^{NS5AB-EGFP-} or Jc1^{p7-Gluc-2A-}-infected cells at 4–16 days post infection were treated with 4 μM SC-26196 or as mock-control (ctr.) for 5 days. Supernatants were subjected to iodixanol density ultracentrifugation and fractions were analyzed for HCV RNA copy numbers and the viral titer (TCID₅₀/ml). RNA copy numbers were determined by RT-qPCR and viral titer by limited dilution assay. B) Shown are the distributions of HCV RNA copy number and the viral titer (TCID₅₀/ml) according to the density of the fraction (mean ± SD; n = 4).

2.7.5. FADS2 inhibition increases intracellular ApoE levels

The unaltered particle densities and infectivity raised the question if the secretion of viral particles is disturbed upon SC-26196 treatment. HCV is suggested to use the same secretion route as lipoproteins for cell exit and it was therefore investigated whether the treatment with SC-26196 causes decreased lipoprotein secretion in naïve Huh7.5 cells (Herker and Ott, 2011). The secretion of lipoproteins was measured by the amount of apolipoproteins in the supernatant. Intracellular and extracellular ApoE levels of uninfected Huh7.5 cells were measured upon a 3 day treatment with 0.1 μM or 4 μM SC-26196 by western blotting (Figure 42 A). The extracellular amount of ApoE was not altered, but the intracellular amount of ApoE increased significantly upon treatment with 4 μM SC-26196. The treatment with 0.1 μM SC-26196 had no effect on the intracellular ApoE level (Figure 42 B). Therefore, FADS2 inhibition affects the lipoprotein metabolism.

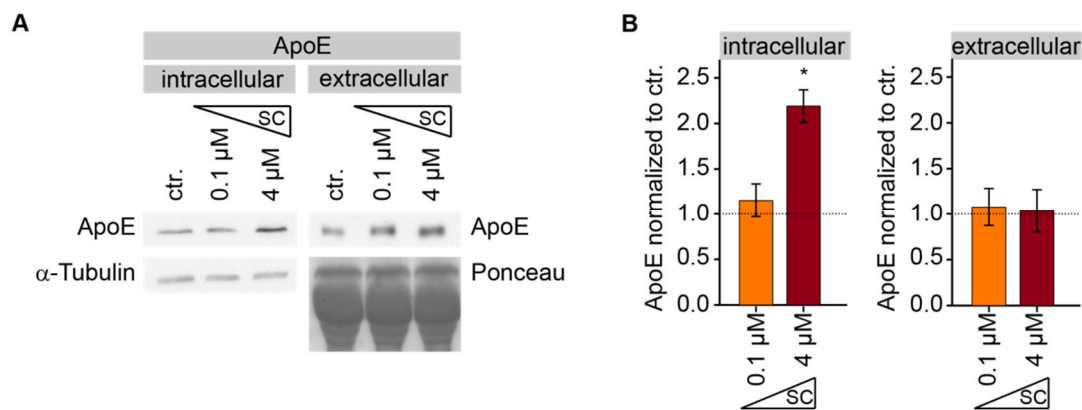


Figure 42: Secretion and intracellular amounts of ApoE.

Huh7.5 cells were treated with 0.1 μM and 4 μM SC-26196 or as mock-control (ctr.) for 3 days and supernatants and cell lysates were subjected to western blot analysis. A) Exemplary western blots from cell lysates (intracellular) and supernatants (extracellular) and α -tubulin or Ponceau S staining as loading control, respectively. B) Western blots were quantified by densitometric analysis with Fiji. Results are shown as ApoE normalized to mock-control (for supernatants) or ApoE fold over α -tubulin normalized to mock-control (intracellular) (mean \pm SEM; n = 3; * p < 0.05).

3. Discussion

3.1. HCV infection causes a higher abundance of lipids with longer fatty acyl chains in Huh7.5 cells

Lipidomics uses mass spectrometry to precisely determine lipid classes and their lipid species. This method enabled a detailed comparison between the lipid composition of HCV-infected and uninfected Huh7.5 cells. In addition, metabolomics provided data concerning lipids and amines. HCV-related lipidomic and metabolomic studies have been conducted before, but these studies concentrated on the early “acute” phase of infection from 1–3 days post infection (Diamond et al., 2010; Roe et al., 2011). This study focused on the long-term effect of “chronic/established” HCV infection. Therefore, the cells were infected for at least 6 days. An organelle doubtlessly connected with both, the host lipid metabolism and the HCV life cycle, are lipid droplets. Lipid droplets store lipids mainly as triglycerides and cholesteryl ester and HCV uses them as virus assembly platform. Whether the lipids stored in lipid droplets are required for this function is unknown (Lindenbach and Rice, 2013; Walther and Farese, 2012). By hijacking lipid droplets for its own purpose, HCV has been shown to alter the lipid droplet proteome. Several lipid modulating proteins were identified and most of them were reduced at lipid droplets from HCV-infected cells (Rosch et al., 2016). These observations make lipid droplets an interesting organelle for lipidomic studies. So far lipidomics of lipid droplets isolated from HCV genotype 2a- and 3a core overexpressing cells have been published, but without showing detailed profiles of lipid classes (Loizides-Mangold et al., 2014). A phospholipid profile of HCV genotype 2a core overexpressing Huh7 cells in the same publication has revealed either a slight increase or no change in the amount of several phosphatidylcholine species from PC[30:0] to PC[36:4]. This is in contrast to the observations made in this study, demonstrating differences between the core overexpression system and the fully replicating virus.

Before the samples were subjected to lipidomics they were analyzed for HCV-infection and comparability among the replicates. The whole cell extracts had similar protein quantities (Figure 17). Isolated lipid droplet fractions constantly contained less protein when isolated from HCV-infected cells compared to uninfected cells, while the post-nuclear supernatants were equal (Figure 27). This might be an HCV-induced phenotype either changing the protein/lipid ratio at lipid droplets or changing the environment such that proteins less likely co-fractionate. The lipidomic profile was generated by determining the mol% of each lipid species in a lipid class. This type of analysis excluded the impact of sample quantity differences.

The lipidomic analysis revealed an increased proportion of membrane lipids than neutral lipids in HCV-infected cells compared to uninfected cell. The higher demand in membrane lipids is most likely due to the formation of the membranous web for HCV RNA replication (Gosert et al., 2003; Romero-Brey et al., 2012). The main increase was observed for phosphatidylcholine, while the abundance of sphingomyelins was reduced in HCV-infected cells. The metabolomics measurement, by generating absolute concentrations, strengthened this observation by revealing that all measured sphingomyelin species were reduced. This result is in line with previous findings in acute infection. A decline of certain sphingomyelins has been described at 72 h post infection (Diamond et al., 2010). The authors suggested an increased conversion of sphingomyelins into ceramides or an incorporation of sphingomyelins into the viral particle (Diamond et al., 2010). The latter has been supported by lipidomic analysis of lipovirions: lipovirions have a higher amount of sphingomyelins than lipoproteins from uninfected cells (Merz et al., 2011). However, a detailed description of single sphingomyelin species in lipovirions is not available so far. Ceramides were not evaluated in this study. Therefore, no conclusion can be made whether the sphingomyelin production from ceramides is reduced or the reversed synthesis of ceramides from sphingomyelins increased. Alternatively, the decline in sphingomyelins might be connected to the increase in phosphatidylcholines. A higher demand in phosphatidylcholine may accompany a lower availability of phosphorylcholine as a sphingomyelin head group (Stryer ed. and Tymoczko ed., 2003).

As mentioned above, lipid droplets are mainly composed of neutral lipids. Thus, an alteration in the lipid droplet morphology and the total lipid droplet volume per cell reflects changes in the amount of neutral lipids. Neither the morphology of lipid droplets nor the number of lipid droplets per cell was altered in HCV-infected cells. Consequently the total lipid droplet volume per cell did not change (Figure 25). The occurrence of steatosis, a lipid accumulation in the cell, has been mainly described for HCV genotype 3 (Asselah et al., 2006). Here, the experiments were performed with HCV genotype 2a. Therefore, lipid droplet volumes may be unchanged due to the different genotype or due to full virus replication as most other studies were performed with core overexpression only. A study of genotype 3a core overexpressing cells has shown an increase in lipid droplet size caused by a higher amount of cholesteryl ester. The similar experiment in genotype 2a overexpressing cells has neither demonstrated any increase in the amount of cholesteryl ester nor in the amount of triglycerides (Loizides-Mangold et al., 2014). In this study, the total amount of cholesteryl ester was not determined, but the amount of triglycerides was similar in HCV-infected and uninfected cells (Figure 24). The latter correlates with unchanged lipid droplet morphology, at least for HCV genotype 2a-infected cells used in this study. However, lipid droplets smaller than $0.063 \mu\text{m}^3$ were excluded from the analysis because of resolution limitations of the microscope. Imaging with

a higher resolution is needed to evaluate smaller lipid droplets and to draw final conclusions concerning HCV-induced changes on the lipid droplet morphology. Although the total amount of triglycerides was not altered upon HCV infection, the detailed lipidomic analysis uncovered differences in triglyceride species. Triglycerides with shorter fatty acyl chains had a reduced abundance while triglycerides with longer fatty acyl chains had a higher abundance in whole cell extracts of HCV-infected cells. This effect was similar in isolated lipid droplets. Measuring similar triglyceride profiles from lipid droplets and whole cell extract was not surprising because most of the cellular triglycerides are found in lipid droplets. However, phosphatidylcholines that make up a low portion of the lipid droplets and a high portion in the whole cell extract also displayed highly comparable profiles in lipid droplets and whole cell extracts. Again, the same trend was observed: HCV-infected cells had a lower abundance of phosphatidylcholines with shorter fatty acyl chains and a higher abundance of phosphatidylcholines with longer fatty acyl chains compared to uninfected cells. This clearly shows that lipid droplets are not metabolically isolated in regard to their lipid composition when cells are infected with HCV. But it also raises the question where the changes occur first. If the lipid composition of lipid droplets changes, it will consequently affect other cellular compartments that receive lipids generated from the lipid depot of the lipid droplets. Alternatively, if *de novo* lipid synthesis is already affected, it will cause changes in the whole cell and this consequently includes lipid droplets. Therefore, the question whether the high demand in membrane lipids, especially phosphatidylcholines, is covered by *de novo* synthesis or by the remodeling of triglycerides from the lipid droplet pool needs to be elucidated in the future. The relation between diglycerides, triglycerides, and phosphatidylcholines becomes clear by comparing the profiles. Nearly all lipids with fatty acyl chains shorter than TAG[52:3], DAG[36:2], and PC[36:2] had a lower abundance in infected cells, while those with longer fatty acyl chains had a constantly higher abundance. Although the single fatty acyl residues were not exactly determined, the total carbon number and amount of double bonds in DAG[36:2] and PC[36:2] suggests similar fatty acyl chain combinations. The connection between these three lipid classes is probably due to the related synthesis of diglycerides, triglycerides, and phosphatidylcholines. The connection of the synthesis pathways might also be the reason why the less related sphingomyelins and cholesteryl ester are affected in a different manner. Incidentally, amongst the phosphatidylcholines with shorter fatty acyl chains the abundance of PC[32:0] was increased in lipid droplets and whole cell extracts as well as in the metabolomics approach. This effect was detected by lipidomics and metabolomics of whole cell extracts as well as by lipidomics of lipid droplets. But for all conclusions drawn from the metabolomics in this study, it needs to be considered that only one experiment was performed so far and repetition is needed. As mentioned above, there is a relation between the effects on diglycerides and phosphatidylcholines. However, the

diglyceride with potentially matching fatty acyl chains, DAG[32:0], is reduced in samples from infected cells, in line with other diglycerides harboring similar fatty acyl chain length. This suggests a special role for PC[32:0].

The shift between a lower and higher abundance of certain lipids in HCV-infected cells was dependent on the total fatty acyl chain length but independent from the degree of desaturation. Different metabolic changes may cause this shift in the fatty acyl chain length of lipids in HCV-infected cells. A higher abundance of lipids with longer fatty acyl chains can result from an induced selective lipolysis of lipids with shorter fatty acyl chains. Lipolysis is the dissection of lipids into their backbone and free fatty acids. Lipolysis displays substrate specificities. An *in vitro* study with the murine adipose triglyceride lipase (ATGL) has revealed that triglycerides with C16:1 fatty acyl chains are more prone to degradation than C18:1 showing a dependency of chain length (Eichmann et al., 2012). As mentioned above, lipids are also remodeled and this occurs with substrate preferences. For example, lysophosphatidylacyltransferases (LPCAT) introduce fatty acyl chains to the sn-2 position of phosphatidylcholine upon the removal of the fatty acyl chain by a phospholipid lipase. LPCAT3 has the highest activity for linoleic acid (C18:2). However, the *LPCAT3* expression was slightly decreased in this experiment, rather suggesting a slightly reduced lipid modulation in HCV-infected cells by LPCAT3 (Figure 35). Alternatively, the incorporation of long chain fatty acids into diglycerides, triglycerides, and phosphatidylcholines may occur in HCV-infected cells to a higher extent. This can be due to a higher availability of long chain free fatty acids or a lower availability of short chain fatty acids in HCV-infected cells. An increase in the very long chain polyunsaturated free fatty acids arachidonic acid, eicosapentaenoic acid, and docosahexaenoic acid was observed by lipidomics of whole cell extracts from HCV-infected cells. Unfortunately, due to technical issues other free fatty acids were not measurable. Therefore, it is not possible to conclude whether only distinct free fatty acids or all free fatty acids are enriched from this experiment. Two earlier studies have described an impact of HCV infection on free fatty acids but with diverging observations. In one study, the free fatty acids from C10:0 to C14:0 have been increased while longer chain free fatty acids have been unaffected in a significant manner. This study has been performed at early time points of infection (Roe et al., 2011). The second study has focused on a later time point of infection (10 days post infection) and palmitic acid (C16:0) and all fatty acids larger than C16:0 have been increased but myristic acid has remained unaffected (Douglas et al., 2016). Of note, amongst them have been the n3 and n6 polyunsaturated fatty acids arachidonic acid and docosahexaenoic acid. The contrary results of these two studies might be due to a short term versus a long term infection. The finding of an increased amount of arachidonic acid and docosahexaenoic acid upon a long term infection of 10 days is in line with findings from this study. Therefore, one may speculate that the longer fatty acids are

also increased in this set up. The availability of free fatty acids and the amount of certain lipid species comprising these fatty acids should be analyzed in parallel to draw final conclusions about their connection.

Arachidonic acid, eicosapentaenoic acid, and docosahexaenoic acid are the desaturation and elongation products of the essential fatty acids α -linolenic acid and linolenic acid. The human body is not capable of producing α -linolenic acid and linolenic acid. Both have to be provided by nutrition (Ridgway ed., 2015). Therefore, an increase in arachidonic acid, eicosapentaenoic acid, and docosahexaenoic acid may have different causes: an increased cellular uptake of free fatty acids, a decrease in their β -oxidation, or an increased breakdown of lipids containing these fatty acids as discussed above. An increased uptake might be facilitated by an overexpression of CD36, a protein that is involved in fatty acid transport (Koonen et al., 2007). Moreover, CD36 has been described as an HCV co-receptor and a higher expression of CD36 has been shown in patients infected with HCV genotype 1 (Cheng et al., 2016; Miquilena-Colina et al., 2011). Whether β -oxidation is increased or decreased in HCV-infection is still under debate. The metabolomics approach identified propionylcarnitine to be decreased upon HCV-infection. Propionylcarnitine is the esterification product of carnitine and propionyl-CoA (Ridgway ed., 2015). Propionyl-CoA originates from β -oxidation of uneven fatty acids and is a hint for an impaired β -oxidation. Propionyl-CoA is also produced during amino acid metabolism and several synthesis products of amino acids were reduced while the amino acids were increased in HCV-infected cells (Figure 22). Thus, the metabolomics study suggests a generally reduced cellular metabolism. In addition to an altered intensity of β -oxidation, there might be changes in the preference of fatty acids that are subjected to β -oxidation. β -Oxidation occurs in the mitochondria and peroxisomes and both of them have preferences towards fatty acids. Peroxisomes rather oxidize very-long-chain-fatty acids and are exclusively responsible for oxidization of the fatty acids C24:0 and C26:0, while short-chain fatty acids are only oxidized by mitochondria (Alexson and Cannon, 1984; Wanders et al., 2010). However, whether there is an alteration in the contribution of peroxisomal and mitochondrial β -oxidation due to HCV infection has to be further elucidated.

In summary, these experiments showed the capacity of HCV to modulate the host cellular lipid composition. Future experiments need to clarify the mechanisms behind these observations.

3.2. Fatty acid incorporation is comparable in HCV-infected and uninfected cells upon prolonged fatty acid treatment

As discussed above, the higher abundance of triglycerides with longer fatty acid chains may underlie certain preferences in the triglyceride synthesis. Therefore, the induction of triglyceride production was analyzed for different fatty acids in HCV-infected and uninfected cells. Fatty acid supplementation induced the production of triglycerides but not for all fatty acids in a similar manner. The triglyceride amount increases constantly with increasing chain length from lauric acid (C12:0) to oleic acid (C18:1) and linoleic acid (C18:2n6). Afterwards, the induction of triglyceride production decreased with increasing fatty acid chain length (Figure 30). Therefore, oleic acid and linoleic acid are preferentially incorporated into triglycerides. The fact that the other fatty acids have a lower capacity to increase the amount of triglycerides might be due to their incorporation into other lipid classes or their degradation by β -oxidation. Also, the uptake rate may differ and has to be taken into account. Lauric acid only caused a slight increase in the triglyceride levels. Lauric acid is known for rapid degradation via β -oxidation and subsequently a lower incorporation into lipids (Christensen et al., 1989). This indicates that β -oxidation for the short fatty acid lauric acid is functional in HCV-infected cells. Differences between triglyceride levels in HCV-infected and uninfected cells were only observable upon treatment with oleic acid and linoleic acid. However, variances of the single experiments are high in the infected samples. Therefore, further experiments with more sensitive methods would be required for confirmation. Altogether, the triglyceride production was similar in HCV-infected and uninfected cells, suggesting no striking changes regarding substrate specificities in triglyceride synthesis upon fatty acid treatment. But, of note, this assay was performed with an excess of fatty acids in the culture medium that might also skew the results. Thus, it is still possible that the uptake and incorporation of fatty acids into triglycerides is manipulated by HCV. As fatty acid uptake and incorporation is a rapid process this experiment should be repeated with time points earlier than 24 h (Bruce and Salter, 1996).

3.3. Fatty acids have diverse effects on viral replication depending on chain length and desaturation

An earlier study has described an impact of fatty acid supplementation on viral RNA replication in cells harboring an HCV replicon. In this case mono- and polyunsaturated fatty acids reduced viral RNA replication, while saturated fatty acids promoted viral RNA replication (Kapadia and Chisari, 2005). As described above, fatty acid supplementation mainly increases the amount of triglycerides and consequently this has been shown to affect lipid droplet morphology (Klabes, unpublished data). In turn, alterations of lipid droplet

morphology may impair virus production. Thus, new insights might be provided by studying the impact of fatty acids on a full replicating virus.

Electroporating the viral RNA into the cells enables the analysis of viral RNA replication and virus production is measured by infecting naïve cells with their supernatant (Figure 32 A). However, the electroporation rate was not determined and viral spreading cannot be completely excluded but should account for a rather low proportion of the measured effect. Lauric acid treatment had a unique effect as it was the only fatty acid that increased viral replication. At 3 days post electroporation, lauric acid might be beneficial during the establishment of the membranous web and thereby promoting viral RNA replication, but without affecting virus production. While on day 5 post infection lauric acid supplementation is rather beneficial for the later steps of the HCV life cycle, such as assembly and release. As mentioned previously, lauric acid is known for a rapid β -oxidation and thereby provides energy (Christensen et al., 1989). Therefore, lauric acid might be used as an energy source for viral replication. The switch from promoting viral RNA replication to promoting virus production may reflect the more important step in the viral life cycle at the corresponding time point. Further experiments did not reveal any changes of the particle density upon lauric acid treatment that would cause a higher specific infectivity, which would subsequently be measurable as increased virus production in the luciferase assay. It has been shown that a lower viral particle density corresponds to a higher infectivity (Hijikata et al., 1993). Gradient ultracentrifugation resulted in a similar density profile of viral particles from lauric acid-treated or untreated cells. The infectivity in lauric acid-treated cells additionally peaked at a slightly lower density, which would even indicate a decreased infectivity but certainly no increase in infectivity. Myristic acid and palmitic acid had no effect on viral replication but slightly decreased virus production at least at one time point. Here, further experiments should elucidate whether they impair viral assembly, release, or specific infectivity. Stearic acid significantly impaired viral replication and virus production at day 5 post treatment. Stearic acid may have an effect on its own but it can also be converted into oleic acid by SCD and SCD5 and, thus, may result in an effect comparable to oleic acid. The prolonged time that is needed until it showed an effect might be due to the reduced concentration that was used to assure cell viability. A reduction in viral replication and virus production was observed for oleic acid and all polyunsaturated fatty acids, except for docosahexaenoic acid. However, docosahexanoic acid might not have had an impact at the low dose that was used due to toxicity. The reduction in viral RNA replication upon polyunsaturated fatty acid treatment has been demonstrated earlier. In contrast, oleic acid has been shown to promote viral RNA replication (Kapadia and Chisari, 2005). In their case the authors have used lower fatty acid concentrations. Furthermore, the genotype and replication system has been different from this study. They have used a genotype 1a replicon and here a genotype 2a full

replicating virus was used. This eventually causes these contrary outcomes. A reduced viral RNA replication upon fatty acid treatment is most likely caused by an impaired membranous web formation. An unusual morphology of the membranous web was proven upon oleic acid, linoleic acid, and α -linolenic acid treatment by electron microscopy (Figure 34). Further fatty acids were not tested so far but comparable morphological changes are expectable. Especially oleic acid, α -linolenic acid, and eicosapentaenoic acid had an even stronger impact on virus production compared to viral RNA replication. Thus, they may have an additional negative effect on the later stages of the viral life cycle. In particular oleic acid and α -linolenic acid strongly elevated the amount of triglycerides, possibly affecting lipid droplets and thereby viral assembly. The reduction in viral replication upon the treatment with arachidonic acid and eicosapentaenoic acid seems to be contrary to the increased amount of these fatty acids induced by HCV-infection. The intracellular amount of arachidonic acid and eicosapentaenoic acid upon the treatment was not tested. But the supplementation was of a very high concentration, suggesting a much higher intracellular concentration of these fatty acids upon treatment than induced by HCV on its own. On the other hand, HCV might somehow influence the lipid synthesis to avoid the introduction of fatty acids into lipids that impair the viral life cycle.

3.4. Cholesterol plays a role in the HCV life cycle

Cholesterol is present in HCV RNA replication complexes and a dysfunctional cholesterol synthesis reduces viral replication (Aizaki et al., 2004; Amemiya et al., 2008; Saito et al., 2015). But not only an active cholesterol synthesis seems to be important: HCV also increases the intracellular cholesterol level (Roe et al., 2011). The measurement of cholesterol was not possible under the experimental conditions used in this study. Therefore, a fluorescent microscopic method has helped to study this important lipid class. Due to their morphology Huh7-lunet cells are more suitable for microscopy analysis than their related Huh7.5 cells and therefore served as host cell in this approach. When cells were stained with Fillipin III, it was visible that there was an accumulation of cholesterol in the perinuclear region in most of the HCV-infected cells. Indeed, the quantification confirmed this subjective observation (Figure 23). Due to the localization it can be speculated that the membranous web accounts for this increased amount of cholesterol in the perinuclear region. Correlative electron microscopy would be a great tool to map the Fillipin III staining from fluorescent confocal microscopy within the high resolution images generated by electron microscopy. So far, the role of cholesterol is mainly attributable to viral RNA replication (Aizaki et al., 2004; Amemiya et al., 2008; Saito et al., 2015). However, in this study cholesterol supplementation had a greater impact on virus production than on viral RNA replication (Figure 29). The

highest impact on virus production was the decrease obtained upon a 3-day cholesterol treatment, which was reversed to a promoted virus production upon a 5-day treatment. This diverging and in addition dose-dependent outcome might reflect the capability of the cells to adapt to treatment conditions. The cholesterol synthesis is a highly regulated process with a feedback mechanism that may lead to an inhibition of its own synthesis upon cholesterol treatment (DeBose-Boyd, 2008). However, an active cholesterol synthesis is required for viral replication (Aizaki et al., 2004; Amemiya et al., 2008; Saito et al., 2015). This might be one explanation for the slightly reduced viral RNA replication and the obviously reduced virus production on day 3 post treatment. Furthermore, the cell may respond to the cholesterol treatment by an increased cholesterol export, either by cholesterol efflux or via lipoproteins upon cholesterol esterification (Ridgway ed., 2015). HCV production may benefit from an increased lipoprotein secretion by presumably sharing similar secretion routes (Lindenbach and Rice, 2013). This might explain the increased virus production upon a 5 day cholesterol treatment. The role of the cholesterol efflux in HCV-replication in the background of cholesterol supplementation has not been elucidated so far. Not to forget, excess cholesterol can change the membrane composition and subsequently its properties and thereby affecting the HCV replication. Of course, several effects might go in line with each other. It should further be elucidated which impact the cholesterol treatment has on the expression of enzymes involved in *de novo* cholesterol synthesis. Furthermore, the intracellular and extracellular cholesterol and cholesteryl ester level upon treatment should be determined in a time-dependent manner to correlate the effects on viral replication with certain cholesterol concentrations. Finally, defining the extracellular amount of the apolipoproteins ApoE and ApoB may elucidate the impact of cholesterol in HCV particle production.

3.5. Fatty acid elongation and desaturation is important for HCV replication

As discussed above, one explanation for the relative increase of diglycerides, triglycerides, and phosphatidylcholines with longer fatty acid chains might be a higher availability of long chain fatty acids in HCV-infected cells. Fatty acid elongases elongate fatty acids by introducing two carbon atoms to the fatty acid chain (Ridgway ed., 2015). The role of elongases in HCV infection has not been investigated so far. Interestingly, the human cytomegalovirus (HCMV) has been shown to upregulate several elongases, especially ELOVL7, to produce very-long-chain fatty acids that are incorporated into its envelope (Koyuncu et al., 2013; Purdy et al., 2015).

First, the expression level of elongases and desaturases upon infection was determined (Figure 35 B). In the next step it was assessed whether these enzymes play a role in the viral life cycle (Figure 36). The elongases *ELOVL4* and *ELOVL7* were upregulated upon HCV-

infection. ELOVL4 elongates n3- and n6-polyunsaturated fatty acids, while ELOVL7 can additionally act in the elongation pathway of non-essential fatty acids (Figure 8, Figure 9). In fact, *ELOVL7* showed the highest increase in expression upon infection, as described previously for HCMV, although the induction by HCV was to a lesser extent. In contrast to HCMV, the virus production, which may reflect virus infectivity, was not decreased upon ELOVL7 knockdown. This suggests a role of ELOVL7 in a step prior to HCV virion production. Contrary results were obtained for ELOVL2. HCV infection reduced the *ELOVL2* expression and it could be assumed that in turn a knockdown of ELOVL2 is beneficial for HCV replication. Nonetheless, the knockdown of ELOVL2 had a negative impact on viral replication. This could be due to the fact that the knockdown reduced the *ELOVL2* expression by 80%, while the HCV-dependent reduction was only 30-45% (Scherer, unpublished data and Figure 35 B). Elongases are not exclusively responsible for one synthesis step and other elongases may compensate for the loss of ELOVL2 upon HCV infection. Interestingly, the ELOVL6 knockdown decreased viral replication but increased virus production. ELOVL6 plays a role in long-chain-fatty acid synthesis by elongating C12, C14, and C16 carbon fatty acids (Matsuzaka and Shimano, 2009). Its dual role in the viral life cycle should be further elucidated. The only knockdown without an effect was ELOVL5. ELOVL5 mainly acts in the polyunsaturated fatty acid synthesis pathway. However, it cannot be excluded that the knockdown efficiency is too low to have strong effects on lipid levels. ELOVL5 was well expressed in uninfected Huh7.5 cells but the knockdown has previously been shown to reduce the *ELOVL5*-expression by only 20–40% (Scherer, unpublished data). Overall, the knockdown experiment underlines the importance of fatty acid elongation for the HCV life cycle. As a result, fatty acid elongation, especially in regard to the elevated ELOVL7 mRNA expression, is a potential explanation for the increased abundance of longer fatty acyl chains in lipids upon HCV-infection. In addition, the knockdown experiments also suggest that the elongases are not able to fully compensate each other, although several elongases are described to have overlapping specificities.

The altered abundance of lipids in HCV-infected cells was mainly independent from the desaturation degree. As elongation and desaturation are consecutive processes, desaturases came into the focus of these investigations. As shown by the knockdown experiments, 3 out of 5 tested desaturases play a role in viral replication. FADS6 clearly reduced viral replication. Unfortunately, this enzyme is not well described so far making it difficult to draw any conclusion about its role in the HCV life cycle.

An active palmitic acid and stearic acid desaturation by SCD is necessary for a functional membranous web formation and subsequently for HCV replication (Lyn et al., 2014). Unexpectedly, the knockdown of SCD had no effect on viral replication or virus production in the luciferase assays. *SCD* was highly expressed in Huh7.5 cells. Therefore, it is not known

whether the SCD knockdown, despite a reduction of 60–80%, was strong enough to efficiently block this synthesis step (Scherer, unpublished data). SCD has an isoform, SCD5, catalyzing the same synthesis steps. In contrast to SCD, SCD5 is only low expressed in Huh7.5 cells. Nevertheless, SCD5 was upregulated in HCV-infected cells and its knockdown significantly decreased viral replication. In line with the first observation, a publication is describing an upregulation of SCD5 in liver samples from HCV patients (Wu et al., 2010). The decreased HCV replication indicates that SCD does not compensate for the loss of SCD5, although both catalyze the same synthesis step and the high expression of SCD would suggest a sufficient palmitoleic- and oleic acid production. In addition, different subcellular localizations of SCD and SCD5 might lead to distinct roles in cell physiology or HCV replication because the membrane composition is determined by the lipid synthesizing enzymes at first (van Meer et al., 2008). The effect of SCD5 on HCV replication might also be distinct from membrane modulation. The SCD and SCD5 desaturation product, palmitoleic acid, has been described as post-translational modification in murine cells (Takada et al., 2006). NS4B, an HCV protein which is important for membranous web formation, is known to be palmitoylated (Yu et al., 2006). However, their experiment does not exclude a modification by palmitoleic acid.

3.6. FADS2 has a dose- and time-dependent effect on the HCV life cycle

The knockdown experiments highlighted an interesting enzyme for further investigation: FADS2. Only the FADS2 knockdown decreased virus production without affecting viral replication at the corresponding time points (Figure 36 B). This suggests a function of FADS2 in the late steps of the HCV life cycle which are not well understood so far. FADS2 is a $\Delta 6$ -desaturase that converts α -linolenic acid to stearidonic acid and linoleic acid to γ -linolenic acid, which are the first steps in the n3 and n6 synthesis pathway. In addition, it desaturates palmitic acid and oleic acid (Ridgway ed., 2015). The availability of the specific FADS2 inhibitor SC-26196 enabled the analysis of dose-dependences (Harmon et al., 2003). The FADS2 inhibition was studied by approaches that differed in the timing of SC-26196 treatment and infection. This enabled the separation of entry and early replication, viral RNA replication, and virus production (Figure 38).

The pretreatment with SC-26196 followed by an infection and the measurement 1 day post infection mainly reflects the impact on virus entry and early replication steps. With 3 day SC-26106 pretreatment the virus entry and early replication was significantly reduced by the highest (4 μ M) SC-26196 dose. This result confirms the first time point of the FADS2-knockdown experiment. Both approaches are comparable insofar that the pretreatment with

SC-26196 was carried out for 3 days and the knockdown was induced 4 days before infection. In both approaches the viral replication was measured at 1 day post infection.

Next, the pretreatment was carried out for only 1 day before HCV-infection. The lowest (0.1 μM) SC-26196 dose increased entry and early replication and this effect is diminished dose dependently. This approach clearly showed the dose dependence of the treatment. The increased surface expression of the HCV-entry receptor SR-BI upon the 1 day SC-26196 treatment supports the hypothesis of an increased HCV entry. SR-BI was not only upregulated with the low (0.1 μM) SC-26196 concentration but also with the high (4 μM) SC-26196 concentration. This observation was surprising because the 1 day 4 μM SC-26196 pretreatment did not have any effect on viral replication. Therefore, this experiment suggests a bivalent role of the treatment with SC-26196 on the viral life cycle. On the one hand, the pretreatment with SC-26196 promotes viral replication most likely by virus attachment and entry. On the other hand, a subsequent step in the viral life cycle is inhibited as, for instance, endocytosis or viral RNA replication. The dose- and time-dependency of the SC-26196 pretreatment suggests that a certain lipid turnover needs to be fulfilled to induce the negative impact of the SC-26196 treatment on viral replication. Further, the results indicate that this negative effect counteracts the promoting effect on viral entry.

In addition, the impact of the FADS2 inhibition on viral replication and virus production was assessed. In this assay Huh7.5 cells with an established HCV replication were treated with SC-26196. Although the infection rate was not tested, an infection for 8–18 days should be sufficient for the virus to infect a high portion of cells. Assuming that most of the cells are HCV-positive, the measurement of viral replication mainly represents viral RNA replication and not virus production and entry due to spreading. In conclusion, viral RNA replication was not influenced by the FADS2 inhibition. The virus production was measured in parallel to viral replication. Therefore, the dose-dependent decrease in virus production at 3 and 5 days post treatment is caused by a late step in the viral life cycle, for example, assembly and release, and is not due to a previous decreased viral RNA replication. A reduced infectivity due to a higher lipovirion density was not observed in the density gradient centrifugation assay (Figure 41). This result should be verified with a more sensitive titer assay because of the overall strong variances between the replicates in this assay. However, the viral RNA distribution revealed that the major peak was slightly lower in SC-26196-treated samples compared to the control. In addition, SC-26196-treated samples had a higher peak at low densities, where particles are of low infectivity. This observation may have two causes. The lipovirions do not properly mature upon SC-26196 treatment. Alternatively, the amount of lipovirions secreted at low densities is similar in SC-26196 treated cells and the control, but the total amount of secreted lipovirions is less. Further experiments should be performed to compare the amount of secreted lipovirions between SC-26196 treated

cells and the untreated control. The virus secretion pathway is still under debate. One suggestion is the release via the lipoprotein secretion pathway through the Golgi (Lindenbach and Rice, 2013). Therefore, the question arises whether SC-26196 treatment has the capability to interrupt the lipoprotein secretion in uninfected Huh7.5 cells at the same time point and concentration when virus production was decreased. One determinant of lipoprotein secretion is the amount of apolipoproteins in the supernatant. In this study, the treatment with SC-26196 had no impact on the extracellular amount of ApoE, suggesting a functional lipoprotein secretion. Nevertheless, the increase in the intracellular ApoE level upon SC-26196 treatment still suggests a connection between lipoproteins and reduced virus production after FADS2 inhibition. Especially because the effective SC-26196 concentration on virus production and intracellular ApoE levels in uninfected cells was 4 μM and not 0.1 μM . Of note, ApoB levels were undeterminable in the supernatant. The ApoB antibody showed unspecific binding to lipoproteins present in the fetal calf serum in full growth medium. The attempt to culture the cells in OPTI-MEM resulted in a loss of cell growth upon treatment with 4 μM SC-26196 already at 24 h. This suggests that the cells rely almost exclusively on external lipid supplementation upon inhibition of FADS2, which made FCS containing full-medium necessary.

In a third approach an early SC-26196 treatment of HCV electroporated cells was investigated (Figure 39). This enabled the possibility of studying the impact of FADS2 inhibition on the establishment of a viral RNA replication compartment without a confounding impact of virus entry. In this case, the lower SC-26196 concentrations (0.1 μM and 2 μM) slightly impaired viral RNA replication and clearly reduced virus production. The slight reduction observed in viral RNA replication might result from spreading events due to an incomplete electroporated cell population. Thus, a replicon assay is needed to exclusively evaluate viral RNA replication. Nevertheless, the electroporation assay strengthens the importance of a functional desaturation by FADS2 for virus production, especially for the establishment of the viral infection.

Taken together, the treatment with the FADS2 inhibitor SC-26196 has a dose- and time-dependent effect on the viral life cycle. So far, the effects were linked to two proteins involved in the viral life cycle: the HCV entry receptor SR-BI and the apolipoprotein ApoE. Understanding the relation between FADS2 and SR-BI as well as ApoE will help to understand the role of FADS2 in the viral life cycle. SR-BI is a receptor for lipoproteins, mainly HDL, and functions in transport of cholesterol from peripheral tissues back to the liver (Grove et al., 2007; Rhainds and Brissette, 2004). A direct connection between FADS2 and SR-BI has not been described. Safflower oil, rich in linoleic acid, has been shown *in vivo* to increase the expression of hepatic SR-BI (Spady et al., 1999). Linoleic acid is the substrate of FADS2 and might be enriched upon FADS2 inhibition, pointing to a putative connection.

So far, a direct relation between FADS2 and ApoE has neither been described. In the future, the source of enriched ApoE should be elucidated to discriminate between newly synthesized ApoE and recycled ApoE obtained from lipoprotein uptake (Heeren et al., 2006). The increased surface expression of SR-BI and the increased amount of ApoE, both involved in lipid transport through lipoproteins, suggest that the cell tries to compensate the alterations in the lipid composition caused by the FADS2 inhibition and thereby affects the HCV life cycle.

3.7. Conclusion

This study illustrates that HCV replication relies on the host lipid metabolism and further elucidated cellular changes that are caused by HCV infection. HCV increased the proportion of cellular membrane lipids, most likely to cover its demand for the membranous web. Further, the infection drives the cell to change its lipid composition by decreasing the amount of lipids with shorter fatty acyl chains and increasing the amount of lipids with longer fatty acyl chains. However, it is unclear whether this is antiviral or beneficial for HCV to replicate. The supplementation of monounsaturated and polyunsaturated fatty acids changed the membranous web morphology and decreased HCV RNA replication. This demonstrates the importance of the cellular lipid composition of membrane structures and its impact on the viral life cycle. Interfering with the lipid metabolism does not only affect membrane properties, but also causes cellular responses. This is shown in the increased SR-BI surface expression as well as increased ApoE levels upon FADS2 inhibition. The dose dependent inhibition of FADS2 additionally revealed that different stages of the viral life cycle can be affected even in an opposing manner.

3.8. Outlook

Regarding the lipidomic results further fragmentation of the lipid species in mass spectrometry is needed to identify the exact fatty acyl chains of diglycerides, triglycerides, and phosphatidylcholines. This, in combination with the analysis of a broader range of free fatty acids, will help to understand the availability and incorporation of fatty acids. So far, only the membrane lipids phosphatidylcholine and sphingomyelin were investigated. Lipids can be conical (for example phosphatidylethanolamine), cylindrical (for example phosphatidylcholine, sphingomyelin) or inverted conical (for example lysophospholipids). The lipid composition of a membrane determines the membrane shape and properties (Holthuis and Menon, 2014; Thiam et al., 2013). Thus, the variety of lipid classes should be analyzed to determine preferences of HCV. Additionally, the lipid composition of cellular compartments

should be determined. This would help to understand whether HCV induces precise changes of compartments that are known to be important for its replication, such as lipid droplets and the ER, or whether HCV-infection induces global cellular changes affecting all compartments in a similar manner.

Lipidomics will also help to further understand the decline in sphingomyelins observed in this study and previously by others (Diamond et al., 2010). Sphingomyelins are synthesized from ceramides and can be converted back (Ridgway ed., 2015). Therefore, the amount of ceramides in correlation to sphingomyelins will provide information whether the sphingomyelin metabolism is manipulated in HCV-infected cells. Diamond et al. have additionally suggested that the decline in sphingomyelins is due to their incorporation into the viral particles. This could be studied by additionally analyzing the supernatants from infected and uninfected cells by lipidomics.

One hypothesis for the increase in free fatty acids is an upregulated fatty acid uptake. Different tools are available to study fatty acid uptake. First of all, the expression of the fatty acid transporter CD36 on the cells surface should be tested on HCV-infected and uninfected Huh7.5 cells by antibody staining, following the analysis by flow cytometry. Furthermore, the fatty acid uptake can be measured by supplementation of fluorescently labeled fatty acids, for example, a Bodipy conjugate. The evaluation can be performed by flow cytometry or in a plate reader (Dubikovskaya et al., 2014). Alternatively, click chemistry can be used to determine the uptake of fatty acids. For this protocol alkyne-fatty acids are supplemented to the cell. Alkyne-fatty acids carry an alkyne group at their methyl terminus, which has the advantage that these fatty acids are not fused to a large fluorophore which may impair their physiology. Upon lipid extraction, the alkyne-group is conjugated with a fluorophore by a click reaction, followed by thin layer chromatography. This method additionally allows the study of the incorporation of fatty acids into other lipid classes, for example, phosphatidylcholines and triglycerides, to elucidate potential substrate preferences (Thiele et al., 2012). The click-chemistry approach would additionally allow time course experiments to study the kinetics and selectivity of the fatty acid incorporation. The kinetics may help to elucidate whether lipid synthesis is decelerated upon infection. Here, the fatty acids identified by mass spectrometry would be of foremost interest. Instead of analyzing the incorporation the lipolysis can be measured with this approach in a pulse-chase setup. A prolonged treatment with a mixture of different alkyne-fatty acids should result in an incorporation of the alkyne-fatty acids into lipids. The loss of alkyne-fatty acid chains upon removal of the alkyne-fatty acids can give hints about the kinetics of lipolysis.

As mentioned previously, mitochondria and peroxisomes have different substrate preferences for β -oxidation. This leads to the question whether the contribution to β -oxidation of one organelle is altered in HCV-infected cells. The peroxisomal β -oxidation can be

measured by the conversion of the fatty acid C24:0 to C16:0, which exclusively occurs in the peroxisomes. Deuterium labeled C24:0 enables the identification by mass spectrometry (Kemp et al., 2004).

In this study, various knockdown experiments of elongases and desaturases had an impact on viral replication. Therefore, further experiments focusing on the distinct role of these enzymes in the viral life cycle should be performed. One desaturase, FADS2, was already taken under further investigation but there are still several open questions. So far, it was not investigated whether the surface receptor SR-BI is also upregulated upon a 3 day pretreatment with the FADS2 inhibitor SC-26196. Next, it should be elucidated whether the increased surface expression of SR-BI on 1 day and potentially 3 days post FADS2 inhibition indeed results in an increased virus uptake. Therefore, entry assays should be performed with commercially available branched DNA assays to stain viral RNA at early time points post infection following the analysis by fluorescence microscopy (Neufeldt et al., 2016). SR-BI is known to function in lipoprotein uptake, mainly the cholesterol rich HDL (Ridgway ed., 2015). Therefore, the question arises if FADS2 inhibition increases the intracellular cholesterol or triglyceride level by upregulation of lipoprotein import. As shown in this study, alterations in the intracellular cholesterol level can affect the virus production. An easy way to test the intracellular cholesterol and triglyceride level upon FADS2 inhibition in uninfected and HCV-infected cells would be the analysis by commercially available colorimetric quantification kits. A second connection of FADS2 inhibition and lipoproteins was the intracellular increase of ApoE. It should further be tested by RT-qPCR whether the ApoE mRNA expression is increased, the protein stabilized, or if ApoE is derived from lipoprotein uptake. Moreover, it would be interesting to determine the localization of ApoE by immunofluorescence co-staining with PDI (ER-marker), G130 (Golgi marker), and recycling endosomes (Rab11). It is of great importance to determine the intracellular and extracellular ApoE levels upon FADS2 inhibition in HCV-infected cells. Additionally, the intracellular localization of the viral protein core to lipid droplets should be determined since changes in the lipid composition might also influence the binding properties of membrane anchored proteins. Overall, solving the mechanism of how FADS2 inhibition impairs virus production will provide further insights to the so far not well understood late steps of the viral life cycle.

Understanding the way in which HCV interferes with the lipid metabolism will raise further options to intervene in the viral replication and to identify potential cellular drug targets. Although highly effective direct acting antivirals are available, the problem of drug resistance due to the error-prone RNA synthesis remains. Cellular drug targets have a lower potential to give rise to drug resistant viruses, therefore lipid modulating enzymes can be considered as potential targets to indirectly inhibit viral replication (Li et al., 2015).

4. Materials

4.1. HCV full replicating cell culture system

In 2005 the HCV genotype 2a strain JFH-1 was isolated from a Japanese patient with fulminant hepatitis. This strain was able to fully replicate in the hepatoma cell line Huh7 (Wakita et al., 2005). This strain was further adapted and the highly infectious J6/JFH1 chimera Jc1 was generated (Pietschmann et al., 2006). Meanwhile, several modifications were introduced into the genome, such as reporter or resistant genes. By flanking those proteins either with the NS5A/B cleavage site or the cleavage site of p7 and a 2A sequence, HCV infection can be monitored without the generation of viral fusion proteins that may influence their function (Marukian et al., 2008; Webster et al., 2013).

4.2. Plasmids

Table 1: HCV plasmids

Number	Plasmid	Description	Reference
pMO711	pBR322 EGFP-Jc1	Bicistronic reporter virus with the HCV 5' UTR and part of the core virus fused to EGFP followed by the ECMV IRES and the full length Jc1.	(Herker et al., 2010)
pMO977	pBR322 Jc1 ^{NS5AB-EGFP}	EGFP flanked by the duplicated NS5A and NS5B cleavage site in the Jc1.	(Webster et al., 2013)
pMO983	pBR322 Jc1 ^{NS5AB-Fluc}	<i>Firefly</i> luciferase flanked by the duplicated NS5A and NS5B cleavage site in the Jc1.	(Webster et al., 2013)
pGL4.75	pGL4.75[hRluc/CMV]	Control plasmid encoding for <i>Renilla</i> luciferase.	Promega
HH183	pBR322 Jc1 ^{p7-Gluc-2A}	HCV Jc1 carrying a <i>Gaussia</i> luciferase which is flanked by the p7 cleavage site and a 2A sequence. <i>Gaussia</i> luciferase is a secreted protein.	Overlap extension PCR as described in (Marukian et al., 2008). Cloned by Anja Schöbel.
HH14	pBR322 Jc1 ^{Flag-E2 NS5AB-EGFP}	Jc1 expressing a Flag-tagged E2 and an EGFP flanked by the duplicated NS5A and NS5B cleavage site.	Overlap extension PCR as described in (Merz et al., 2011). Cloned during this thesis.
HH21	pBR322 Jc1 ^{Flag-E2}	Jc1 expressing a Flag-tagged E2	(Eggert et al., 2014)

Table 2: Lentiviral plasmids

Number	Plasmid	Description	Reference
	pSicoR-MS1	Backbone for shRNA constructs encoding mCherry	(Wissing et al., 2011)
HH264	pSicoR-EL2	pSicoR carrying ELOVL2 shRNA	(Scherer, unpublished)
HH262	pSicoR-EL4	pSicoR carrying ELOVL4 shRNA	(Scherer, unpublished)
HH252	pSicoR-EL5	pSicoR carrying ELOVL5 shRNA	(Scherer, unpublished)
HH263	pSicoR-EL6	pSicoR carrying ELOVL6 shRNA	(Scherer, unpublished)
HH265	pSicoR-EL7	pSicoR carrying ELOVL7 shRNA	(Scherer, unpublished)
HH253	pSicoR-SCD	pSicoR carrying SCD shRNA	(Scherer, unpublished)
HH254	pSicoR-SCD5	pSicoR carrying SCD5 shRNA	(Scherer, unpublished)
HH256	pSicoR-FADS2	pSicoR carrying FADS2 shRNA	(Scherer, unpublished)
HH257	pSicoR-FADS3	pSicoR carrying FADS3 shRNA	(Scherer, unpublished)
HH266	pSicoR-FADS6	pSicoR carrying FADS6 shRNA	(Scherer, unpublished)
HH98	Trip-RFP-NLS-IPS	HCV reporter	(Jones et al., 2010)
pMO86	pCMV Δ R8.91	Lentiviral packaging plasmid	(Naldini et al., 1996)
pMO87	pMD.G	VSV-G envelope glycoprotein	(Naldini et al., 1996)

4.3. Oligonucleotides

Table 3: Oligonucleotides for overlap extension PCR

Primer	Sequence 5'-3'	Description	Reference
BsiWI_J6 sense	GGACATGATGATGAACTGG	Primer set 1	(Merz et al., 2011)
E1_FLAG as	CCCTTGTCATCGTCGTCCTTGTAGT CCGCGTCCACCCCGCGGCC	Primer set 1	(Merz et al., 2011)
E1_FLAG sense	GGACGACGATGACAAGGGATCAGG AGCACGCACCCATACTGTTGGGGG	Primer set 2	(Merz et al., 2011)
NS2_JFH1 Not as	CCATCGCGGCCGCGCGCAC	Primer set 2	
J6 Seq 1200	GCCCAAATGTTTCATTGTCTC	Sequencing	

Oligonucleotides were purchased from Sigma-Aldrich, Taufkirchen

Table 4: Oligonucleotides for qPCR

Gene	Primer	Sequence 5'-3'	Harvard Primer Bank ID
ELOVL1	ELOVL1 fw	TTATTCTCCGAAAGAAAGACGGG	373938451c1
	ELOVL1 rev	ATGACATGCACGGAAGAGTTTAT	
ELOVL2	ELOVL2 fw	ATGTTTGGACCGCGAGATTCT	157388944c1
	ELOVL2 rev	CCCAGCCATATTGAGAGCAGATA	
ELOVL3	ELOVL3 fw	GTATTGGGCAACCTCATTCCC	23097309c2
	ELOVL3 rev	CCTTGCGTTCCTTCATGTAGT	
ELOVL4	ELOVL4 fw	AAGGACCGAGAACCTTTTCAGA	169646356c3
	ELOVL4 rev	TCCCGCATTATATGATCCCATGA	
ELOVL5	ELOVL5 fw	ATGGTTTGTCTGTCAGTCCCTT	11464975a3
	ELOVL5 rev	AGCTGGTCTGGATGATTGTCA	
ELOVL6	ELOVL6 fw	AACGAGCAAAGTTTGAAGTGG	195539341c1
	ELOVL6 rev	TCGAAGAGCACCGAATATACTGA	
ELOVL7	ELOVL7 fw	GCCTTCAGTGATCTTACATCGAG	157388948c1
	ELOVL7 rev	AGGACATGAGGAGCCAATCTT	
SCD	SCD fw	TCTAGCTCCTATACCACCACCA	(Liu et al., 2016)
	SCD rev	TCGTCTCCAACCTTATCTCCTCC	
SCD5	SCD5 fw	TGCGACGCCAAGGAAGAAAT	148596960c1
	SCD5 rev	CCTCCAGACGATGTTCTGCC	
FADS1	FADS1 fw	CTACCCCGCGCTACTTCAC	214831729c1
	FADS1 rev	CGGTTCGATCACTAGCCACC	
FADS2	FADS2 fw	TGACCGCAAGGTTTACAACAT	14141180c1
	FADS2 rev	AGGCATCCGTTGCATCTTCTC	
FADS3	FADS3 fw	CCCTGGTGAACCTTGAAGTGG	34304362c3
	FADS3 rev	GGAGGTAGGATAAGAAGAAGCGG	
FADS6	FADS6 fw	TCGGATTCACATGATGAGCCT	116812625c3
	FADS6 rev	CTTCTCACGTAGGAACTGGGA	
DEGS1	DEGS1 fw	GAGATCCTGGCAAAGTATCCAGA	360039229c1
	DEGS1 rev	CAAACGCATAGGCCCCAAA	
β Actin	β Actin fw	CATGTACGTTGCTATCCAGGC	
	β Actin rev	CTCCTTAATGTCACGCACGAT	
18S rRNA	18S rRNA fw	GTAACCCGTTGAACCCATT	
	18S rRNA rev	CCATCCAATCGGTAGTAGCG	

JFH1	JFH1 fw JFH1 rev	CGGGAGAGCCATAGTGG AGTACCACAAGGCCTTTTCG	(Herker et al., 2010)
------	---------------------	---	-----------------------

The qPCR-primer mix contains 10 μ M forward primer and 10 μ M reverse primer diluted in nuclease-free H₂O.

Oligonucleotides were purchased from Sigma-Aldrich, Taufkirchen

4.4. Bacteria

Table 5: Bacteria strain

Bacterial strain	Genotype	Company
DH5 α	F ⁻ Φ 80 <i>lacZ</i> Δ M15 Δ (<i>lacZYA-argF</i>) U169 <i>recA1 endA1 hsdR17</i> (r ⁻ , m ^{k+}) <i>phoA supE44 thi-1 gyrA96 relA1 λ</i>	ThermoFisher Scientific, St. Leon-Rot

Table 6: Bacterial media

Name	Components	Quantity
LB-medium	Trypton Yeast extract NaCl 5 N NaOH dH ₂ O	10 g 5 g 10 g 200 μ l ad 1 l

The medium was autoclaved and supplemented with 100 μ g/ml ampicillin if needed.

LB-agar	Trypton Yeast extract NaCl 5N NaOH Agar bacteriology grade dH ₂ O	10 g 5 g 10 g 200 μ l 15 g ad 1 l
---------	---	--

The LB-agar was autoclaved and cooled to approximately 60 °C before 100 μ g/ml ampicillin was supplemented. The LB-agar was plated into sterile petri dishes.

4.5. Cell lines and cell culture materials

HEK 293T

HEK 293T is a human embryonic kidney cell line expressing the SV40 large T antigen. This promotes the replication of plasmids carrying the SV40 origin of replication (DuBridge et al., 1987). HEK 293T cells were purchased from the American Type Culture Collection (ATCC).

Huh7.5

Huh7.5 cells are derived from the hepatocellular carcinoma cell line Huh7. Huh7 cells carried an HCV replicon that was removed by IFN treatment. Huh7.5 cells are highly permissive for HCV replication (Blight et al., 2002). This has been attributed to a mutation in the RIG-I gene (Sumpter et al., 2005). Huh7.5 cells were kindly provided by Charles M. Rice.

Huh7-Lunet

Huh7-Lunet cells are derived from the hepatocellular carcinoma cell line Huh7. Huh7 cells harboring an HCV replicon were cured with a specific inhibitor. Huh7-Lunet cells are more permissive for HCV replication than Huh7 cells (Friebe et al., 2005). Huh7-Lunet cells were kindly provided by Ralf Bartenschlager.

Huh7.5-RFP-NLS

Huh7.5 cells stably transduced with Trip-RFP-NLS-IPS. This plasmid contains a red fluorescent protein (RFP) fused to a nuclear localization sequence (NLS) and the mitochondrial antiviral-signaling protein (MAVS/IPS-1). Thus, in uninfected cells the RFP localizes to the mitochondria. IPS-1 is a target for the HCV NS3/NS4A protease and upon cleavage the NLS is accessible and the RFP translocates into the nucleus. This system enables monitoring HCV infection in cell culture (Jones et al., 2010).

Table 7: Cell culture media and buffer

Name	Components	Final concentration
DMEM ⁺⁺	Dulbecco's modified eagle medium (High glucose) Fetal bovine calf serum (FCS) GlutaMAX 100x	10% (v/v) 1% (v/v)
DMEM ⁺⁺⁺	DMEM ⁺⁺ Penicillin/Streptomycin 100x	1% (v/v)
Freezing medium	DMSO FCS	10% (v/v) 90% (v/v)
Cytomix	Potassium phosphate buffer (pH 7.6) KCl MgCl ₂ HEPES CaCl ₂ EGTA (pH 7.6) adjust pH 7.6 with 1 N KOH dH ₂ O sterile filtered (0.22 µm filter)	10 mM 120 mM 5 mM 25 mM 0.15 mM 2 mM
	ATP Glutathione	2 mM 5 mM } add before electroporation

1 M Potassium phosphate buffer	1 M KH_2PO_4 1 M K_2HPO_4 adjust pH 7.4	19% (v/v) 81% (v/v)
2x HBS	NaCl KCl Na_2HPO_4 HEPES Glucose adjust pH 7.05	275 mM 10 mM 1.4 mM 42 mM 11 mM
25 mM Chloroquin	Chloroquin diphosphate ddH ₂ O	25 mM
4 mg/ml Polybrene	Polybrene DPBS	4 mg/ml
40% PEG	PEG-8000 DPBS autoclaved	40% (w/v)
Glutaraldehyde	Glutaraldehyde PBS	5% (v/v)
Osmium tetroxyde	OsO_4 PBS	2% (w/v)

Table 8: Solutions used for fatty acid complexation to albumin

Name	Component	Quantity
Fatty acid stocks	Fatty acid Ethanol (99.8%)	100 mM
0.5 mM albumin solution	Bovine albumin (fatty acid free) DMEM (high glucose)	33 mg/ml

For complexation the fatty acids were diluted in 0.5 mM albumin solution to a concentration of 2 mM. As mock-control the same volume of ethanol was diluted in albumin solution. The mixture was shaken at 1200 rpm at 37 °C for 1 h in an Eppendorf Thermomixer. The complexation was always freshly prepared.

4.6. Solvents and buffers for biochemical methods

4.6.1. Agarose gel electrophoresis

Table 9: Chemicals used for agarose gel electrophoresis

Name	Component	Final concentration
Agarose gel	Agarose EtBr 1x TAE Buffer	0.7–1.5% (w/v) 1 µg/ml
10x TAE buffer	Tris base Acetic acid EDTA (pH 8) dH ₂ O	2 M 5.71% (v/v) 50 mM

4.6.2. SDS-PAGE

Table 10: SDS-PAGE and analysis

Name	Component	Final concentration
6x Laemmli	Tris-HCl (pH 6.8) Glycerol SDS Bromphenol blue β-Mercaptoethanol dH ₂ O	375 mM 25.8% (v/v) 12.3% (w/v) 600 µg/ml 6% (v/v)
10x Running buffer	Tris base Glycine SDS dH ₂ O	3.02% (w/v) 18.8% (w/v) 1% (w/v)
10x Blotting buffer	Tris base Glycin dH ₂ O	3.03% (w/v) 14.4% (w/v)
1x Blotting buffer	10x Blotting buffer Methanol dH ₂ O	1:10 20% (v/v)
20x TBS-T	Tris base NaCl Tween 20 dH ₂ O adjust to pH 7.4	200 mM 3 M 1% (v/v)

<u>Polyacrylamidgel</u>		
Running gel (12%)	1.5 M Tris (pH 8.8) Acrylamid (30%) SDS (10%) APS (10%) TEMED ddH ₂ O	33% (v/v) 40% (v/v) 1% (v/v) 1% (v/v) 0.08% (v/v)
Stacking gel	1M Tris (pH 6.8) Acrylamid (30%) SDS (10%) APS (10%) TEMED ddH ₂ O	13 % 17% 1% (v/v) 1% (v/v) 0.1% (v/v)
Blocking buffer	Nonfat dried milk powder 1x TBS-T	5% (w/v)
<u>Ponceau staining</u>		
Ponceau	PonceauS Acetic acid	0.1% w/v 5% v/v
<u>Coomassie staining</u>		
Coomassie staining buffer	Coomassie brilliant blue R Methanol Acetic acid dH ₂ O	0.5% (w/v) 40% (v/v) 10% (v/v)
Coomassie destain buffer	Acetic acid Methanol dH ₂ O	10% (v/v) 10% (v/v)
<u>Silver staining</u>		
Fixation solution	Methanol Acetic acid Formaldehyde dH ₂ O	50% (v/v) 12% (v/v) 0.0185% (v/v)
Wash solution	Methanol dH ₂ O	50% (v/v)
Pretreatment solution	Na ₂ S ₂ O ₃ dH ₂ O	0.02% (w/v)
Impregnate solution	AgNO ₃ Formaldehyde dH ₂ O	0.2% (w/v) 0.0278% (v/v)
Develop solution	Na ₂ CO ₃ Formaldehyde Na ₂ S ₂ O ₃ dH ₂ O	6% (w/v) 0.0185% (w/v) 0.0004% (w/v)

Stop solution	Methanol Acetic acid dH ₂ O	50% (v/v) 12% (v/v)
---------------	--	------------------------

4.6.3. DNA and protein ladder

Table 11: Utilized DNA and protein ladders

Application	Ladder	Company
DNA	GeneRuler DNA Ladder Mix	Fermentas, Darmstadt
Protein	PageRuler Prestained (10-170 kDa)	Fermentas, Darmstadt

4.6.4. Cell lysis

Table 12: Lysis Buffer

Lysis Buffer	Component	Final concentration
RIPA	Tris-HCl (pH 7.4)	50 mM
	EDTA	1 mM
	NaCl	150 mM
	NP-40	1%
	Na-Desoxycholat	0,5%
	SDS	0,1%
	dH ₂ O	1:100
	100 mM PMSF	1:100
	Protease Inhibitor Cocktail	
	Supplement PMSF and Protease Inhibitor Cocktail before use	
SDS lysis buffer	EDTA (pH 7.6)	5 mM
	Tris-HCl (pH 6.8)	50 mM
	SDS	4%
	dH ₂ O	

4.6.5. Buffers used for lipid droplet isolation

Table 13: Buffers used for lipid droplet isolation

Buffer	Component	Quantity
Hypotonic buffer	HEPES	50 mM
	MgCl ₂	2 mM
	dH ₂ O	
	Adjust pH 7.4 with 1M KOH	
	100 mM PMSF	1:100
	Protease inhibitor cocktail	1:100
	Add PMSF and protease inhibitor cocktail before usage	
Isotonic buffer	HEPES	50 mM
	KCl	100 mM
	MgCl ₂	2 mM
	100 mM PMSF	1:100
	Add PMSF before usage	
Sucrose in isotonic buffer	Sucrose	1.05 M
	Isotonic buffer	
	100 mM PMSF	1:100
	Add PMSF before usage	

4.6.6. Solutions used for acidified Bligh & Dyer

Table 14: Solutions used for acidified Bligh & Dyer

Solution	Component	Quantity
3% acetic acid + BHT	Acetic acid 99.9%	3% v/v
	Methanol	97%
	BHT 1 mg/ml	5.62 µl
BHT 1 mg/ml	2,6-Di-tert-butyl-4-methyl-phenol	1 mg
	Methanol	1 ml

4.6.7. Density gradient

Table 15: Buffers to prepare a density gradient

Buffer	Component	Quantity
40% Iodixanol	Optiprep 60%	33.3 ml
	0.1 M EDTA (pH 7.6)	1 ml
	1.5 M Tris-HCl (pH 6.8)	1.6 ml
	0.25 M Sucrose	14.1 ml
10% Iodixanol	Optiprep 60%	8.3 ml
	0.1 M EDTA (pH 7.6)	1 ml
	1.5 M Tris-HCl (pH 6.8)	1.6 ml
	0.25 M Sucrose	39.6 ml

Gradients were prepared with a gradient mixer

4.7. Solutions and stainings utilized for microscopy

Table 16: Solutions utilized for Microscopy

Solution	Component	Quantity
16% PFA	Paraformaldehyde	16% (w/v)
	PBS	84% (v/v)
Mowiol	0.2 M Tris-HCl (pH 8.5)	12 ml
	Mowiol 4-88	2.4 g
	Glycerol	6 g
	ddH ₂ O	6 ml
Mowiol + DABCO	Mowiol as described above DAPCO	25 mg/ml

Table 17: Stainings utilized for microscopy

Staining	Dilution	Company
Bodipy 493/503 (1mg/ml)	1:1000	Life technologies, Darmstadt
Filipin III (1mg/ml)	1:20	Sigma-Aldrich GmbH, Taufkirchen
Hoechst (10 mg/ml)	1:5000	Sigma-Aldrich GmbH, Taufkirchen

4.8. Antibodies

Table 18: Utilized antibodies

Antibody	Dilution	Application	Company
<u>Primary antibodies</u>			
Core, ms	1:1000	Western blot	Santa Cruz Biotechnology, Heidelberg
Tubulin	1:2000	Western blot	Sigma-Aldrich GmbH, Taufkirchen
ADRP, rb	1:1000	Western blot	Abcam, Cambridge
ApoE, rb	1:2500	Western blot	Abcam, Cambridge
LDLR, ms	1:20	Flow cytometry	Santa Cruz Biotechnology, Heidelberg
SR-BI, rb	1:100	Flow cytometry	Novus Biologicals, Littleton
CD81, ms	1:300	Flow cytometry	(Fritzsching et al., 2002)
<u>Secondary antibodies</u>			
Peroxidase-AffiniPure Goat Anti-Mouse IgG (H+L)	1:10000	Western blot	JacksonImmunoResearch Laboratories, Suffolk
Peroxidase-conjugated AffiniPure Goat Anti-Rat IgG(H+L)	1:10000	Western blot	JacksonImmunoResearch Laboratories, Suffolk
Alexa Flour 488 goat anti-mouse IgG (H+L)	1:1000	Flow cytometry	Life Technologies, Darmstadt
Alexa Flour 488 donkey anti-rabbit IgG (H+L)	1:1000	Flow cytometry	Life Technologies, Darmstadt

All antibodies were diluted in 5% milk/TBS-T for western blot or 1% FCS/DPBS for flow cytometry staining.

4.9. Enzymes

Table 19: Utilized Enzymes

Enzymes	Units	Company
BsiWI	10,000 units/ml	New England BioLabs GmbH, Frankfurt a.M.
MluI	10,000 units/ml	New England BioLabs GmbH, Frankfurt a.M.
NotI	10,000 units/ml	New England BioLabs GmbH, Frankfurt a.M.
SspI	5,000 units/ml	New England BioLabs GmbH, Frankfurt a.M.

alkaline phosphatase (CIP)	10,000 units/ml	New England BioLabs GmbH, Frankfurt a.M.
T4 DNA Ligase	5 U/ μ l	Thermo Fisher Scientific, St. Leon-Rot
Taq DNA polymerase	5 U/ μ l	Thermo Fisher Scientific, St. Leon-Rot
Phusion High-Fidelity DNA Polymerase	2 U/ μ l	Thermo Fisher Scientific, St. Leon-Rot
Super Script III Reverse Transcriptase	200 U/ μ l	Thermo Fisher Scientific, St. Leon-Rot

4.10. Inhibitors

Table 20: Utilized Inhibitors

Inhibitor	Stock concentration	Company
Phenylmethylsulfonyl fluorid (PMSF)	100 mM in isopropanol	Sigma-Aldrich GmbH, Taufkirchen
Protease Inhibitor Cocktail	100x	Sigma-Aldrich GmbH, Taufkirchen
RNase Away		Carl Roth GmbH, Karlsruhe
RNaseOut	5000 units	Thermo Fisher Scientific, St. Leon-Rot
SC-26196	2 mM or 0.1 mM in DMSO	Sigma-Aldrich GmbH, Taufkirchen

4.11. Chemicals

Table 21: Utilized chemicals

Chemical	Company
α -Linolenic acid	Sigma-Aldrich, Taufkirchen
γ -Linolenic acid	Sigma-Aldrich, Taufkirchen
1,4-Dithiothreitol (DTT)	Sigma-Aldrich GmbH, Taufkirchen
100x BSA (Bovine serum albumin for restriction enzymes)	New England BioLabs, Frankfurt a. M
10x MungBean nuclease buffer	New England Biolabs, Frankfurt a.M.
10x NEBuffer 3	New England Biolabs, Frankfurt a.M.
10x T ₄ -Ligase Buffer	Thermo Fischer Scientific, St. Leon-Rot
10x Taq Buffer KCl	Thermo Fischer Scientific, St. Leon-Rot
2,6-Di-tert-butyl-4-methyl-phenol >99.0% (GC) (BHT)	Sigma-Aldrich GmbH, Taufkirchen

25 mM MgCl ₂ (PCR)	Thermo Fischer Scientific, St. Leon-Rot
5x Phusion HF buffer	Thermo Fischer Scientific, St. Leon-Rot
6x DNA loading dye	Thermo Fisher Scientific, St. Leon-Rot
Acetic acid	AppliChem GmbH, Darmstadt
Acetic acid (used for lipidomics)	Sigma-Aldrich, Taufkirchen
Acrylamide solution (30%) - Mix 37.5	AppliChem GmbH, Darmstadt
Adenosine triphosphate (ATP)	AppliChem GmbH, Darmstadt
Agar bacteriology grade	AppliChem GmbH, Darmstadt
Agarose basic	AppliChem GmbH, Darmstadt
Ampicillin	AppliChem GmbH, Darmstadt
APS (Ammonium persulfate)	AppliChem GmbH, Darmstadt
Arachidonic acid	Sigma-Aldrich GmbH, Taufkirchen
ATP (Adenosine triphosphate)	AppliChem GmbH, Darmstadt
β-Mercaptoethanol	Sigma-Aldrich GmbH, Taufkirchen
Bovine albumin (fatty acid free)	Sigma-Aldrich GmbH, Taufkirchen
Bromophenol blue	AppliChem GmbH, Darmstadt
Calcium chloride (CaCl ₂)	AppliChem GmbH, Darmstadt
Chloroform	AppliChem GmbH, Darmstadt
Chloroform CHROMASOLV Plus, for HPLC, 99.9% (used for lipidomics)	Sigma-Aldrich GmbH, Taufkirchen
Chloroquine diphosphate	Sigma-Aldrich GmbH, Taufkirchen
Coomassie brilliant blue G	Sigma-Aldrich GmbH, Taufkirchen
Cut Smart buffer	New England BioLabs, Frankfurt a. M.
D(+)-Glucose Monohydrat	AppliChem GmbH, Darmstadt
DAPCO	Roth GmbH + Co. KG, Karlsruhe
Dimethyl sulfoxide (DMSO)	AppliChem GmbH, Darmstadt
<i>di</i> -potassium hydrogen phosphate (K ₂ HPO ₄)	AppliChem GmbH, Darmstadt
Disodium phosphate (Na ₂ HPO ₄)	AppliChem GmbH, Darmstadt
dNTP Mix 10 mM	Thermo Fischer Scientific, St. Leon-Rot
Docosahexanoic acid	Sigma-Aldrich, Taufkirchen

Dulbecco's modified eagle medium (High glucose) (Gibco)	Thermo Fischer Scientific, St. Leon-Rot
Dulbecco's phosphate buffered saline (DPBS)	Sigma-Aldrich, Taufkirchen
ECL lumi-light	Roche Diagnostics, Basel
EDTA	AppliChem GmbH, Darmstadt
EGTA	AppliChem GmbH, Darmstadt
Eicosapentaenoic acid	Sigma-Aldrich, Taufkirchen
EtBr (Ethidium bromide)	AppliChem GmbH, Darmstadt
Ethanol absolute (used for RNA isolation)	AppliChem GmbH, Darmstadt
Ethanol ROTIPURAN 99,8%	Roth GmbH + Co. KG, Karlsruhe
Fetal Calf Serum (FCS)	Biochrom AG, Berlin
Formaldehyde - Solution 37%	AppliChem GmbH, Darmstadt
GlutaMAX 100x (Gibco)	Thermo Fischer Scientific, St. Leon-Rot
Glutaraldehyde	Electron Microscopy Sciences, Pennsylvania
Glutathione	AppliChem GmbH, Darmstadt
Glycerol anhydrous	AppliChem GmbH, Darmstadt
Glycine	AppliChem GmbH, Darmstadt
HEPES	Sigma-Aldrich GmbH, Taufkirchen
Hydrochloric acid (HCl)	AppliChem GmbH, Darmstadt
Hydrogen peroxide 10%	AppliChem GmbH, Darmstadt
Isopropanol	AppliChem GmbH, Darmstadt
Isopropanol (used for RNA isolation)	Sigma-Aldrich, Taufkirchen
Lauric Acid	Sigma-Aldrich, Taufkirchen
Linoleic acid	Sigma-Aldrich, Taufkirchen
Magnesium chloride (MgCl ₂)	AppliChem GmbH, Darmstadt
Magnesium chloride (MgCl ₂)	AppliChem GmbH, Darmstadt
Methanol (MeOH)	AppliChem GmbH, Darmstadt
Methanol LC-MS CHROMASOLV (used for lipidomics)	Sigma-Aldrich GmbH, Taufkirchen
Monopotassium phosphate (KH ₂ PO ₄)	AppliChem GmbH, Darmstadt
Mowiol 4-88	AppliChem GmbH, Darmstadt

Myristic Acid	Sigma-Aldrich, Taufkirchen
Nonfat dried milk powder	AppliChem GmbH, Darmstadt
Nonidet-P40	AppliChem GmbH, Darmstadt
Nuclease-free water	Thermo Fischer Scientific, St. Leon-Rot
Oleic acid	Sigma-Aldrich, Taufkirchen
OPTI-MEM (Gibco)	Thermo Fischer Scientific, St. Leon-Rot
OptiPREP (60% Iodixanol)	Sigma-Aldrich GmbH, Taufkirchen
Osmium tetroxide	Roth GmbH + Co. KG, Karlsruhe
Palmitic Acid	Sigma-Aldrich, Taufkirchen
Paraformaldehyde (PFA)	AppliChem GmbH, Darmstadt
Penicillin/Streptomycin 100x	Sigma-Aldrich, Taufkirchen
Phenol-Chloroform-Isoamyl alcohol (25:24:1 v/v/v)	AppliChem GmbH, Darmstadt
Phenylmethylsulfonyl fluoride (PMSF)	AppliChem GmbH, Darmstadt
Polybrene (Hexadimethrine bromide)	Sigma-Aldrich GmbH, Taufkirchen
Polyethylene glycol (PEG) - 8000	AppliChem GmbH, Darmstadt
Ponceau S	AppliChem GmbH, Darmstadt
Potassium chloride (KCl)	AppliChem GmbH, Darmstadt
Potassium hydroxide (KOH)	AppliChem GmbH, Darmstadt
Random Hexamer	Qiagen, Hilden
RNA Stat-60	AMS Biotechnology (Europe) Ltd, Abington
RNase Away	Molecular Bio Products / Thermo Fischer Scientific, St. Leon-Rot
RNase free water (Ambion)	Thermo Fischer Scientific, St. Leon-Rot
Silver nitrate (AgNO ₃)	AppliChem GmbH, Darmstadt
Sodium acetate (C ₂ H ₃ NaO ₂) 3 M pH 5.2	AppliChem GmbH, Darmstadt
Sodium carbonate (Na ₂ CO ₃)	AppliChem GmbH, Darmstadt
Sodium chloride (NaCl)	AppliChem GmbH, Darmstadt
Sodium deoxycholate	AppliChem GmbH, Darmstadt
Sodium dodecyl sulfate (SDS)	AppliChem GmbH, Darmstadt
Sodium hydroxide	AppliChem GmbH, Darmstadt

Sodium hypochlorite	Merck, Darmstadt
Sodium thiosulfate (Na ₂ S ₂ O ₃)	AppliChem GmbH, Darmstadt
Sspl-Buffer	New England Biolabs, Frankfurt a.M.
Stearic Acid	Sigma-Aldrich, Taufkirchen
Sucrose	AppliChem GmbH, Darmstadt
SuperSignal West Femto	Thermo Fischer Scientific, St. Leon-Rot
TEMED (Tetramethylethylenediamine)	AppliChem GmbH, Darmstadt
Thiocarbohydrazide	Sigma-Aldrich GmbH, Taufkirchen
TRI Reagent	Sigma-Aldrich GmbH, Taufkirchen
Tris ultrapure (Tris-base)	AppliChem GmbH, Darmstadt
Tris-HCl	AppliChem GmbH, Darmstadt
Triton X-100	AppliChem GmbH, Darmstadt
Trypan blue solution 0,4%	Amresco, Ohio, USA
Trypan Blue Stain (0.4%) for Countess Automated Cell Counter	Life Technologies GmbH, Darmstadt
Trypsin/EDTA (0,05 % / 0,02 % w/v) (Gibco)	Thermo Fischer Scientific, St. Leon-Rot
Tryptone	AppliChem GmbH, Darmstadt
Tween 20 molecular biology grade	AppliChem GmbH, Darmstadt
Water LC-MS CHROMASOLV (used for lipidomics)	Sigma-Aldrich, Taufkirchen
Water nuclease-free	Thermo Fischer Scientific, St. Leon-Rot
Water Rotisolv HPLC grade	Roth GmbH + Co. KG, Karlsruhe
Yeast extract	AppliChem GmbH, Darmstadt

4.12. Kits

Table 22: Utilized kits

Kit	Company
CellTiter 96® AQueous One Solution Reagent	Promega Corporation, Mannheim
DNA-free DNA removal kit (Ambion)	Thermo Fischer Scientific, St. Leon-Rot
DC Protein Assay	BioRad GmbH, München
Dual-Luciferase® Reporter Assay System	Promega GmbH, Mannheim

Infinity Triglyceride Reagent	Thermo Fischer Scientific, St. Leon-Rot
Luciferase Assay System	Promega GmbH, Mannheim
Maxima SYBR Green qPCR Master Mix	Life Technologies, Darmstadt
Megascript T7 Transcription Kit	Life Technologies, Darmstadt
NucleoBond® XtraMaxi Kit	Macherey-Nagel, Düren
Nucleospin RNA® Virus	Macherey-Nagel GmbH + Co KG, Düren
NucleoSpin® Gel and PCR Clean-Up Kit	Macherey-Nagel, Düren
NucleoSpin® Plasmid Kit	Macherey-Nagel, Düren
Pierce Coomassie Plus Assay	Thermo Fischer Scientific, St. Leon-Rot
PS-Speck™ Microscope Point Source Kit	Thermo Fischer Scientific, St. Leon-Rot
<i>Renilla</i> Luciferase Assay System	Promega GmbH, Mannheim

4.13. Consumables

Table 23: Utilized consumables

Name	Company
Adhesive PCR seal	Sarstedt AG & Co KG, Nümbrecht
μ-Dish with grid for tissue culture	IBIDI GmbH, Planegg
1.5 ml-reaction tubes RNase free	Sarstedt AG & Co KG, Nümbrecht
15 ml- and 50 ml-tubes (conical)	Greiner GmbH, Frickenhausen
2 ml-Eppendorf tube	Eppendorf AG, Hamburg
5 Prime Phase-Lock Tube	5Prime GmbH, Hilden
96 Fast PCR Plate half skirt	Sarstedt AG & Co KG, Nümbrecht
96-Well microtestplate conical bottom	Sarstedt AG & Co KG, Nümbrecht
Adhesive qPCR seal	Sarstedt AG & Co KG, Nümbrecht
Adhesive qPCR seal	Sarstedt AG & Co KG, Nümbrecht
Amersham Hyperfilm ECL	Geyer Th. GmbH & Co.KG, Renningen
Amersham Protran Premium Nitrocellulose membrane	Geyer Th. GmbH & Co.KG, Renningen
Art Tip (used for lipidomics)	Thermo Fischer Scientific, St. Leon-Rot

Beckmann Ultra-clear tube	Beckman Coulter GmbH, Krefeld
Biosphere Filter Tips	Sarstedt AG & Co KG, Nümbrecht
Blunt-end cannula	Kleiser Medical GmbH, Messkirch
Cell culture dishes	Sarstedt AG & Co KG, Nümbrecht
Cell culture flasks	Sarstedt AG & Co KG, Nümbrecht
Cell culture plates	Sarstedt AG & Co KG, Nümbrecht
Cell scraper	VWR International GmbH, Darmstadt
Cellstar serological pipettes	Greiner GmbH, Frickenhausen
Combitips advanced	Eppendorf AG, Hamburg
Cover slips	VWR International GmbH, Darmstadt
Cryo tubes	Sarstedt AG & Co KG, Nümbrecht
Electroporation cuvette 0.4 mm	VWR International GmbH, Darmstadt
Eppendorf Research plus pipettes	Eppendorf AG, Hamburg
Erlenmeyer flask	VWR International GmbH, Darmstadt
Glass flask	VWR International GmbH, Darmstadt
Glass slides	VWR International GmbH, Darmstadt
Luer-Lok syringe	BD Plastipak, Heidelberg
Microtest plate	Sarstedt AG & Co KG, Nümbrecht
Nunc-Immuno MicroWell 96 well polystyrene plates (white)	Thermo Fischer Scientific, St. Leon-Rot
Parafilm	Bemis, Oshkosh, USA
PCR tubes	Sarstedt AG & Co KG, Nümbrecht
Pipette tips	VWR International GmbH, Darmstadt
Pipette tips RNase free	Sarstedt AG & Co KG, Nümbrecht
Rotilabo liquid-reservoirs (sterile and non-sterile)	Roth GmbH + Co. KG, Karlsruhe
SafeSeal 1.5 ml-reaction tube	Sarstedt AG & Co KG, Nümbrecht
Steriflip 0.22 µm	Merck Millipore, Darmstadt
Sterile filter 0.22 µm	Fisher Scientific GmbH, Darmstadt
Syringe	neoLab GmbH, Heidelberg
Whatman paper	GE Healthcare, München

4.14. Devices

Table 24: Utilized devices

Device	Company
7500 fast real time PCR system	Applied Biosystems, Darmstadt
Agarose casting stand	BioRad Laboratories GmbH München
Agarose gel chamber comb	BioRad Laboratories GmbH München
Agilent 1100	Agilent Technologies, Santa Clara, USA
Apex Qe FT-ICR	Bruker Daltonics, Bremen, Germany
BD FACSCanto Flow Cytometer	BD Science, Heidelberg
BD LSR Fortessa flow cytometer	BD Bioscience, Heidelberg
Beaker 50- 1000 ml	VWR International GmbH, Darmstadt
Centrifuge 5424R	Eppendorf, Hamburg
Centrifuge 5810R	Eppendorf, Hamburg
Centrifuge Multifuge 3 SR	Thermo Fischer Scientific, St. Leon-Rot
Centrifuge Sorvall RC5C Plus	Thermo Fischer Scientific, St. Leon-Rot
Countess automated counter	Invitrogen AG, Carlsbad
GelDoc	BioRad Laboratories GmbH München
Gene Pulser Xcell electroporation system	Biorad GmbH, Munich
Hera freezer	Thermo Fischer Scientific, St. Leon-Rot
HERAsafe incubator	Thermo Fischer Scientific, St. Leon-Rot
Herasafe sterile bench	Thermo Fischer Scientific, St. Leon-Rot
Infinite M200 plate reader	Tecan Group Ltd, Männedorf
Leica DMIL microscope	Leica Camera AG, Wetzlar
Magnetic stirrer heating plate IKA RH basic	IKA®-Werke GmbH & CO. KG, Staufen
Micro centrifuge	Carl Roth GmbH, Karlsruhe
Mini Protean Tetra system	BioRad Laboratories GmbH München
Multipipette plus	Eppendorf AG, Hamburg
Nanodrop 1000 Spectrophotometer	Peqlab Biotechnologie GmbH, Erlangen
Neubauer Counting Chamber	Cellomics Technology, Halethopre (MD)
Nikon C2plus	Nikon, Düsseldorf

Nikon Eclipse Ti	Nikon, Düsseldorf
Optima ultracentrifuge	Beckman Coulter GmbH, Krefeld
Phenomenex Luna	Phenomenex Inc, Torrance, USA
Pipetboy	Integra Biosciences GmbH, Biebertal
Pipettes Research plus	Eppendorf AG, Hamburg
Pipettes Research plus	Eppendorf AG, Hamburg
Plan Apo VC 60x H Oil objective	Nikon, Düsseldorf
Plan Fluor 40x Air objective	Nikon, Düsseldorf
PM4600 DeltaRange	Mettler Toledo, Gießen
Q Exactive	Thermo Fischer Scientific, St. Leon-Rot
Q TOF Ultima	Waters, Milford, USA
Refractometer DR 201-95	Krüss GmbH, Hamburg
Tecnai G ² transmission electron microscope	FEI Company, Eindhoven, Netherlands
Thermomixer comfort	Eppendorf, Hamburg
UV Illuminator	VWR International GmbH, Darmstadt
Vortex-Genie 2	VWR International GmbH, Darmstadt
Water bath WBT-series	LTF Labortechnik, Wasserburg
Wide Mini Sub Cell GT	BioRad Laboratories GmbH München

4.15. Software

Table 25: Utilized software

Software	Company
7500 Software v2.3	Life Technologies Corporation 2014
AutoQuant X2	Media Cybernetics
BD FACSDiva 5.0.3	BD Science
BD FACSDiva 8.0.1	BD Science
Fiji/ ImageJ 1.48t	Wayne Resband, National Institutes of Health
FloJo 7.6.5	Tree Star Inc.
GraphPad Prism 5.0	GraphPad Software, Inc.

Imaris 7.6.4	Bitplane AG
LipidXplorer	Herzog et al. Genome Biology 2011
MassLynx 4.0 software package	Waters
Microsoft office	Microsoft
NIS-Element Viewer 4.2	Nikon
NIS-Element Ar 4.3	Nikonf
R Studio Version 0.99.484	R Studio, Inc.
Serial Cloner 2.6.1	Serial Basics Software

5. Methods

5.1. Molecular biology

5.1.1. Overlap-extension polymerase chain reaction and cloning of Jc1^{Flag-E2 NS5AB-EGFP}

The introduction of a Flag-tag to the envelope protein E2 was performed with an overlap extension polymerase chain reaction (overlap extension PCR). In the first step two PCRs were performed with pBR322 EGFP-Jc1 as template and either primer set 1 or primer set 2 (Table 5.3) as primers. The PCR mixture was used as described in Table 26 and the program run after Table 27.

Table 26: PCR mixture

Component	Volume
5x Phusion HF Buffer	10 μ l
10 mM dNTPs	1 μ l
Primer sense (10 μ M)	2.5 μ l
Primer antisense (10 μ M)	2.5 μ l
Template Plasmid	100 ng
Phusion DNA-Polymerase	0.5 μ l
ddH ₂ O	x μ l
Total volume	50 μ l

Table 27: PCR program

Cycle Step	Temperature	Time	
1. Initial Denaturation	98 °C	2'	
2. Denaturation	98 °C	10"	} 25 repeats
3. Annealing	55 °C	30"	
4. Extension	72 °C	45"	
5. Final Extension	72 °C	10'	
6. Hold	4 °C	forever	

After the PCR, 10 μ l of 6x DNA loading dye were added to the PCR mixture and subjected to agarose gel electrophoresis with a 1% agarose gel. The corresponding bands from primer set 1 and primer set 2 were excised and purified with the NucleoSpin Gel and PCR cleanup kit according to manufacturer's instructions and eluted in 22 μ l elution buffer. The DNA concentration was determined with a NanoDrop 1000. The next step was an overlap PCR to

merge the two PCR products. $\frac{1}{2}$ to $\frac{3}{4}$ of the overlap PCR reaction should contain equimolar amounts of the purified PCR products. The reaction mixture is described in Table 28 and the PCR program is shown in Table 29.

Table 28: Overlap PCR reaction

Component	Volume	
Product Primer set 1	x μ l	} Equimolar amounts of purified PCR-fragments; $\frac{1}{2}$ - $\frac{3}{4}$ of total volume
Product Primer set 2	x μ l	
5x Pfusion HF Buffer	10 μ l	
10 mM dNTPs	1 μ l	
Phusion DNA-Polymerase	0.5 μ l	
ddH ₂ O	x μ l	
Total volume	45 μ l	

Table 29: Cyclor program for overlap PCR

Cycle Step	Temperature	Time	
1. Initial Denaturation	98 °C	2'	
2. Denaturation	98 °C	10"	} 15 repeats
3. Annealing	60 °C	30"	
4. Extension	72 °C	45"	

Next, a purification PCR was performed by supplementation of 2.5 μ l of the outer forward primer BsiWI_J6 sense and 2.5 μ l of the outer reverse primer NS2_JFH1 Not. The PCR program is depicted in Table 30.

Table 30: Cyclor program for purification PCR

Cycle Step	Temperature	Time	
1. Initial Denaturation	98 °C	2'	
2. Denaturation	98 °C	10"	} 20 repeats
3. Annealing	60 °C	30"	
4. Extension	72 °C	45"	
5. Final Extension	72 °C	10'	
6. Hold	4 °C	forever	

The PCR mixture was subjected to a 1% agarose gel for electrophoresis and the PCR product purified with the NucleoSpin Gel and PCR cleanup kit and eluted in 20 μ l elution buffer.

The PCR product was cloned into pBR322 Jc1^{NS5AB-EGFP}. Therefore, the purified PCR product (insert) and the vector were digested with restriction enzymes after the NEB manufacturer's instructions as indicated in Table 31.

Table 31: DNA digestion with restriction enzymes

Component	Insert	Vector
DNA	0.1-0.5 μ g	1 μ g
10x NEB 3	2 μ l	2 μ l
10x BSA	2 μ l	2 μ l
NotI	1 μ l	1 μ l
ddH ₂ O	x μ l	x μ l
Total volume	20 μ l	20 μ l

After incubation for 1 h at 37 °C, 1 μ l BsiWI was added and further incubated for 1 h at 55 °C. The vector was dephosphorylated with 1 μ l CIP for 20 min at 37 °C. The digestion samples were supplemented with 4 μ l 6x DNA loading dye and subjected to electrophoresis with a 1% agarose gel. Afterwards, the corresponding bands were excised and purified the NucleoSpin Gel and PCR cleanup kit according to manufacturer's instructions. 15 μ l elution buffer were used for elution. The ligation was performed as described in Table 32. A negative control was performed without supplementation of the insert. The ligation was performed for 1h at room temperature.

Table 32: Ligation

Component	Volume
Linear vector	10-50 ng
Insert	3:1 or 5:1 molar ratio over vector
10x T ₄ -Ligase Buffer	1 μ l
T ₄ -Ligase	0.5 μ l
dH ₂ O	x μ l
Total volume	10 μ l

The transformation into DH5 α (Table 5) was performed with 5 μ l ligation and 50 μ l DH5 α . The mixture was incubated on ice for 30 min and a heat shock was performed for 20 sec at 42 °C. Afterwards, bacteria were incubated on ice for 2 min. 300 μ l pre-warmed LB medium were added and the bacteria shaken for 30 min at 37 °C with 350 rcf. The complete transformation samples were plated on LB-agar plates containing 100 μ g/ml ampicillin. The plates were incubated at 37 °C over night. The colonies were tested by colony-PCR and further analyzed by sequencing.

5.1.2. Colony PCR

The bacterial colonies were picked and dipped into an empty sterile PCR tube and further scratched on a LB-agar plate. 20 μ l of the PCR mixture (Table 33) were subjected to the PCR tubes and PCR was performed as described in Table 34. The PCR products were analyzed by agarose gel electrophoresis. Positive clones were verified by sequencing.

Table 33: PCR mixture for colony PCR

Component	1x
10x Taq Buffer KCl	2 μ l
10mM dNTP	0,4 μ l
fw Primer	1 μ l
rev Primer	1 μ l
25mM MgCl ₂	1,6 μ l
Taq Polymerase	0,1 μ l
ddH ₂ O	13,9 μ l
Total volume	20 μ l

Table 34: Cyclor program for colony PCR

Cycle Step	Temperature	Time
1. Initial Denaturation	95 °C	10'
2. Denaturation	95 °C	30"
3. Annealing	55 °C	30"
4. Extension	72 °C	1'
5. Final Extension	72 °C	10'
6. Hold	4 °C	

} 25 repeats

5.1.3. Agarose gel electrophoresis

Agarose gel electrophoresis was used to visualize DNA and RNA for size determination. 0.7-1% of agarose were dissolved in 1x TAE buffer by heating in a microwave. The agarose was supplemented with approximately 1 µg/ml EtBr. Samples were mixed with 6x DNA loading dye to a final concentration of 1 x DNA loading dye. As a marker 7 µl of GeneRuler DNA Ladder Mix were loaded for size determination. The electrophoresis was carried out in 1x TAE at 100 V for 30–40 min. The visualization was performed with a BioRad Gel Doc or a UV-table.

5.1.4. Miniprep

Plasmid isolation in a small scale was performed with a NucleoSpin Plasmid Kit. Therefore, 3–5 ml LB-medium containing 100 µg/ml ampicillin were inoculated with bacteria picked from a LB-agar plate or from glycerol stock. The bacteria were grown in a rotation shaker at 250 rpm and 37 °C over night. The plasmid extractions was performed according to manufacturer's instructions The DNA concentration was determined with a NanoDrop 1000.

5.1.5. Maxiprep

Plasmid isolation in a large scale was performed with the NucleoBond XtraMaxi Kit. Therefore, a pre-culture was made by inoculating 5 ml LB-medium containing 100 µg/ml ampicillin with bacteria from glycerol stock or a LB-agar plate. The pre-culture was incubated in a rotation shaker for 6–8 h at 37 °C and 250 rpm. The pre-culture was transferred to 250–300 ml LB medium with 100 µg/ml ampicillin and incubated over night at 37 °C in a rotation shaker at 250 rpm. The suspension was centrifuged for 15 min at 4221 x g and 4 °C. The next steps were performed after the manufacturer's instruction. Plasmid DNA was resuspended in 500–1000 µl TE-buffer or ddH₂O. The DNA concentration was determined with a NanoDrop.

5.1.6. Sequencing

Sequencing was performed at Eurofins MWG or GATC according to the companies' instructions.

5.1.7. Glycerol stocks

Bacteria were grown over night in LB-medium containing appropriate antibiotics in a rotation shaker at 250 rpm and 37 °C. 700 µl of bacterial suspension were mixed with 300 µl glycerol in a 1.5 ml-reaction tube and carefully vortexed. The glycerol stocks were stored at -80 °C.

5.2. Cell biology

5.2.1. Thawing of eukaryotic cells

Cells were thawed for approximately 1 min in a water bath at 37 °C and immediately transferred into 5 ml pre-warmed DMEM⁺⁺ or DMEM⁺⁺⁺ in a 15 ml-tube. After spinning the cells for 5 min, 290 x *g* at room temperature, the pellet was resuspended in 10 ml of DMEM⁺⁺ or DMEM⁺⁺⁺ and transferred into a 75 cm²-cell culture flask. Cells were cultured as described in 5.2.2.

5.2.2. Cell culture

Cells were cultured at 37 °C, 5% CO₂, and 95% relative humidity. The cells were kept in either DMEM⁺⁺⁺ or DMEM⁺⁺ and splitted every 3–4 days, when confluency was about 70–80%. Therefore, cells were washed once with DPBS and detached with trypsin/EDTA for 3–5 min at 37 °C. Afterwards, cells were splitted into new cell culture flasks in a 1:4–1:8 ratio, depending on the confluency. Used volumes are depicted in Table 35.

Table 35: Volumes utilized for cell culture

Component	75 cm ² -cell culture flask	175 cm ² -cell culture flask
DMEM ⁺⁺⁺ or DMEM ⁺⁺	10–15 ml	20–25 ml
DPBS	5 ml	5–10 ml
Trypsin/EDTA	1.5 ml	2.5 ml

5.2.3. Freezing of eukaryotic cells

When cells reached 70–80% confluence they were detached as described in 5.2.2. The cell number was determined by counting in a Neubauer counting chamber. The cells were centrifuged for 5 min, 290 x *g* at room temperature. The pellet was resuspended in freezing medium to a cell count of 1·10⁶ cells/ml and 1 ml of the cell suspension was transferred per cryovial. The cells were carefully frozen in a freezing container with a 1 °C/min cooling rate at -80 °C. Afterwards the cells were transferred into liquid nitrogen for long-term storage.

5.2.4. Electroporation of Huh7.5 cells with *in vitro* transcribed RNA

Huh7.5 cells were washed with DPBS and detached with trypsin/EDTA (see Table 35). They were resuspended in medium and counted with a Neubauer counting chamber. 4·10⁶ cells were centrifuged for 5 min, 290 x *g* at room temperature. Afterwards cells were washed in OPTI-MEM and resuspended in 400 µl cytomix containing ATP and glutathione. Cells were mixed with 10 µg *in vitro* transcribed HCV RNA and transferred into a 4 mm electroporation

cuvette. Electroporation was carried out in a BioRad electroporator with the setup shown in Table 36. The electroporated cells were immediately transferred into a 75 cm²-flask containing 10 ml of DMEM⁺⁺⁺ or DMEM⁺⁺. The medium was changed 4 h after electroporation.

Table 36: BioRad electroportator settings

Settings	
Voltage	260 V
Capacitance	950 μ F
Resistance	∞
Cuvette	4

5.2.5. HCV stock production

Huh7.5 cells were infected with supernatant from electroporated cells or virus stock. The supernatants were collected every 1–2 days for 1–2 weeks and kept at 4 °C until the last supernatants were taken. The supernatants were pooled in 50 ml-tubes and centrifuged for 5 min, 290 x *g* at room temperature. Afterwards supernatants were filtered in a Steriflip filter. 40% PEG was added to the supernatants to a final concentration of 10% PEG and mixed by inverting the tube and incubated at 4 °C overnight. The virus was concentrated by centrifugation for 45 min at 1270 x *g* and 4 °C. The supernatant was removed and the pellet resuspended in 200–300 μ l DMEM⁺⁺⁺. The resuspended pellets were pooled and mixed by pipetting. 150–200 μ l aliquots were stored in cryo vials at -80 °C.

5.2.6. Viral titer assay

8·10³ up to 1.4·10⁴ Huh7.5 RFP-NLS cells were seeded per well of a 96-well-plate. The virus stock was diluted from 10²–10⁷/10⁸ and 6 wells per dilution were infected with 100 μ l. The cells were fixed at 3–4 days post infection by the addition of 100 μ l 4% PFA. Cells were evaluated by fluorescence microscopy on a Nikon Eclipse Ti. Each well containing HCV positive cells, indicated by RFP in the nucleus, was marked as positive. Virus titer was calculated according to the Reed & Muench calculator by Brett Lindenbach (Lindenbach, 2009).

5.2.7. Production of lentivirus stocks and lentiviral transduction

5·10⁶ HEK293T cells were seeded per 15 cm-cell culture dish. Cells were transfected 1 day after seeding. The transfection mixture was prepared as described in Table 37.

Table 37: Transfection mixture

Component	Quantity
Transfer plasmid	20 µg
Packaging plasmid	15 µg
Envelope plasmid	6 µg
CaCl ₂ (2.5 M)	50 µl
ddH ₂ O	x µl
Total volume	500 µl

The transfection mixture was slowly dropped into 500 µl HBS under constant bubbling with air and further incubated for 25 min at room temperature. During the incubation time the medium of the HEK293T cells was replaced with 15 ml fresh DMEM⁺⁺/DMEM⁺⁺⁺ supplemented with 25 µM chloroquine. The transfection mixture/HBS was slowly dropped into the medium. The medium was replaced at 6–8 h post transfection with DMEM⁺⁺/DMEM⁺⁺⁺.

3 days post transfection the supernatant was centrifuged for 5 min and 1830 x *g* at room temperature to remove cell debris. The supernatant was filtered with a 0.22 µm sterile filter and further centrifuged for 2 h and 89.454 x *g* at 4 °C with a SW28 rotor in Beckmann Coulter ultracentrifuge. The supernatant was removed until approximately 1 ml was left in the Beckmann tube and the residual media was used to resuspend the lentiviral particles at the bottom of the tube. The concentrated lentivirus was aliquoted and stored at -80 °C.

The lentiviral transduction was performed in DMEM⁺⁺/DMEM⁺⁺⁺ supplemented with 4 µg/ml polybrene. The medium was changed the next day. The transduction efficiency was determined by titrating 2.5 µl to 50 µl to 3·10⁴ Huh7.5 cells. After 3 days the cells were fixed and analyzed by flow cytometry.

5.2.8. Flow cytometry

The cells were washed once with DPBS and detached with Trypsin/EDTA for approximately 5 min at 37 °C. The cells were resuspended in DMEM medium and centrifuged for 3 min and 153 x *g* at room temperature. The cell pellet was resuspended in DPBS and mixed 1:1 with 4% PFA/DPBS and vortexed. Fixation was carried out for at least 20–60 min at 4 °C. Flow cytometry was carried out on a BD Canto or BD LSRFortessa. The quantification was performed with FlowJo.

5.2.9. Surface receptor staining for flow cytometry

Cells were washed once with DPBS and detached with 0.5 mM EDTA/PBS at 37 °C for approximately 5 min. 0.5 ml DMEM⁺⁺ was added and cells scraped off with a cell scraper. After spinning for 5 min at 300 x *g* at room temperature the cells were washed once with DPBS containing 1% FCS. The pellet was resuspended in 100 µl primary antibody diluted in DPBS containing 1% FCS and incubated for 15 min at room temperature. The cells were washed once with DPBS containing 1% FCS. Next, the cells were incubated with 100 µl Alexa labeled secondary antibody diluted in DPBS containing 1% FCS for 15 min at room temperature in the dark. After one washing step the cells were fixed in DPBS mixed 1:1 with 4% PFA. The analysis was performed on a BD FACSCanto.

5.2.10. Cell viability assay

5·10³ Huh7.5 cells were seeded in a 96-well plate. The medium was exchanged with 100 µl DMEM⁺⁺⁺ supplemented with treatment compounds 4 h after seeding. 6 wells were analyzed per treatment condition. Treatment with 1 mM H₂O₂ or 5% DMSO served as negative control. At 3 or 5 days post treatment the cell viability was measured with the CellTiter 96® AQueous One Solution Reagent according to manufacturer's instructions. The absorbance was measured at 490 nm using a plate reader with several measurements in a time frame of 1–4 h. The values at 2–2.5 h were used for evaluation of cytotoxicity.

5.2.11. Luciferase assays to study HCV replication

5.2.11.1. Analyzing viral RNA replication and virus production in HCV-electroporated Huh7.5 cells

Huh7.5 cells were electroporated as described in 5.2.4. For these experiments 10 µg *in vitro* transcribed Jc1^{NS5AB-Fluc} RNA and 250 ng *Renilla* luciferase reporter plasmid pGL7.5 were co-electroporated. Two electroporations were pooled in 40 ml DMEM⁺⁺⁺ with a final concentration of 2·10⁵ cells/ml. Cells were seeded into 12-well plates with 2·10⁵ cells per well.

The electroporation control cells were lysed 4 h after electroporation. Therefore, the cells were washed once with DPBS and lysed by addition of 150 µl 1x Passive Lysis Buffer (Promega). After swinging the plate to distribute the lysis buffer it was stored at -20 °C until further analysis. The treatment of the remaining cells was started 4 h after electroporation and was performed in triplicates. Therefore, the supernatant was removed and each well received 1 ml of DMEM⁺⁺⁺ containing treatment compounds as described in Table 38. The treatment was renewed on day 3 post treatment when cells were treated for 5 days in total. After 3 and 5 days treatment the cells were lysed to study viral RNA replication and the

supernatants were used for infection of naïve Huh7.5 cells to study virus production. Lysis was performed as described above for the electroporation control. The supernatants were transferred to 1.5 ml-reaction tubes and centrifuged for 3 min at $153 \times g$ and room temperature. 800 μ l of the supernatant were transferred to a 12-well plate with naïve Huh7.5 cells. These cells had been seeded the day before with $1 \cdot 10^5$ cells/well. The medium was changed 3 h post infection and cells were lysed 2 days post infection as described above. For the measurement plates were thawed and incubated for 1 h at room temperature. The cells were resuspended by pipetting up and down. Lysates were transferred into a 96-well plate with a conical bottom, centrifuged for 2 min at $290 \times g$ and $4 \text{ }^\circ\text{C}$, and lysates were transferred into a new 96-well plate with a conical bottom. The luciferase assay was performed according to manufacturer's instructions in a white 96-well plate. The electroporated cells were analyzed with the Dual-Luciferase® Reporter Assay System and infected cells with the Luciferase Assay System. The injection and luminescence measurement were performed in a Tecan plate reader.

Protein concentration in the lysate was determined with the Coomassie plus protein assay. Therefore 5 μ l of lysate were incubated with 150 μ l Coomassie plus reagent for 10 min. Lysates of infected cells were diluted 1:2 in Passive Lysis Buffer and lysates from treated cells were used undiluted. The albumin standard provided by the supplier was diluted as well in 1x Passive Lysis Buffer. Absorption was measured at 595 nm. Each sample was measured in duplicates.

Relative light units (RLU) from the luciferase assay were normalized with the corresponding protein concentrations. The triplicate values were averaged and normalized to the mock-control.

Table 38: Treatment components used for Luciferase assays in HCV-electroporated cells

Treatment	Stock concentration	Dilution	Final concentration
Ethanol/albumin (mock)		1:20	
Lauric acid/albumin	2 mM	1:20	100 μ M
Myristic acid/albumin	2 mM	1:20	100 μ M
Palmitic acid/albumin	2 mM	1:20	100 μ M
Stearic acid/albumin+ Ethanol/albumin	2 mM	1:200 1:22	10 μ M
Oleic acid/albumin	2 mM	1:20	100 μ M
Linoleic acid/albumin	2 mM	1:20	100 μ M
α -Linolenic acid/albumin	2 mM	1:20	100 μ M

γ -Linolenic acid/albumin	2 mM	1:20	100 μ M
Arachidonic acid/albumin + Ethanol/Albumin	2 mM	1:40 1:40	50 μ M
Eicosapentaenoic acid/albumin	2 mM	1:20	100 μ M
Docosahexaenoic acid/albumin+ Ethanol/albumin	2 mM	1:200 1:22	10 μ M
Cholesterol + Ethanol/albumin	5 mM	1:500 1:20	10 μ M
Cholesterol + Ethanol/albumin	5 mM	1:100 1:20	50 μ M
Cholesterol + Ethanol/albumin	5 mM	1:50 1:20	100 μ M
DMSO (mock)		1:1000	
SC-26196	2 mM	1:1000	2 μ M
SC-26196	0.1 mM	1:1000	0.1 μ M

5.2.11.2. Analyzing viral RNA replication and virus production in Huh7.5 cells with an established HCV infection

For infection $6 \cdot 10^5$ Huh7.5 cells were seeded into a 75 cm²-cell culture flask. Cells were infected at the same day or the day after with Jc1^{p7-GLuc-2A}. The luciferase assay was started 7–18 days post infection. For analyzing the effect of SC-26196 on an established HCV infection, $1 \cdot 10^5$ infected cells were seeded per well of a 12-well plate and treatment was started 4 h post seeding. The treatment was prepared in DMEM⁺⁺ as described in Table 39. The supernatant was removed from the cells and cells were washed once with DPBS before 1 ml of treatment compound was added. Each treatment was performed in triplicates.

Table 39: Treatment components for FADS2 inhibition

Treatment	Stock concentration	Dilution
DMSO		1:500
4 μ M SC-26196	2 mM	1:500
2 μ M SC-26196	2 mM	1:1000
DMSO		1:1000
0.1 μ M SC-26196	100 μ M	1:1000
DMSO		1:1000

3 days post treatment the supernatants were transferred into 1.5 ml-reaction tubes and centrifuged for 3 min, 153 g, room temperature. 800 μ l of the supernatants were transferred into a new 1.5 ml-reaction tube and stored at 4 °C. The cells were washed once with DPBS and the treatment was renewed. The supernatants were taken again at 5 days post treatment as described above. The supernatants were stored at 4 °C for a maximum of 6 days or kept at -20 °C before lysis for the luciferase assay. $1.3 \cdot 10^4$ Huh7.5 cells were seeded per well of a 96-well plate the day before infection. For infection the supernatants were diluted 1:10 in DMEM⁺⁺ and 100 μ l were transferred per well of a 96-well plate. The infection was performed in duplicates. 3 h after infection the medium was changed and cells were incubated for 2 days. Afterwards 50 μ l supernatant from treated cells (stored at 4 °C) or infected cells were mixed with 50 μ l 2x *Renilla* Luciferase Assay Lysis Buffer and incubated for 1 h at room temperature. Lysates were directly measured or stored at -20 °C. The measurement was performed with *Renilla* Luciferase assay system. For measurement 10 μ l of lysate were transferred into a white 96-well plate and 50 μ l of *Renilla* Luciferase substrate were injected per well and bioluminescence was measured by using the Tecan plate reader. Each treatment was performed in triplicates. The triplicates were averaged and normalized to the mock-control DMSO.

5.2.11.3. SC-26196 pretreatment and analysis of early steps in the viral life cycle

Huh7.5 cells were seeded in a 12-well plate with $5 \cdot 10^4$ cells/well. 4 h after seeding cells were treated as specified in Table 39. Cells were infected 1 day post treatment with an MOI = 1 or 3 days post treatment cells with an MOI = 0.5 of Jc1^{p7-GLuc-2A} for 3 h. Cells were washed once with DPBS and 1 ml fresh medium was added. 1 day post infection 50 μ l supernatant of each sample was lysed with 50 μ l 2x *Renilla* Luciferase Assay Lysis Buffer. Luciferase measurement was performed as described 5.2.11.2.

5.2.11.4. Analysis of HCV replication in knockdown cells

The impact of desaturase and elongase downregulation on HCV replication and virus production were assessed with luciferase assays. $2 \cdot 10^5$ Huh7.5 cells per 6-well plate were transduced with lentiviral stocks 5–6 h after seeding. 3 days after transduction $5 \cdot 10^4$ Huh7.5 cells were seeded per 12-well. The cells were infected with Jc1^{p7-Gluc-2A} with an MOI of 0.5. The cells were washed once with DPBS 3 h post infection and supplemented with 1 ml of DMEM⁺⁺⁺.

Viral replication was analyzed after 1, 3, and 5 days post infection. The samples from day 1 were immediately lysed 2x *Renilla* Luciferase Assay Lysis Buffer. On day 3 and 5 the complete supernatant was removed from the cells, centrifuged for 5 min at 153 x g, room

temperature. The supernatants were transferred to a new tube and stored at 4 °C until lysis or infection of uninfected Huh7.5 cells to study virus production. Therefore, $1.3 \cdot 10^4$ Huh7.5 cells were seeded per well of a 96-well plate 1 day prior infection. The supernatants taken on 3 and 5 days post infection were diluted 1:10 and 100 μ l were added to the naive Huh7.5 cells. 3 h after infection the medium was changed and cells were incubated for 2 days. 40 μ l of supernatant were as well mixed with 40 μ l of 2x *Renilla* Luciferase Assay Lysis Buffer. The measurement was performed as described in 5.2.11.2.

5.2.12. Gradient centrifugation

$3 \cdot 10^5$ – $5 \cdot 10^5$ HCV-infected Huh7.5 cells were seeded per 6-well or $1.6 \cdot 10^6$ cells per 10 cm-cell culture dish. 4 h after seeding the cells were washed once with DPBS and received 2 ml or 10 ml DMEM⁺⁺ containing treatment, respectively. The 100 μ M lauric acid and 4 μ M SC-26196 treatment was prepared as described in Table 38 and Table 39. The treatment was renewed at day 3 post treatment. On day 5 the supernatants were harvested, centrifuged for 5 min at $153 \times g$, room temperature. The supernatants from the 10 cm-cell culture dish were precipitated with PEG as described in 5.2.5 and the pellet was resuspended in 1.4 ml DMEM⁺⁺. The supernatants from 6-well plates were filtered with a 0.22 μ m filter. 1 ml supernatant or concentrate were transferred to an iodixanol gradient in 14 x 89 mm ultracentrifugation tubes and centrifuged for 16 h at 34.500 rpm and 4 °C in a Beckmann Coulter ultracentrifuge using a SW40-Ti rotor. The acceleration was set to maximum and the deceleration was reduced.

Gradients were harvested by taking the first 15 fractions à 500 μ l from the top of the gradient and transferring them into RNase-free tubes. 150 μ l of the fraction were transferred into a new tube and the viral titer and density of the fractions were determined. Other fractions were kept at -80 °C for RNA isolation. For the titer assay, $3 \cdot 10^3$ Huh7.5 RFP cells were seeded in a 96-well plate in DMEM⁺⁺⁺ one day prior to infection. Fractions were diluted 1:10–1:10⁵ and input was diluted 1:10–1:10⁶. For each dilution 3 wells were infected. Titer cells were fixed with 100 μ l 4% PFA 4 days after the infection. The evaluation was performed as described in 5.2.6. The refraction index (RI) was measured with a refractometer and densities were calculated.

RNA isolation was performed with the Nucleospin RNA Virus kit. 600 μ l RAV1 with carrier were provided in RNase-free tubes and 150 μ l of fraction were added, vortexed, and transferred into new RNase-free tubes. Samples were incubated for 1 h on ice. Further steps were performed according to manufacturer's instructions.

5.2.13. Preparation of samples for lipidomic analysis

$6 \cdot 10^5$ or $2 \cdot 10^6$ Huh7.5 cells were seeded in 75 cm²- or 175 cm² tissue culture flasks, respectively. Two flasks were seeded for each experiment and after 1 day cells of one flask were infected with an MOI of 0.03–0.5 of Jc1^{Flag-E2 NS5AB-EGFP} while a second flask remained uninfected as control. 4–8 days after infection similar amounts of infected and uninfected cells were seeded for the experiment. For seeding the cells were washed with DPBS and incubated for 5 min at 37 °C with trypsin/EDTA. Cells were resuspended in 10 ml DMEM⁺⁺⁺ and transferred into a 50 ml-tube and cells were pooled. After spinning at 301 x *g*, room temperature for 3 min, the supernatant was discarded and cells resuspended in 20 ml medium. For cell counting a 30 µl aliquot was fixed with 30 µl 4% PFA for 5 min at room temperature, stained with trypan blue, and counted in a Neubauer counting chamber. Jc1^{Flag-E2 NS5AB-EGFP}-infected and uninfected Huh7.5 cells were seeded as follows: 175 cm²-cell culture flasks with $4 \cdot 10^6$ cells, 75 cm²-cell culture flasks with $1.7 \cdot 10^6$ cells or 15 cm-cell culture dishes with $4 \cdot 10^6$ cells. In each experiment flasks or dishes containing only DMEM⁺⁺⁺ were treated in a similar manner and were used as background control. 2 days after seeding the cells were harvested. Therefore, cells were washed once with DPBS and detached by incubation for 5 min at 37 °C with accutase. After resuspending the cells in 5–15 ml DMEM⁺⁺⁺, cells were pooled, samples were mixed by pipetting and kept on ice until further processing. To analyze the percentage of infected cells 500 µl of the sample were fixed with 4% PFA at a final concentration of 2% for flow cytometry. For cell counting 25 µl of cells were fixed with 25 µl 4% PFA for 1 h at room temperature and cell number was determined with a Countess automated cell counter (Life Technologies). Therefore, 20 µl of fixed cells were stained with 20 µl trypan blue and 9–10 µl were filled to a Countess counting chamber slides. Each sample was counted twice. $6 \cdot 10^5$ or $8 \cdot 10^6$ cells of each sample were transferred into a 2 ml-Eppendorf tube and centrifuged for 5 min, 153 x *g* at 4 °C. One sample was resuspended in 500 µl RNA-Stat60 reagent for RNA isolation. Other samples were washed twice with DPBS and cell pellets were stored at -80 °C until lipids were extracted after acidified Bligh & Dyer.

5.2.14. Lipid droplet isolation for lipidomics

Huh7.5 cells were infected with an MOI of 0.1 of Jc1^{Flag-E2 NS5AB-EGFP}. $2 \cdot 10^6$ of infected and uninfected Huh7.5 cells were seeded in 15 cm-dishes 6–7 days post infection. 15 cm-dishes containing only medium were used as background control. At the time point of seeding, cells were fixed for flow cytometry to analyze the infection rate. At day 1 after seeding the cells were washed twice with 5 ml DPBS and additional 5 ml DPBS remained on the cells for harvesting with a cell scraper. Cells were pooled in a 50 ml-tube and remained on ice. 50 µl of cells were fixed with 40 µl 4% PFA for 1 h at room temperature, mixed 1:2 with trypan blue

and counted with the Countess automated cell counter. Equal numbers of uninfected and infected cells, as well as a medium control, were centrifuged for 5 min at 200 x *g* and room temperature. The cell pellet was resuspended in 500 µl hypotonic buffer and lysed in a Dounce homogenizer by approx. 200 strokes (or 5–10 min). Cell lysis was confirmed by trypan blue staining. The cell lysates were centrifuged for 10 min at 500 x *g* and 4 °C and transferred into an ultracentrifugation tube. 50 µl of the sample were stored at -20 °C as input control. These samples were later on mixed with 25 µl 6x Laemmli buffer. 450 µl of 1.05 M sucrose were added to the lysates and overlaid with isotonic buffer. After centrifuging for 2 h at 100,000 x *g* and 4 °C, the lipid droplets were transferred into a 2 ml-Eppendorf tube using a bended syringe. The samples were centrifuged for 20 min at 20000 x *g* and 4 °C and the underlying buffer was removed until the total volume was around 100 µl. LDs were stored at -80 °C and lipid extraction was performed according to acidified Bligh & Dyer.

5.3. Biochemical methods

5.3.1. RNA *in vitro* transcription

16 µg of the HCV plasmid were linearized with 1 µl SspI or MluI for 2 h or overnight at 37 °C. This was followed by a phenol/chloroform extraction using phase-lock tubes as described in 5.3.2. In case of digestion with MluI it is necessary to remove the sticky ends with a MungBean digestion. Therefore, 2 µl of MungBean nuclease, 5 µl of 10x MungBean nuclease buffer, and 45 µl digested plasmid were incubated for 30 min at 30 °C. Afterwards a second phenol-chloroform extraction was performed. The linearization was controlled on a 0.7–1% agarose gel, as linearized plasmids migrate slower than supercoiled and faster than nicked plasmids. The *in vitro* transcription was performed with the MegaScript T7 kit according to manufacturer's instructions. An RNA aliquot was diluted 1:10 to determine the RNA concentration with a NanoDrop and the quality of the RNA by electrophoresis on a 1% agarose gel. RNA aliquots containing 10 µg RNA were stored at -80 °C.

5.3.2. Phenol/chloroform extraction using 5 Prime Phase Lock Gel tube

The 5 Prime Phase Lock Gel Heavy 2 ml Tube was centrifuged for 30 sec and 12000 x *g* at room temperature. 1 volume of sample was transferred to the tube and mixed 1:1 with phenol:chloroform:isoamylalcohol and mixed by flicking the tube. After centrifugation for 15 min and 12000 x *g* at room temperature 1 volume chloroform was added and mixed by flicking the tube. After centrifugation for 5 min and 12000 x *g* at room temperature the aqueous sample was transferred into a 1.5 ml-reaction tube and supplemented with 1/10 vol 3M sodium acetate and 2.5x volumes 99.5% Ethanol. The mixture was incubated for 5 min at room temperature and centrifuged for 20 min and 12000 x *g* at 4 °C. The supernatant was

discarded and the pellet washed with 500 μ l 70% Ethanol. After centrifugation for 15 min and 12000 \times g at 4 $^{\circ}$ C the supernatant was discarded and the pellet dried at room temperature. The pellet was resuspended in nuclease free water or TE-buffer.

5.3.3. RNA isolation with TriReagent/Stat60

Medium was removed from the cells and 1 ml TriReagent/Stat60 was added and mixed by pipetting. Lysates were transferred to a 1.5 ml-reaction tube and stored at -80 $^{\circ}$ C or immediately used for extraction. Therefore 200 μ l chloroform were added and the tube inverted for 15 sec. After 3 min incubation at room temperature the samples were centrifuged for 15 min at 12000 \times g and 4 $^{\circ}$ C. The upper phase was transferred into a new 1.5 ml-reaction tube. 500 μ l isopropanol were added, mixed by inverting and incubated for 10 min at room temperature. Centrifugation was performed for 10 min at 1200 \times g and 4 $^{\circ}$ C and supernatant was drained. The pellet was washed with 1 ml 75% Ethanol and centrifuged for 5 min at 7500 \times g and 4 $^{\circ}$ C. The supernatant was drained and residual liquid was removed by pipetting. The pellet was dried for 10–15 min and resuspended in 18 μ l dH₂O. To remove DNA 1.8 μ l 10x rDNase Buffer and 1 μ l rDNaseI were added and incubated for 30 min at 37 $^{\circ}$ C. After adding 1.8 μ l DNase inactivator, samples were incubated for 2 min at room temperature and afterwards centrifuged for 1.5 min at 1000 \times g and room temperature. The supernatant was transferred into a fresh 1.5 ml-reaction tube and the concentration was measured with a Nano-Drop. The RNA was stored at -80 $^{\circ}$ C.

5.3.4. cDNA synthesis

The RNA was reverse transcribed into cDNA by supplementing the reagents depicted in Table 40. The reaction mixture was incubated for 1 min on ice, 5 min at 65 $^{\circ}$ C and 5 min at 4 $^{\circ}$ C in a PCR cycler.

Table 40: Reaction mixture for cDNA synthesis

Component	Quantity
RNA	1 μ g
dNTP (10 mM)	1 μ l
Random hexamer primer (1:10)	1 μ l
ddH ₂ O	x μ l
Total volume	14 μ l

Afterwards the components listed in Table 41 were added to the reaction mixture and incubation was performed for 5 min at 25 $^{\circ}$ C, 60 min at 50 $^{\circ}$ C and 15 min at 70 $^{\circ}$ C. The cDNA was stored at -80 $^{\circ}$ C.

Table 41: cDNA synthesis reaction mixture

Component	Quantity
5x First-Strand Buffer	4 μ l
SuperScript III reverse transcriptase	0.5 μ l
RNaseOut	0.5 μ l
DTT (0.1 M)	1 μ l

5.3.5. HCV PCR standard preparation

To prepare a qPCR standard 1 μ g of *in vitro* transcribed Jc1 RNA was synthesized into cDNA as described in 5.3.4. The cDNA standard diluted from 1:10² to 1:10⁸. From each dilution 1 μ l was used for qPCR corresponding to 0.01–10000 pg RNA per qPCR reaction.

5.3.6. Real-time quantitative PCR

The real-time quantitative PCR (qPCR) was performed with 10 μ l 2x SYBRGreen, 0.04 μ l ROX (5 μ M), 0.6 μ l qPCR-primer mix, 8.34 μ l ddH₂O and 1 μ l cDNA were mixed per well of a 96-well plate. The measurement was performed on a 7900HT Fast Real-Time PCR System.

5.3.7. Coomassie staining

Lysates were supplemented with 6x Laemmli buffer to a final concentration of 1x Laemmli buffer and heated for 5 min at 95 °C. The samples and 3 μ l PageRuler ladder were subjected to SDS-PAGE with a 12% polyacrylamide gel. The Coomassie staining was performed with Coomassie staining buffer at room temperature, over night. To destain the gel was incubated in Coomassie destain buffer at room temperature, over night. Images of the gel were acquired on a BioRad Gel Doc.

5.3.8. Silver staining

Lysates were supplemented with 6x Laemmli buffer to a final concentration of 1x Laemmli buffer and heated for 5 min at 95 °C. The samples and 3 μ l PageRuler marker were loaded on a 12% polyacrylamide gel. The SDS-PAGE was performed in running buffer and started at 200 V for at least 10 min. The polyacrylamide gel was fixed in fixation solution for 1 h and afterwards washed in washing solution three times for 10 min. This was followed by a 1 min incubation in pretreatment solution. The polyacrylamide gel was washed twice for 30 sec with tap water and incubated for 20 min in impregnate solution. After washing twice with tap water for 30 sec the development solution was added for 3–10 min, depending on the amount of protein. When bands appeared, the reaction was stopped by washing twice for 2 min with tap

water and incubation for 10 min with stop solution. All steps were performed at room temperature on a shaker. After washing with washing solution the gel was stored. Images of the gel were acquired on a BioRad Gel Doc.

5.3.9. Western blot

8–25 µg protein were used to perform an SDS-PAGE with a 12% polyacrylamide gel. The electrophoresis was performed at 200 V for at least 10 min and the electrophoresis was completed when the bromphenol blue reached the bottom of the polyacrylamide gel, but was still visible. The proteins were blotted to a nitrocellulose membrane for 90 min at 80 V using a wet blot system. The membrane was incubated with Ponceau staining for approximately 30 sec. The membrane was washed with tap water and scanned. The Ponceau was removed by washing with TBS-T. Afterwards the membrane was incubated with blocking buffer for 1 h at room temperature. Next, the primary antibody was subjected to the membrane over night at 4 °C or for 1 h at room temperature. Afterwards the membrane was washed in TBS-T for at least 45 min with exchanging TBS-T several times. The incubation with the secondary HRP-linked antibody was carried out for 1 h at room temperature. For detection, ECL Lumi-light or SuperSignal West Femto were incubated for 1 min with the membrane and signals were exposed to an ECL Hyperfilm. Development was performed with a GE StrucutrixM Eco developer.

5.3.10. Lipid extraction, shotgun lipidomics and free fatty acid measurement

The lipid extraction was performed according to acidified Bligh & Dyer (Weerheim et al., 2002). 320 µl ice cold chloroform and 640 µl ice cold acidic acid (3% in methanol, 0.3 µg/ml butylated hydroxytoluene) were added to the cells and vortexed for 10 sec, inverted, and the samples were incubated for 1 h at room temperature in the dark. 320 µl H₂O were added to the samples, vortexed for 10 sec, and incubated for 5 min at room temperature. Afterwards samples were centrifuged for 10 min, 3700 x g at 4 °C, and the organic phase was transferred into a new 2 ml-Eppendorf tube. The aqueous phase was mixed again with 320 µl chloroform and incubated for 20 min at room temperature. During incubation the samples were vortexed twice for 10 sec. The organic phase was pooled with the previous organic phase and the purification step was performed for 3 times in total. The pooled organic phases were centrifuged for 10 min, 15000 x g at 4 °C and transferred into a new 2 ml-Eppendorf tube to remove residual water. The organic phases were stored at -80 °C. For protein isolation the aqueous phase was mixed with 320 µl acidic acid (3% in Methanol, 0.3 µg/ml BHT) and vortexed for 10 sec. Samples were centrifuged for 5 min, 15000 x g at room temperature. The supernatant was discarded and pellets dried for 1 h at room temperature. Pellets were resuspended in 100–300 µl of SDS-lysis buffer vortexed, and incubated for 1–

12 h at 50 °C and 750 rpm in a ThermoMixer. Proteins were used for Coomassie staining or silver staining and western blotting.

The lipidomic and free fatty acid analysis was performed by the group of Dominik Schwudke (Bioanalytical Chemistry, Research Center Borstel). Prior to mass spectrometry, 25 µl AA-d11, which served as standard for the free fatty acid measurement, were added to the samples. The solvent was evaporated under a nitrogen stream at room temperature and the dried lipids were resuspended in 250 µl chloroform/methanol (1/2; v/v). 50-70 µl of the samples were diluted 1:10 in MS-Mix (chloroform/0.5mM ammoniumchloride in methanol/isopropanol; 1/2/4; v/v/v) for shotgun lipidomics. The residual samples were dried under nitrogen stream and resolved in water/acetonitrile/1M ammonium acetate pH=5.5 (59/40/1; v/v/v) for analysis of free fatty acids. The analysis of phosphatidylcholines, diglycerides, triglycerides, and cholesteryl ester was performed in the positive ion mode.

The lipid analysis was performed using an Agilent 1100 for flow injection and either a Q Exactive Plus or an Apex Qe FT-ICR with electrospray ionization (ESI) for tandem mass spectrometric analysis. The lipidomics screening approach (Schwudke et al., 2007; Schwudke et al., 2011) was applied where lipids were identified on basis of accurate masses using the LipidXplorer software (Herzog et al., 2011). The mol-percentage (mol%) of each lipid species in a lipid class was calculated and normalized according the most abundant species in uninfected samples.

Free fatty acids were analyzed by liquid chromatography-tandem mass spectrometry (LC-MS/MS) on an Agilent 1100 micro-LC system using a Phenomenex Luna C18 HPLC column. Tandem mass spectrometric experiments were performed using a Q-ToF Ultima (Waters, Milford, USA) with electrospray ionization (ESI). The complete analysis including data acquisition and quantitation was performed with MassLynx 4.0 software package.

5.3.11. Metabolite extraction and analysis

$1.5 \cdot 10^4$ Jc1^{NS5AB-EGFP}-infected or uninfected cells were seeded per 10 cm-cell culture dish. Plates containing only DMEM⁺⁺⁺ were used as background control. 2 days after seeding the cells were washed twice with 4 ml DPBS and scratched in 300 µl DPBS. After spinning for 5 min at 153 x g and 4 °C the supernatant was removed and ice cold methanol/chloroform/H₂O (1/1/0.1; v/v/v) was added. The mixture was vortexed for 15 sec and incubated for 1 h with shaking at 300 rpm and 21 °C in a ThermoMixer. After centrifugation for 5 min at 5725 x g and 4 °C, the supernatant was transferred into a new 2ml-Eppendorf tube and kept on ice. 400 µl ice cold methanol/chloroform/H₂O were added to the pellet, vortexed for 15 sec and incubated for 30 min at 300 rpm and 4 °C in a ThermoMixer. The centrifugation was carried out for 10 min at 13000 x g and 4 °C. The supernatants were pooled and again centrifuged for 10 min at 13000 x g and 4 °C to remove contaminating protein. The supernatant was

evaporated under liquid nitrogen stream at room temperature. Dried lipid extracts were stored at -80 °C.

The protein pellet was dried for 50 min at room temperature and resuspended in 150 µl SDS-lysis buffer. After the incubation of minimally 60 min at 50 °C, 750 rpm in a ThermoMixer the protein quantity was determined with a DC protein assay according to manufacturer's instructions.

The metabolomic analysis was performed by BIOCRATES Life Sciences. The dried samples were resuspended in Ethanol/phosphate buffer to a concentration of 10 µg/µl total protein, processed, and subjected to mass spectrometry by usage of an AbsoluteIDQ® p180 Kit assay (Biocrates Life Science AG). The analysis was performed by FIA-MS/MS or LC-MS/MS on a Thermo TSQ or SCIEX 4000 QTRAP® with ESI.

5.3.12. Bligh & Dyer lipid extraction for triglyceride measurement

Huh7.5 cell, either naïve or HCV-infected at 6–12 days post infection, were seeded at $4 \cdot 10^5$ cells per well of a 6-well plate. 4 h after seeding the cells were treated with 2 ml DMEM⁺⁺ or DMEM⁺⁺⁺ containing 0.1 mM fatty acids for 24 h. Afterwards cells were washed twice with DPBS and stored at -80 °C. The extraction was performed after the Bligh and Dyer method. Here, 600 µl methanol were added per well and cells were scraped off with a cell scraper and transferred into a 2 ml-Eppendorf reaction tube. Afterwards 300 µl chloroform were added and vortexed for 10 sec. After 1 h incubation time at room temperature, 300 µl ddH₂O was added. Afterwards the lipids were further extracted according to two variants of the Bligh & Dyer method.

Variant 1: The mixture was vortexed for 10 sec and incubated for 5 min at room temperature. Afterwards samples were centrifuged for 10 min, 3700 x *g* at 4 °C and the organic phase was transferred into a new 2 ml Eppendorf tube. The aqueous phase was mixed again with 300 µl chloroform and incubated for 20 min at room temperature. During incubation the samples were vortexed twice for 10 sec. The organic phase was pooled with the previous organic phase and the purification step was performed for 3 times in total. The pooled organic phases were centrifuged for 10 min, 15000 x *g* at 4 °C and transferred into a new Eppendorf tube to remove residual water.

Variant 2: The mixture was vortexed for 10 sec and incubated for 30 min at 300 rpm and 20 °C in a ThermoMixer. Afterwards the phases were separated by centrifugation for 10 min at 13500 x *g* and 4 °C. The organic phase was transferred into a new 2 ml-Eppendorf tube. The aqueous phase was again extracted with chloroform and the organic phases were pooled.

The organic phase was transferred into a glass tube and supplemented with 50 µl chloroform containing 5% Triton-X. The solvent was evaporated under a nitrogen stream at 50 °C and

the lipids were resolved in 100 μl ddH₂O. This results in a final concentration of 2.5% Triton-X, thus when less ddH₂O was used for resuspension the amount of Triton-X needed to be adjusted. The triglyceride assay was performed with the Infinity Triglyceride Reagent. The glycerol standard spanned concentrations from 0.0625 mg/ml to 2.5 mg/ml in ddH₂O. 1.5 μl Standard or 20–30 μl lipid extract were mixed with 150 μl Infinity Triglyceride Reagent in a 96-well plate and were incubated for 30 min at 37 °C. The absorbance was measured in a Tecan plate reader at 570 nm.

5.4. Microscopic analysis

5.4.1. Determination of z-elongation factor

An elongation to the z-axis occurs due to the different refractive indices of oil and mowiol. Therefore, nano beads of a certain size were measured to determine the elongation factor. 2–5 μl of PS-speck nano beads (green) were placed on a cover slip, dried and embedded with mowiol/DAPCO on a microscopy slide. The measurement was performed with a Nikon C2plus confocal microscope containing four different lasers (405 nm diode laser; 488 nm DPSS laser; 543 nm HeNe laser; 642 nm diode laser) using a Plan Apo VC 60x H oil objective. The z-sections had a distance of 0.05 or 0.1 μm . The quantification was performed with Imaris. Therefore, a 3D reconstruction of the stacks was performed and the diameter of the nano beads was determined in y-, x-, and z-direction. 13–19 beads were analyzed in one image. The average diameter in y-, x-, and z-direction, designated as $av\text{-}y$, $av\text{-}x$, and $av\text{-}z$, was calculated for the nano beads in of one image. The z-elongation factor was then determined as follows: $av\text{-}z/[(av\text{-}x+av\text{-}y)/2]$. Finally, the average of the elongation factors from 6 different images was calculated, resulting in 1.98, which was further used as elongation factor.

5.4.2. Microscopy and volumetric analysis of lipid droplets

Uninfected and Jc1^{Flag-E2}-infected Huh7.5-RFP-NLS cells were mixed 1:1 and a total of $8 \cdot 10^4$ cells were seeded per well of a 6-well plate containing cover slips. 1 day after seeding the cells were fixed by supplementation of 16% PFA to a final concentration of 3.2% PFA. After incubation for 1 h at room temperature the cells were washed twice with DPBS. The staining was performed with Bodipy and Hoechst for 30 min at room temperature in the dark. Afterwards the cells were washed three times with DPBS and shortly dipped into ddH₂O. The coverslips were embedded in mowiol/DAPCO on a microscopy slide. The microscopic analysis was performed on a Nikon C2plus confocal scanning microscope containing four different lasers (405 nm diode laser; 488 nm DPSS laser; 543 nm HeNe laser; 642 nm diode laser) with a Plan Apo VC 60x H oil objective. 3D stacks were recorded with slices in 0.15 μm

distance. The images were deconvoluted with 75 iterations and a high noise level with AutoQuant X2. The volumetric analysis was performed using Imaris software. The z-length was reduced by the determined elongation factor to 0.076 μm . A surface was generated for the cell of interest. Therefore, a region of interest was determined. The smoothing parameter was set to 0.06 and the intensity threshold was reduced to approximately 1/3 of the highest intensity. All lipid droplets with a size below 0.068 had to be excluded. This was determined by the minimal resolution at an emission wavelength of 514 nm when using a 514/30 nm LSM filter. Imaris generated the lipid droplet volume for each lipid droplet. The average lipid droplet volume was calculated, as well as the total number of lipid droplets per cell and the total lipid droplet volume per cell.

5.4.3. Microscopy analysis of unesterified cholesterol

Huh7-lunet RFP-NLS transduced cells were infected with Jc1^{Flag-E2} for 5 days. $8 \cdot 10^4$ cells were seeded per 6-well containing cover slips. Cells were fixed with 16% PFA at a final concentration of 3.2% PFA for 1 h at room temperature 2 days after seeding. Cells were washed three times with DPBS, stained with Filipin III or co-stained with Filipin III and Bodipy for 1 h at room temperature. After washing with DPBS three times and shortly in ddH₂O, the coverslips were embedded in mowiol on a microscopy slide. The microscopic analysis was performed on a Nikon C2plus confocal microscope and a 60x oil objective. The analysis was performed with Fiji. Therefore, a region of interest was manually drawn to mark the nucleus and a 20 px band was set around the nucleus. Furthermore, an area outside the cell was used for background subtraction. The corrected fluorescence was calculated as follows: Integrated Density – (Area of interest x mean fluorescence of background) (McCloy et al., 2014).

5.4.4. Electron microscopy

Huh7.5 RFP-NLS cells were infected with Jc1^{NS5AB-EGFP} for 2 days. $9 \cdot 10^4$ cells were seeded per IBIDI dish and treated with DMEM⁺⁺ containing 100 μM oleic acid/albumin, linoleic acid/albumin, or α -linolenic acid/albumin, or treated as mock-control for 3 days. The position of infected cells was determined by fluorescence microscopy on a Nikon Eclipse Ti. The electron microscopy study was performed by Valerie Mordhorst at the Microscopy & Image analysis facility of the Heinrich Pette Institute. The protocol for sample preparation and transmission electron microscopy was established by Valerie Mordhorst (Mordhorst, unpublished data). All following steps were performed on ice or at 4 °C. Briefly, the medium was removed and cells were fixed with 2.5% glutaraldehyde/1% osmiumtetroxide on ice and incubated for 30 min on ice in the dark. The cells were washed 3 times with DPBS and incubated with 0.1% thiocarbohydrazide for 30 min. After washing three times with DPBS the

cells were incubated with 1% reduced osmium tetroxide for 12 min in the dark. Cells were washed for three times, incubated with 1% gallic acid for 30 min at room temperature, and washed again three times with DPBS. The area containing the cells of interest was cut and dehydrated by the progressive lowering of temperature method. Therefore, cells were incubated in dilutions of ethanol, while with increasing concentrations of ethanol the temperature decreases. Each incubation step was performed for 10 min, starting with 10% ethanol at 0 °C, 30% ethanol at -10 °C, 50% ethanol at -30 °C, 70% ethanol at -30 °C and at least three times 10 min with 100% ethanol at -35 °C. Finally, the cells were incubated in ethanol/Epon over night at 0 °C and embedded in Epon at 4 °C. Sections of the embedded samples were analyzed in a FEI TECNAI G2 transmission electron microscope.

5.5. Statistical analysis

Unless otherwise stated, not normalized data were evaluated with a two-tailed student's *t*-test. Normalized data were analyzed with a one sample *t*-test.

Bibliography

Aizaki, H., Lee, K.J., Sung, V.M., Ishiko, H., and Lai, M.M. (2004). Characterization of the hepatitis C virus RNA replication complex associated with lipid rafts. *Virology* 324, 450-461.

Akil, A., Peng, J., Omrane, M., Gondeau, C., Desterke, C., Marin, M., Tronchere, H., Taveneau, C., Sar, S., Briolotti, P., *et al.* (2016). Septin 9 induces lipid droplets growth by a phosphatidylinositol-5-phosphate and microtubule-dependent mechanism hijacked by HCV. *Nat Commun* 7, 12203.

Alexson, S.E., and Cannon, B. (1984). A direct comparison between peroxisomal and mitochondrial preferences for fatty-acyl beta-oxidation predicts channelling of medium-chain and very-long-chain unsaturated fatty acids to peroxisomes. *Biochim Biophys Acta* 796, 1-10.

Amemiya, F., Maekawa, S., Itakura, Y., Kanayama, A., Matsui, A., Takano, S., Yamaguchi, T., Itakura, J., Kitamura, T., Inoue, T., *et al.* (2008). Targeting lipid metabolism in the treatment of hepatitis C virus infection. *J Infect Dis* 197, 361-370.

Asabe, S.I., Tanji, Y., Satoh, S., Kaneko, T., Kimura, K., and Shimotohno, K. (1997). The N-terminal region of hepatitis C virus-encoded NS5A is important for NS4A-dependent phosphorylation. *J Virol* 71, 790-796.

Asselah, T., Rubbia-Brandt, L., Marcellin, P., and Negro, F. (2006). Steatosis in chronic hepatitis C: why does it really matter? *Gut* 55, 123-130.

Bayer, K., Banning, C., Bruss, V., Wiltzer-Bach, L., and Schindler, M. (2016). Hepatitis C Virus Is Released via a Noncanonical Secretory Route. *J Virol* 90, 10558-10573.

Bettters, J.L., and Yu, L. (2010). NPC1L1 and cholesterol transport. *FEBS Lett* 584, 2740-2747.

Bidell, M.R., McLaughlin, M., Faragon, J., Morse, C., and Patel, N. (2016). Desirable Characteristics of Hepatitis C Treatment Regimens: A Review of What We Have and What We Need. *Infect Dis Ther* 5, 299-312.

Blight, K.J., McKeating, J.A., and Rice, C.M. (2002). Highly permissive cell lines for subgenomic and genomic hepatitis C virus RNA replication. *J Virol* 76, 13001-13014.

Boulant, S., Montserret, R., Hope, R.G., Ratinier, M., Targett-Adams, P., Lavergne, J.P., Penin, F., and McLauchlan, J. (2006). Structural determinants that target the hepatitis C virus core protein to lipid droplets. *J Biol Chem* 281, 22236-22247.

Brasaemle, D.L. (2007). Thematic review series: adipocyte biology. The perilipin family of structural lipid droplet proteins: stabilization of lipid droplets and control of lipolysis. *J Lipid Res* 48, 2547-2559.

Bruce, J.S., and Salter, A.M. (1996). Metabolic fate of oleic acid, palmitic acid and stearic acid in cultured hamster hepatocytes. *Biochem J* 316 (Pt 3), 847-852.

Chang, K.S., Jiang, J., Cai, Z., and Luo, G. (2007). Human apolipoprotein e is required for infectivity and production of hepatitis C virus in cell culture. *J Virol* 81, 13783-13793.

Chen, S.L., and Morgan, T.R. (2006). The natural history of hepatitis C virus (HCV) infection. *Int J Med Sci* 3, 47-52.

Cheng, J.J., Li, J.R., Huang, M.H., Ma, L.L., Wu, Z.Y., Jiang, C.C., Li, W.J., Li, Y.H., Han, Y.X., Li, H., *et al.* (2016). CD36 is a co-receptor for hepatitis C virus E1 protein attachment. *Sci Rep* 6, 21808.

Christensen, E., Hagve, T.A., Gronn, M., and Christophersen, B.O. (1989). Beta-oxidation of medium chain (C8-C14) fatty acids studied in isolated liver cells. *Biochim Biophys Acta* 1004, 187-195.

Cooper, A.D. (1997). Hepatic uptake of chylomicron remnants. *J Lipid Res* 38, 2173-2192.

Da Poian A.T., E.-B.T., Luz M.R.M.P. *Nutrient Utilization in Humans: Metabolism Pathways.* Nature Education.

Dashti, N., Gandhi, M., Liu, X., Lin, X., and Segrest, J.P. (2002). The N-terminal 1000 residues of apolipoprotein B associate with microsomal triglyceride transfer protein to create a lipid transfer pocket required for lipoprotein assembly. *Biochemistry* 41, 6978-6987.

DeBose-Boyd, R.A. (2008). Feedback regulation of cholesterol synthesis: sterol-accelerated ubiquitination and degradation of HMG CoA reductase. *Cell Res* 18, 609-621.

Diamond, D.L., Syder, A.J., Jacobs, J.M., Sorensen, C.M., Walters, K.A., Prohl, S.C., McDermott, J.E., Gritsenko, M.A., Zhang, Q., Zhao, R., *et al.* (2010). Temporal proteome and lipidome profiles reveal hepatitis C virus-associated reprogramming of hepatocellular metabolism and bioenergetics. *PLoS Pathog* 6, e1000719.

Ding, Q., von Schaewen, M., and Ploss, A. (2014). The impact of hepatitis C virus entry on viral tropism. *Cell Host Microbe* 16, 562-568.

Douglas, D.N., Pu, C.H., Lewis, J.T., Bhat, R., Anwar-Mohamed, A., Logan, M., Lund, G., Addison, W.R., Lehner, R., and Kneteman, N.M. (2016). Oxidative Stress Attenuates Lipid Synthesis and Increases Mitochondrial Fatty Acid Oxidation in Hepatoma Cells Infected with Hepatitis C Virus. *J Biol Chem* 291, 1974-1990.

Dubikovskaya, E., Chudnovskiy, R., Karateev, G., Park, H.M., and Stahl, A. (2014). Measurement of long-chain fatty acid uptake into adipocytes. *Methods Enzymol* 538, 107-134.

DuBridge, R.B., Tang, P., Hsia, H.C., Leong, P.M., Miller, J.H., and Calos, M.P. (1987). Analysis of mutation in human cells by using an Epstein-Barr virus shuttle system. *Mol Cell Biol* 7, 379-387.

Ducharme, N.A., and Bickel, P.E. (2008). Lipid droplets in lipogenesis and lipolysis. *Endocrinology* 149, 942-949.

Eberle, D., Hegarty, B., Bossard, P., Ferre, P., and Foufelle, F. (2004). SREBP transcription factors: master regulators of lipid homeostasis. *Biochimie* 86, 839-848.

Eggert, D., Rosch, K., Reimer, R., and Herker, E. (2014). Visualization and analysis of hepatitis C virus structural proteins at lipid droplets by super-resolution microscopy. *PLoS One* 9, e102511.

Eichmann, T.O., Kumari, M., Haas, J.T., Farese, R.V., Jr., Zimmermann, R., Lass, A., and Zechner, R. (2012). Studies on the substrate and stereo/regioselectivity of adipose triglyceride lipase, hormone-sensitive lipase, and diacylglycerol-O-acyltransferases. *J Biol Chem* 287, 41446-41457.

Fahy, E., Subramaniam, S., Murphy, R.C., Nishijima, M., Raetz, C.R., Shimizu, T., Spener, F., van Meer, G., Wakelam, M.J., and Dennis, E.A. (2009). Update of the LIPID MAPS comprehensive classification system for lipids. *J Lipid Res* 50 *Suppl*, S9-14.

Farese, R.V., Jr., and Walther, T.C. (2009). Lipid droplets finally get a little R-E-S-P-E-C-T. *Cell* 139, 855-860.

Friebe, P., Boudet, J., Simorre, J.P., and Bartenschlager, R. (2005). Kissing-loop interaction in the 3' end of the hepatitis C virus genome essential for RNA replication. *J Virol* 79, 380-392.

Fried, M.W., Shiffman, M.L., Reddy, K.R., Smith, C., Marinos, G., Goncalves, F.L., Jr., Haussinger, D., Diago, M., Carosi, G., Dhumeaux, D., *et al.* (2002). Peginterferon alfa-2a plus ribavirin for chronic hepatitis C virus infection. *N Engl J Med* 347, 975-982.

Fritzsching, B., Schwer, B., Kartenbeck, J., Pedal, A., Horejsi, V., and Ott, M. (2002). Release and intercellular transfer of cell surface CD81 via microparticles. *J Immunol* 169, 5531-5537.

Gao, L., Aizaki, H., He, J.W., and Lai, M.M. (2004). Interactions between viral nonstructural proteins and host protein hVAP-33 mediate the formation of hepatitis C virus RNA replication complex on lipid raft. *J Virol* 78, 3480-3488.

Gastaminza, P., Cheng, G., Wieland, S., Zhong, J., Liao, W., and Chisari, F.V. (2008). Cellular determinants of hepatitis C virus assembly, maturation, degradation, and secretion. *J Virol* 82, 2120-2129.

Gosert, R., Egger, D., Lohmann, V., Bartenschlager, R., Blum, H.E., Bienz, K., and Moradpour, D. (2003). Identification of the hepatitis C virus RNA replication complex in Huh-7 cells harboring subgenomic replicons. *J Virol* 77, 5487-5492.

Grove, J., Huby, T., Stamataki, Z., Vanwolleghem, T., Meuleman, P., Farquhar, M., Schwarz, A., Moreau, M., Owen, J.S., Leroux-Roels, G., *et al.* (2007). Scavenger receptor BI and BII expression levels modulate hepatitis C virus infectivity. *J Virol* 81, 3162-3169.

Guan, M., Wang, W., Liu, X., Tong, Y., Liu, Y., Ren, H., Zhu, S., Dubuisson, J., Baumert, T.F., Zhu, Y., *et al.* (2012). Three different functional microdomains in the hepatitis C virus hypervariable region 1 (HVR1) mediate entry and immune evasion. *J Biol Chem* 287, 35631-35645.

Harmon, S.D., Kaduce, T.L., Manuel, T.D., and Spector, A.A. (2003). Effect of the delta6-desaturase inhibitor SC-26196 on PUFA metabolism in human cells. *Lipids* 38, 469-476.

Harris, C., Herker, E., Farese, R.V., Jr., and Ott, M. (2011). Hepatitis C virus core protein decreases lipid droplet turnover: a mechanism for core-induced steatosis. *J Biol Chem* 286, 42615-42625.

Heeren, J., Beisiegel, U., and Grewal, T. (2006). Apolipoprotein E recycling: implications for dyslipidemia and atherosclerosis. *Arterioscler Thromb Vasc Biol* 26, 442-448.

Herker, E., Harris, C., Hernandez, C., Carpentier, A., Kaehlcke, K., Rosenberg, A.R., Farese, R.V., Jr., and Ott, M. (2010). Efficient hepatitis C virus particle formation requires diacylglycerol acyltransferase-1. *Nat Med* 16, 1295-1298.

Herker, E., and Ott, M. (2011). Unique ties between hepatitis C virus replication and intracellular lipids. *Trends Endocrinol Metab* 22, 241-248.

- Herker, E., and Ott, M. (2012). Emerging role of lipid droplets in host/pathogen interactions. *J Biol Chem* 287, 2280-2287.
- Herms, A., Bosch, M., Ariotti, N., Reddy, B.J., Fajardo, A., Fernandez-Vidal, A., Alvarez-Guaita, A., Fernandez-Rojo, M.A., Rentero, C., Tebar, F., *et al.* (2013). Cell-to-cell heterogeneity in lipid droplets suggests a mechanism to reduce lipotoxicity. *Curr Biol* 23, 1489-1496.
- Herzog, R., Schwudke, D., Schuhmann, K., Sampaio, J.L., Bornstein, S.R., Schroeder, M., and Shevchenko, A. (2011). A novel informatics concept for high-throughput shotgun lipidomics based on the molecular fragmentation query language. *Genome Biol* 12, R8.
- Higashino, K., Fujioka, M., Aoki, T., and Yamamura, T. (1967). Metabolism of lysine in rat liver. *Biochem Biophys Res Commun* 29, 95-100.
- Hijikata, M., Shimizu, Y.K., Kato, H., Iwamoto, A., Shih, J.W., Alter, H.J., Purcell, R.H., and Yoshikura, H. (1993). Equilibrium centrifugation studies of hepatitis C virus: evidence for circulating immune complexes. *J Virol* 67, 1953-1958.
- Holthuis, J.C., and Menon, A.K. (2014). Lipid landscapes and pipelines in membrane homeostasis. *Nature* 510, 48-57.
- Hossain, T., Riad, A., Siddiqi, S., Parthasarathy, S., and Siddiqi, S.A. (2014). Mature VLDL triggers the biogenesis of a distinct vesicle from the trans-Golgi network for its export to the plasma membrane. *Biochem J* 459, 47-58.
- Houten, S.M., and Wanders, R.J. (2010). A general introduction to the biochemistry of mitochondrial fatty acid beta-oxidation. *J Inher Metab Dis* 33, 469-477.
- Jones, C.T., Catanese, M.T., Law, L.M., Khetani, S.R., Syder, A.J., Ploss, A., Oh, T.S., Schoggins, J.W., MacDonald, M.R., Bhatia, S.N., *et al.* (2010). Real-time imaging of hepatitis C virus infection using a fluorescent cell-based reporter system. *Nat Biotechnol* 28, 167-171.
- Kapadia, S.B., and Chisari, F.V. (2005). Hepatitis C virus RNA replication is regulated by host geranylgeranylation and fatty acids. *Proc Natl Acad Sci U S A* 102, 2561-2566.
- Kemp, S., Valianpour, F., Mooyer, P.A., Kulik, W., and Wanders, R.J. (2004). Method for measurement of peroxisomal very-long-chain fatty acid beta-oxidation in human skin fibroblasts using stable-isotope-labeled tetracosanoic acid. *Clin Chem* 50, 1824-1826.
- Koonen, D.P., Jacobs, R.L., Febbraio, M., Young, M.E., Soltys, C.L., Ong, H., Vance, D.E., and Dyck, J.R. (2007). Increased hepatic CD36 expression contributes to dyslipidemia associated with diet-induced obesity. *Diabetes* 56, 2863-2871.
- Koyuncu, E., Purdy, J.G., Rabinowitz, J.D., and Shenk, T. (2013). Saturated very long chain fatty acids are required for the production of infectious human cytomegalovirus progeny. *PLoS Pathog* 9, e1003333.
- Li, Q., Pene, V., Krishnamurthy, S., Cha, H., and Liang, T.J. (2013). Hepatitis C virus infection activates an innate pathway involving IKK-alpha in lipogenesis and viral assembly. *Nat Med* 19, 722-729.
- Li, Y., Yamane, D., Masaki, T., and Lemon, S.M. (2015). The yin and yang of hepatitis C: synthesis and decay of hepatitis C virus RNA. *Nat Rev Microbiol* 13, 544-558.
- Lindenbach, B.D. (2009). Measuring HCV infectivity produced in cell culture and in vivo. *Methods Mol Biol* 510, 329-336.

- Lindenbach, B.D., and Rice, C.M. (2013). The ins and outs of hepatitis C virus entry and assembly. *Nat Rev Microbiol* 11, 688-700.
- Lingwood, D., and Simons, K. (2010). Lipid rafts as a membrane-organizing principle. *Science* 327, 46-50.
- Listenberger, L.L., Han, X., Lewis, S.E., Cases, S., Farese, R.V., Jr., Ory, D.S., and Schaffer, J.E. (2003). Triglyceride accumulation protects against fatty acid-induced lipotoxicity. *Proc Natl Acad Sci U S A* 100, 3077-3082.
- Liu, Q., Yang, M., Fu, X., Liu, R., Sun, C., Pan, H., Wong, C.W., and Guan, M. (2016). Activation of farnesoid X receptor promotes triglycerides lowering by suppressing phospholipase A2 G12B expression. *Mol Cell Endocrinol* 436, 93-101.
- Löffler, G., Heinrich, P.C., Müller, M., Graeve, L., and Petrides, P.E., eds. (2014). *Löffler/Petrides Biochemie und Pathobiochemie*, Vol, 9., vollständig überarbeitete Auflage edn, ISBN: 978-3-642-17971-6.
- Lohmann, V. (2013). Hepatitis C virus RNA replication. *Curr Top Microbiol Immunol* 369, 167-198.
- Loizides-Mangold, U., Clement, S., Alfonso-Garcia, A., Branche, E., Conzelmann, S., Parisot, C., Potma, E.O., Riezman, H., and Negro, F. (2014). HCV 3a core protein increases lipid droplet cholesteryl ester content via a mechanism dependent on sphingolipid biosynthesis. *PLoS One* 9, e115309.
- Lyn, R.K., Singaravelu, R., Kargman, S., O'Hara, S., Chan, H., Oballa, R., Huang, Z., Jones, D.M., Ridsdale, A., Russell, R.S., *et al.* (2014). Stearoyl-CoA desaturase inhibition blocks formation of hepatitis C virus-induced specialized membranes. *Sci Rep* 4, 4549.
- Mankouri, J., Walter, C., Stewart, H., Bentham, M., Park, W.S., Heo, W.D., Fukuda, M., Griffin, S., and Harris, M. (2016). Release of Infectious Hepatitis C Virus from Huh7 Cells Occurs via a trans-Golgi Network-to-Endosome Pathway Independent of Very-Low-Density Lipoprotein Secretion. *J Virol* 90, 7159-7170.
- Marukian, S., Jones, C.T., Andrus, L., Evans, M.J., Ritola, K.D., Charles, E.D., Rice, C.M., and Dustin, L.B. (2008). Cell culture-produced hepatitis C virus does not infect peripheral blood mononuclear cells. *Hepatology* 48, 1843-1850.
- Matsuzaka, T., and Shimano, H. (2009). Elovl6: a new player in fatty acid metabolism and insulin sensitivity. *J Mol Med (Berl)* 87, 379-384.
- McCloy, R.A., Rogers, S., Caldon, C.E., Lorca, T., Castro, A., and Burgess, A. (2014). Partial inhibition of Cdk1 in G 2 phase overrides the SAC and decouples mitotic events. *Cell Cycle* 13, 1400-1412.
- Merz, A., Long, G., Hiet, M.S., Brugger, B., Chlanda, P., Andre, P., Wieland, F., Krijnse-Locker, J., and Bartenschlager, R. (2011). Biochemical and morphological properties of hepatitis C virus particles and determination of their lipidome. *J Biol Chem* 286, 3018-3032.
- Messina, J.P., Humphreys, I., Flaxman, A., Brown, A., Cooke, G.S., Pybus, O.G., and Barnes, E. (2015). Global distribution and prevalence of hepatitis C virus genotypes. *Hepatology* 61, 77-87.
- Michal, G., ed. (1999). *Biochemical pathways = : Biochemie-Atlas*, Vol, ISBN: 3-86025-239-9.

Miquilena-Colina, M.E., Lima-Cabello, E., Sanchez-Campos, S., Garcia-Mediavilla, M.V., Fernandez-Bermejo, M., Lozano-Rodriguez, T., Vargas-Castrillon, J., Buque, X., Ochoa, B., Aspichueta, P., *et al.* (2011). Hepatic fatty acid translocase CD36 upregulation is associated with insulin resistance, hyperinsulinaemia and increased steatosis in non-alcoholic steatohepatitis and chronic hepatitis C. *Gut* 60, 1394-1402.

Mitsche, M.A., Packer, L.E., Brown, J.W., Jiang, Z.G., Small, D.M., and McKnight, C.J. (2014). Surface tensiometry of apolipoprotein B domains at lipid interfaces suggests a new model for the initial steps in triglyceride-rich lipoprotein assembly. *J Biol Chem* 289, 9000-9012.

Mohd Hanafiah, K., Groeger, J., Flaxman, A.D., and Wiersma, S.T. (2013). Global epidemiology of hepatitis C virus infection: new estimates of age-specific antibody to HCV seroprevalence. *Hepatology* 57, 1333-1342.

Moradpour, D., and Penin, F. (2013). Hepatitis C virus proteins: from structure to function. *Curr Top Microbiol Immunol* 369, 113-142.

Moradpour, D., Penin, F., and Rice, C.M. (2007). Replication of hepatitis C virus. *Nat Rev Microbiol* 5, 453-463.

Moriya, K., Yotsuyanagi, H., Shintani, Y., Fujie, H., Ishibashi, K., Matsuura, Y., Miyamura, T., and Koike, K. (1997). Hepatitis C virus core protein induces hepatic steatosis in transgenic mice. *J Gen Virol* 78 (Pt 7), 1527-1531.

Murphy, D.G., Sablon, E., Chamberland, J., Fournier, E., Dandavino, R., and Tremblay, C.L. (2015). Hepatitis C virus genotype 7, a new genotype originating from central Africa. *J Clin Microbiol* 53, 967-972.

Naganuma, T., Sato, Y., Sassa, T., Ohno, Y., and Kihara, A. (2011). Biochemical characterization of the very long-chain fatty acid elongase ELOVL7. *FEBS Lett* 585, 3337-3341.

Naldini, L., Blomer, U., Gallay, P., Ory, D., Mulligan, R., Gage, F.H., Verma, I.M., and Trono, D. (1996). In vivo gene delivery and stable transduction of nondividing cells by a lentiviral vector. *Science* 272, 263-267.

Narayanan, S., Nieh, A.H., Kenwood, B.M., Davis, C.A., Tosello-Trampont, A.C., Elich, T.D., Breazeale, S.D., Ward, E., Anderson, R.J., Caldwell, S.H., *et al.* (2016). Distinct Roles for Intracellular and Extracellular Lipids in Hepatitis C Virus Infection. *PLoS One* 11, e0156996.

Neufeldt, C.J., Joyce, M.A., Van Buuren, N., Levin, A., Kirkegaard, K., Gale, M., Jr., Tyrrell, D.L., and Wozniak, R.W. (2016). The Hepatitis C Virus-Induced Membranous Web and Associated Nuclear Transport Machinery Limit Access of Pattern Recognition Receptors to Viral Replication Sites. *PLoS Pathog* 12, e1005428.

Neumann-Haefelin, C., and Thimme, R. (2013). Adaptive immune responses in hepatitis C virus infection. *Curr Top Microbiol Immunol* 369, 243-262.

Pietschmann, T., Kaul, A., Koutsoudakis, G., Shavinskaya, A., Kallis, S., Steinmann, E., Abid, K., Negro, F., Dreux, M., Cosset, F.L., *et al.* (2006). Construction and characterization of infectious intragenotypic and intergenotypic hepatitis C virus chimeras. *Proc Natl Acad Sci U S A* 103, 7408-7413.

Pike, L.J. (2003). Lipid rafts: bringing order to chaos. *J Lipid Res* 44, 655-667.

- Purdy, J.G., Shenk, T., and Rabinowitz, J.D. (2015). Fatty acid elongase 7 catalyzes lipidome remodeling essential for human cytomegalovirus replication. *Cell Rep* 10, 1375-1385.
- Reiss, S., Harak, C., Romero-Brey, I., Radujkovic, D., Klein, R., Ruggieri, A., Rebhan, I., Bartenschlager, R., and Lohmann, V. (2013). The lipid kinase phosphatidylinositol-4 kinase III alpha regulates the phosphorylation status of hepatitis C virus NS5A. *PLoS Pathog* 9, e1003359.
- Reiss, S., Rebhan, I., Backes, P., Romero-Brey, I., Erfle, H., Matula, P., Kaderali, L., Poenisch, M., Blankenburg, H., Hiet, M.S., *et al.* (2011). Recruitment and activation of a lipid kinase by hepatitis C virus NS5A is essential for integrity of the membranous replication compartment. *Cell Host Microbe* 9, 32-45.
- Rhainds, D., and Brissette, L. (2004). The role of scavenger receptor class B type I (SR-BI) in lipid trafficking. defining the rules for lipid traders. *Int J Biochem Cell Biol* 36, 39-77.
- Ridgway, N., and McLeod, R., eds. (2015). *Biochemistry of Lipids, Lipoproteins and Membranes*, Vol, Sixth Edition edn, ISBN: 978-0-444-63438-2.
- Roe, B., Kensicki, E., Mohney, R., and Hall, W.W. (2011). Metabolomic profile of hepatitis C virus-infected hepatocytes. *PLoS One* 6, e23641.
- Romero-Brey, I., Merz, A., Chiramel, A., Lee, J.Y., Chlanda, P., Haselman, U., Santarella-Mellwig, R., Habermann, A., Hoppe, S., Kallis, S., *et al.* (2012). Three-dimensional architecture and biogenesis of membrane structures associated with hepatitis C virus replication. *PLoS Pathog* 8, e1003056.
- Rosch, K., Kwiatkowski, M., Hofmann, S., Schobel, A., Gruttner, C., Wurlitzer, M., Schluter, H., and Herker, E. (2016). Quantitative Lipid Droplet Proteome Analysis Identifies Annexin A3 as a Cofactor for HCV Particle Production. *Cell Rep* 16, 3219-3231.
- Ross-Thriepland, D., and Harris, M. (2015). Hepatitis C virus NS5A: enigmatic but still promiscuous 10 years on! *J Gen Virol* 96, 727-738.
- Rubbia-Brandt, L., Quadri, R., Abid, K., Giostra, E., Male, P.J., Mentha, G., Spahr, L., Zarski, J.P., Borisch, B., Hadengue, A., *et al.* (2000). Hepatocyte steatosis is a cytopathic effect of hepatitis C virus genotype 3. *J Hepatol* 33, 106-115.
- Ruggles, K.V., Turkish, A., and Sturley, S.L. (2013). Making, baking, and breaking: the synthesis, storage, and hydrolysis of neutral lipids. *Annu Rev Nutr* 33, 413-451.
- Rustan, A., and Devron, C. (2005). Fatty Acids: Structures and Properties. In *Encyclopedia of Life Sciences*
- Saito, K., Shirasago, Y., Suzuki, T., Aizaki, H., Hanada, K., Wakita, T., Nishijima, M., and Fukasawa, M. (2015). Targeting cellular squalene synthase, an enzyme essential for cholesterol biosynthesis, is a potential antiviral strategy against hepatitis C virus. *J Virol* 89, 2220-2232.
- Scheel, T.K., and Rice, C.M. (2013). Understanding the hepatitis C virus life cycle paves the way for highly effective therapies. *Nat Med* 19, 837-849.
- Schwenk, R.W., Holloway, G.P., Luiken, J.J., Bonen, A., and Glatz, J.F. (2010). Fatty acid transport across the cell membrane: regulation by fatty acid transporters. *Prostaglandins Leukot Essent Fatty Acids* 82, 149-154.

- Schwudke, D., Hannich, J.T., Surendranath, V., Grimard, V., Moehring, T., Burton, L., Kurzchalia, T., and Shevchenko, A. (2007). Top-down lipidomic screens by multivariate analysis of high-resolution survey mass spectra. *Anal Chem* 79, 4083-4093.
- Schwudke, D., Schuhmann, K., Herzog, R., Bornstein, S.R., and Shevchenko, A. (2011). Shotgun lipidomics on high resolution mass spectrometers. *Cold Spring Harb Perspect Biol* 3, a004614.
- Shavinskaya, A., Boulant, S., Penin, F., McLauchlan, J., and Bartenschlager, R. (2007). The lipid droplet binding domain of hepatitis C virus core protein is a major determinant for efficient virus assembly. *J Biol Chem* 282, 37158-37169.
- Shepard, C.W., Finelli, L., and Alter, M.J. (2005). Global epidemiology of hepatitis C virus infection. *Lancet Infect Dis* 5, 558-567.
- Shi, S.T., Lee, K.J., Aizaki, H., Hwang, S.B., and Lai, M.M. (2003). Hepatitis C virus RNA replication occurs on a detergent-resistant membrane that cofractionates with caveolin-2. *J Virol* 77, 4160-4168.
- Shi, Y., and Cheng, D. (2009). Beyond triglyceride synthesis: the dynamic functional roles of MGAT and DGAT enzymes in energy metabolism. *Am J Physiol Endocrinol Metab* 297, E10-18.
- Smirnova, E., Goldberg, E.B., Makarova, K.S., Lin, L., Brown, W.J., and Jackson, C.L. (2006). ATGL has a key role in lipid droplet/adiposome degradation in mammalian cells. *EMBO Rep* 7, 106-113.
- Spady, D.K., Kearney, D.M., and Hobbs, H.H. (1999). Polyunsaturated fatty acids up-regulate hepatic scavenger receptor B1 (SR-BI) expression and HDL cholesteryl ester uptake in the hamster. *J Lipid Res* 40, 1384-1394.
- Stryer, L., and Tymoczko, J.L., eds. (2003). *Biochemie*, Vol. 5. Aufl. edn, ISBN: 3-8274-1303-6.
- Sumpter, R., Jr., Loo, Y.M., Foy, E., Li, K., Yoneyama, M., Fujita, T., Lemon, S.M., and Gale, M., Jr. (2005). Regulating intracellular antiviral defense and permissiveness to hepatitis C virus RNA replication through a cellular RNA helicase, RIG-I. *J Virol* 79, 2689-2699.
- Syriopoulou, V., Nikolopoulou, G., Daikos, G.L., Theodoridou, M., Pavlopoulou, I., Nicolaidou, P., and Manolaki, N. (2005). Mother to child transmission of hepatitis C virus: rate of infection and risk factors. *Scand J Infect Dis* 37, 350-353.
- Takada, R., Satomi, Y., Kurata, T., Ueno, N., Norioka, S., Kondoh, H., Takao, T., and Takada, S. (2006). Monounsaturated fatty acid modification of Wnt protein: its role in Wnt secretion. *Dev Cell* 11, 791-801.
- Takeuchi, K., and Reue, K. (2009). Biochemistry, physiology, and genetics of GPAT, AGPAT, and lipin enzymes in triglyceride synthesis. *Am J Physiol Endocrinol Metab* 296, E1195-1209.
- Thiam, A.R., Farese, R.V., Jr., and Walther, T.C. (2013). The biophysics and cell biology of lipid droplets. *Nat Rev Mol Cell Biol* 14, 775-786.
- Thiele, C., Papan, C., Hoelper, D., Kusserow, K., Gaebler, A., Schoene, M., Piotrowitz, K., Lohmann, D., Spandl, J., Stevanovic, A., *et al.* (2012). Tracing fatty acid metabolism by click chemistry. *ACS Chem Biol* 7, 2004-2011.

- Thomssen, R., Bonk, S., Propfe, C., Heermann, K.H., Kochel, H.G., and Uy, A. (1992). Association of hepatitis C virus in human sera with beta-lipoprotein. *Med Microbiol Immunol* *181*, 293-300.
- Tiwari, S., and Siddiqi, S.A. (2012). Intracellular trafficking and secretion of VLDL. *Arterioscler Thromb Vasc Biol* *32*, 1079-1086.
- Todoroki, T., Matsumoto, K., Watanabe, K., Tashiro, Y., Shimizu, M., Okuyama, T., and Imai, K. (2000). Accumulated lipids, aberrant fatty acid composition and defective cholesterol ester hydrolase activity in cholesterol ester storage disease. *Ann Clin Biochem* *37 (Pt 2)*, 187-193.
- van Meer, G., Voelker, D.R., and Feigenson, G.W. (2008). Membrane lipids: where they are and how they behave. *Nat Rev Mol Cell Biol* *9*, 112-124.
- Voisset, C., and Dubuisson, J. (2004). Functional hepatitis C virus envelope glycoproteins. *Biol Cell* *96*, 413-420.
- Wakita, T., Pietschmann, T., Kato, T., Date, T., Miyamoto, M., Zhao, Z., Murthy, K., Habermann, A., Krausslich, H.G., Mizokami, M., *et al.* (2005). Production of infectious hepatitis C virus in tissue culture from a cloned viral genome. *Nat Med* *11*, 791-796.
- Walther, T.C., and Farese, R.V., Jr. (2012). Lipid droplets and cellular lipid metabolism. *Annu Rev Biochem* *81*, 687-714.
- Wanders, R.J., Ferdinandusse, S., Brites, P., and Kemp, S. (2010). Peroxisomes, lipid metabolism and lipotoxicity. *Biochim Biophys Acta* *1801*, 272-280.
- Wang, Y., Botolin, D., Xu, J., Christian, B., Mitchell, E., Jayaprakasam, B., Nair, M.G., Peters, J.M., Busik, J.V., Olson, L.K., *et al.* (2006). Regulation of hepatic fatty acid elongase and desaturase expression in diabetes and obesity. *J Lipid Res* *47*, 2028-2041.
- Waris, G., Felmlee, D.J., Negro, F., and Siddiqui, A. (2007). Hepatitis C virus induces proteolytic cleavage of sterol regulatory element binding proteins and stimulates their phosphorylation via oxidative stress. *J Virol* *81*, 8122-8130.
- Webster, B., Ott, M., and Greene, W.C. (2013). Evasion of superinfection exclusion and elimination of primary viral RNA by an adapted strain of hepatitis C virus. *J Virol* *87*, 13354-13369.
- Weerheim, A.M., Kolb, A.M., Sturk, A., and Nieuwland, R. (2002). Phospholipid composition of cell-derived microparticles determined by one-dimensional high-performance thin-layer chromatography. *Anal Biochem* *302*, 191-198.
- Wilfling, F., Haas, J.T., Walther, T.C., and Farese, R.V., Jr. (2014). Lipid droplet biogenesis. *Curr Opin Cell Biol* *29*, 39-45.
- Wissing, S., Montano, M., Garcia-Perez, J.L., Moran, J.V., and Greene, W.C. (2011). Endogenous APOBEC3B restricts LINE-1 retrotransposition in transformed cells and human embryonic stem cells. *J Biol Chem* *286*, 36427-36437.
- Wu, J.M., Skill, N.J., and Maluccio, M.A. (2010). Evidence of aberrant lipid metabolism in hepatitis C and hepatocellular carcinoma. *HPB (Oxford)* *12*, 625-636.
- Yang, W., Hood, B.L., Chadwick, S.L., Liu, S., Watkins, S.C., Luo, G., Conrads, T.P., and Wang, T. (2008). Fatty acid synthase is up-regulated during hepatitis C virus infection and regulates hepatitis C virus entry and production. *Hepatology* *48*, 1396-1403.

Ye, J., Wang, C., Sumpter, R., Jr., Brown, M.S., Goldstein, J.L., and Gale, M., Jr. (2003). Disruption of hepatitis C virus RNA replication through inhibition of host protein geranylgeranylation. *Proc Natl Acad Sci U S A* *100*, 15865-15870.

Yoon, E.J., and Hu, K.Q. (2006). Hepatitis C virus (HCV) infection and hepatic steatosis. *Int J Med Sci* *3*, 53-56.

Yu, G.Y., Lee, K.J., Gao, L., and Lai, M.M. (2006). Palmitoylation and polymerization of hepatitis C virus NS4B protein. *J Virol* *80*, 6013-6023.

Zayas, M., Long, G., Madan, V., and Bartenschlager, R. (2016). Coordination of Hepatitis C Virus Assembly by Distinct Regulatory Regions in Nonstructural Protein 5A. *PLoS Pathog* *12*, e1005376.

Zhao, Y., Chen, Y.Q., Bonacci, T.M., Bredt, D.S., Li, S., Bensch, W.R., Moller, D.E., Kowala, M., Konrad, R.J., and Cao, G. (2008). Identification and characterization of a major liver lysophosphatidylcholine acyltransferase. *J Biol Chem* *283*, 8258-8265.

Appendix

A. Abbreviations

Abbreviation	Meaning
°C	degree Celsius
µg	microgram
µl	microliter
3D	three dimensional
AA	arachidonic acid
α-AAA	α-amino adipic acid
ACAT	acyl-cholesterol-acyltransferases
ADRP	adipose differentiation-related protein
AGPAT	1-acylglycerol-3-phosphate-O-acyltransferase
ALA	α-linolenic acid
Apo	apolipoprotein
BSA	bovine serum albumin
BSL	biosafety level
CCT	CTP:phosphocholine cytidyltransferase
CD81	cluster of differentiation 81
CDP-Cho	cytidinediphosphate choline
CDP-DAG	cytidine diphosphate-diacylglycerol
CDP-Etn	cytidine diphosphate ethanolamine
CDS	cytidine diphosphate diacylglycerol
CE	cholesteryl ester
CE	cholesteryl ester
CEPT	choline/ethanolaminephosphotransferase
CERS	ceramide synthase
CerS	ceramide synthases
Cho	choline
CL	cardiolipin
CLDN1	claudin-1
CLS	cardiolipin synthase
CLSM	confocal laser scanning microscopy
CM	chylomicron

CoA	coenzyme A
CPE	ceramide phosphoethanolamine
CPT	cholinesphosphotransferase
CTCF	corrected total cell fluorescence
CTP	cytidine triphosphate
d	day
DAA	direct acting antivirals
DNA	deoxyribonucleic acid
DGAT	diglyceride acyltransferases
DGAT1	diacylglycerol transferase 1
DHA	docosahexanoic acid
DIC	differential interference contrast
DMSO	dimethyl sulfoxide
DMV	double-membrane vesicle
DTT	1,4-dithiothreitol
EGFP	enhanced green fluorescent protein
EGFR	epidermal growth factor receptor
EGFR	epidermal growth factor receptor
ELOVL	fatty acid elongase
EPA	eicosapentaenoic acid
ER	endoplasmic reticulum
FADS	fatty acid desaturase
FAS	fatty acid synthase
FCS	fetal calf serum
FFU	focus forming unit
FIA-MS/MS	flow injection analysis-tandem mass spectrometry
Fluc	<i>Firefly</i> luciferase
fw	forward
g	gram
GAG	glucosaminoglycan
GAPDH	glyceraldehyde 3-phosphate dehydrogenase
GCS	glucosylceramide synthase
GLA	γ -linolenic acid
Gluc	<i>Gaussia</i> luciferase
GSL	glycosphingolipids
h	hour
HCV	hepatitic C virus

HDL	high-density lipoprotein
HMG-CoA-reductase	HMG-CoA-reductase
HMGCR	3-hydroxy-3-methylglutaryl-CoA reductase
HMGCS	hydroxymethylglutaryl coenzyme A synthase
IRES	internal ribosomal entry site
IRES	internal ribosome entry site
JFH1	Japanese Fulminant Hepatitis 1
kb	kilo-base pair
l	liter
LA	linoleic acid
LB	Luria-Bertani
LC-MS/MS	liquid chromatography-tandem mass spectrometry
LC-MS/MS	liquid chromatography-tandem mass spectrometry
LD	lipid droplet
LDL	low-density lipoprotein
LDLR	low-density lipoprotein receptor
LPA	lyso-phosphatidic acid
LPC	lysophosphatidylcholine
LPCAT3	lyso-phosphatidylcholine acyltransferase 3
LVP	lipovirion particle
M	mol/l
m/z	mass to charge
MAG	monoglyceride
mg	milligram
min	minutes
ml	milliliter
MMV	multi-membrane vesicle
MOI	multiplicity of infection
mRNA	messenger ribonucleic acid
MS/MS	tandem mass spectrometry
MTTP	microsomal transfer protein
MUFA	monounsaturated fatty acid
NLS	nuclear localization sequence
NPC1L1	Niemann-Pick C1 like1
nt	nucleotides
o/n	over night
OA	oleic acid

OCLN	occludin
ORF	open reading frame
OXPAT	oxidative tissue-enriched PAT protein
PA	phosphatidic acid
PAP	phosphatidic acid phosphatase
PBS	phosphate-buffered saline
PC	phosphatidylcholine
PCae	acyl-alkyl-phosphatidylcholine
P-Cho	phosphocholine
PCR	polymerase chain reaction
PE	phosphatidylethanolamine
PEG	polyethylene glycol
PFA	paraformaldehyde
PG	phosphatidylglycerol
PGP	phosphatidylglycerolphosphate
PI	phosphatidylinositol
PI4P	phosphatidyl-inositol-4-phosphate
PIP	phosphoinositide
PIS	phosphatidylinositol synthase
PL	phospholipid
pmol	picomol
PMSF	phenylmethysulfonyl fluoride
PS	phosphatidylserine
PUFA	polyunsaturated fatty acid
rb	rabbit
rev	reverse
RFP	red fluorescence protein
RLU	relative light units
Rluc	renilla luciferase
RNA	ribonucleic acid
ROI	region of interest
rpm	revolutions per minute
rRNA	ribosomal ribonucleic acid
RT	room temperature
RT-pPCR	reverse transcription quantitative polymerase chain reaction
SCD	stearoyl-CoA desaturase
SDS	sodium dodecyl sulfate

SDS-PAGE	sodium dodecyl sulfate polyacrylamide gel electrophoresis
SEM	standard error of the mean
SFA	saturated fatty acid
shRNA	small hairpin ribonucleic acid
SL	sphingolipids
SM	sphingomyelin
SMS	sphingomyelin synthase
SMSr	sphingomyelin-synthase-related enzyme
SPT	serine palmitoyl transferase
SR-BI	scavenger receptor BI
SRE	sterol regulatory element
SREBP	sterol regulatory element-binding protein
T4-OH-proline	trans-4-hydroxyproline
TAG	triglyceride
TCID ₅₀	50% tissue culture infective dose
TEM	transmission electron microscopy
TIP47	tail-interacting protein 47
UTR	untranslated region
V	volt
v/v	volume/volume
VLDL	very low-density lipoprotein
VTV	VLDL transport vesicles
w/v	weight/volume
WB	western blotting
x g	times gravity

B. List of figures

Figure 1: HCV genotype distribution	6
Figure 2: The HCV life cycle	7
Figure 3: Structure of the virions and HCV entry	9
Figure 4: Viral genome organization and polyprotein processing	10
Figure 5: Viral RNA replication sites.	12
Figure 6: HCV assembly and release.	13
Figure 7: Fatty acid structure.	15
Figure 8: Fatty acid elongation and desaturation.	16
Figure 9: Polyunsaturated fatty acid synthesis pathway.....	17
Figure 10: β -oxidation.....	18
Figure 11: Triglyceride.....	19
Figure 12: Membrane lipids.....	20
Figure 13: Lipid synthesis pathways.....	23
Figure 14: Lipoproteins.....	24
Figure 15: Lipid droplets.....	26
Figure 16: Experimental setup and flow cytometry analysis of HCV-infected and control cells for lipidomics.	32
Figure 17: Western blot analysis of proteins from Bligh & Dyer extraction (whole cell extracts).	33
Figure 18: HCV infection alters the relative abundance of lipid classes.	34
Figure 19: Lipid profile of whole cell extracts from uninfected and HCV-infected cells.	35
Figure 20: Analysis of free fatty acids.....	36
Figure 21: Phosphatidylcholine and sphingomyelin concentrations determined by a targeted metabolomics approach.	38
Figure 22: Intracellular levels of amino acids, biogenic amines, and carnitines determined by targeted metabolomics.	40
Figure 23 Staining of free cholesterol in HCV-infected cells.	41
Figure 24: Amount of triglycerides in infected and uninfected Huh7.5 cells.....	43
Figure 25: Volumetric analysis of lipid droplets.....	44
Figure 26: Experimental setup and flow cytometry analysis for lipidomics of isolated lipid droplets.	46
Figure 27: Western blot analysis of proteins obtained from Bligh & Dyer extraction (lipid droplets).	47
Figure 28: Lipid profile of lipid droplets from uninfected and HCV-infected cells.	48
Figure 29: Luciferase assay to study the impact of cholesterol on the viral life cycle.	50

Figure 30: Triglyceride levels after fatty acid treatment.....	51
Figure 31: Cell viability after fatty acid treatment.	53
Figure 32: Analysis of viral replication after fatty acid treatment.	54
Figure 33: Density distribution of viral particles after lauric acid treatment.	55
Figure 34: Transmission electron microscopy was used to study the membranous web after fatty acid treatment.	56
Figure 35: HCV infection changes the expression of enzymes involved in fatty acid elongation and desaturation and lipid remodeling.....	58
Figure 36: HCV replication after knockdown of different elongases and desaturases.	60
Figure 37: Viability assay and FADS2 expression after SC-26196 treatment.....	61
Figure 38: Evaluation of SC-26196 treatment on the HCV life cycle.	63
Figure 39: Analysis of HCV replication after early SC-26196 treatment.	64
Figure 40: Surface expression of HCV entry factors after SC-26196 treatment.	65
Figure 41: Analysis of viral particle density after SC-26196 treatment.	66
Figure 42: Secretion and intracellular amounts of ApoE.	67

C. List of tables

Table 1: HCV plasmids.....	85
Table 2: Lentiviral plasmids.....	86
Table 3: Oligonucleotides for overlap extension PCR.....	86
Table 4: Oligonucleotides for qPCR.....	87
Table 5: Bacteria strain.....	88
Table 6: Bacterial media.....	88
Table 7: Cell culture media and buffer.....	89
Table 8: Solutions used for fatty acid complexation to albumin.....	90
Table 9: Chemicals used for agarose gel electrophoresis.....	91
Table 10: SDS-PAGE and analysis.....	91
Table 11: Utilized DNA and protein ladders.....	93
Table 12: Lysis Buffer.....	93
Table 13: Buffers used for lipid droplet isolation.....	94
Table 14: Solutions used for acidified Bligh & Dyer.....	94
Table 15: Buffers to prepare a density gradient.....	95
Table 16: Solutions utilized for Microscopy.....	95
Table 17: Stainings utilized for microscopy.....	95
Table 18: Utilized antibodies.....	96
Table 19: Utilized Enzymes.....	96
Table 20: Utilized Inhibitors.....	97
Table 21: Utilized chemicals.....	97
Table 22: Utilized kits.....	101
Table 23: Utilized consumables.....	102
Table 24: Utilized devices.....	104
Table 25: Utilized software.....	105
Table 26: PCR mixture.....	107
Table 27: PCR program.....	107
Table 28: Overlap PCR reaction.....	108
Table 29: Cyclor program for overlap PCR.....	108
Table 30: Cyclor program for purification PCR.....	108
Table 31: DNA digestion with restriction enzymes.....	109
Table 32: Ligation.....	109
Table 33: PCR mixture for colony PCR.....	110
Table 34: Cyclor program for colony PCR.....	110
Table 35: Volumes utilized for cell culture.....	112
Table 36: BioRad electroportator settings.....	113

Table 37: Transfection mixture	114
Table 38: Treatment components used for Luciferase assays in HCV-electroporated cells	116
Table 39: Treatment components for FADS2 inhibition	117
Table 40: Reaction mixture for cDNA synthesis.....	122
Table 41: cDNA synthesis reaction mixture	123

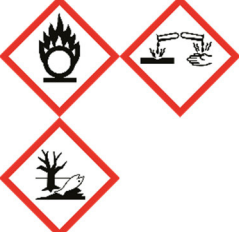
D. Presentations

The author presented parts of this dissertation at the following conferences:

- October 2014 Sarah Hofmann, Matthias Krajewski, Moritz Klages, Michael Melling, Pavel Truschow, Dominik Schwudke, Eva Herker
HCV's Interaction With the Host Lipid Metabolism
HPI Scientific Retreat, Hamburg, Germany (oral presentation)
- November 2014 Sarah Hofmann, Matthias Krajewski, Moritz Klages, Michael Melling, Pavel Truschow, Dominik Schwudke, Eva Herker
HCV's Interaction With the Host Lipid Metabolism
13th Workshop 'Cell Biology of Viral Infections', Kloster Schöntal, Germany (oral presentation, best presentation prize)
- March 2015 Sarah Hofmann, Matthias Krajewski, Moritz Klages, Michael Melling, Pavel Truschow, Dominik Schwudke, Eva Herker
HCV Alters the Cellular Lipid Profile and is Itself Influenced by Fatty Acids
25th Annual Meeting of the Society of Virology, Bochum, Germany (poster)
- September 2015 Sarah Hofmann, Matthias Krajewski, Moritz Klages, Michael Melling, Pavel Truschow, Dominik Schwudke, Eva Herker
HCV Alters the Cellular Lipid Profile and is Itself Influenced by Fatty Acids
14th Workshop 'Cell Biology of Viral Infections', Kloster Schöntal, Germany (oral presentation)
- October 2015 Sarah Hofmann, Matthias Krajewski, Moritz Klages, Michael Melling, Pavel Truschow, Dominik Schwudke, Eva Herker
HCV Alters the Cellular Lipid Profile and is Itself Influenced by Fatty Acids
22nd International Symposium on Hepatitis C and related Viruses, Strasbourg, France (poster)
- April 2016 Sarah Hofmann, Matthias Krajewski, Moritz Klages, Michael Melling, Pavel Truschow, Christina Scherer, Dominik Schwudke, Eva Herker
Hepatitis C Virus Infection Perturbs the Lipid Profile of the Host Cell
26th Annual Meeting of the Society of Virology, Münster, Germany (poster)

-
- October 2016 Sarah Hofmann, Matthias Krajewski, Moritz Klages, Michael Melling, Pavel Truschow, Christina Scherer, Valerie Mordhorst, Rudolph Reimer, Dominik Schwudke, Eva Herker
Hepatitis C Virus Infection Perturbs the Lipid Profile of the Host Cell
6th European Congress of Virology, Hamburg, Germany (poster)
- November 2016 Sarah Hofmann, Matthias Krajewski, Moritz Klages, Michael Melling, Pavel Truschow, Christina Scherer, Valerie Mordhorst, Verena Scholz, Rudolph Reimer, Dominik Schwudke, Eva Herker
Lipidomics Profiling Reveals an Interplay Between HCV Infection and Fatty Acid Remodelling
HPI Scientific Retreat, Hamburg, Germany (oral presentation)

E. Toxicity of chemicals

Chemical	GHS hazard pictogram	GHS hazard statements	GHS precautionary statements
1,4-Dithiothreitol (DTT)		H302-H315-H319	P302+P350-P305+P351+P338
2,6-Di-tert-butyl-4-methylphenol >99.0% (GC) (BHT)		H302-H315-H319-H411	P273-P305 + P351 + P338
2-Propanol		H225-H319-H336	P210-P233-P305+P351+P338
Acetic acid		H314	P301+P330+P331-P303+P361+P353-P305+P351+P338-P313
Acrylamide solution (30%) - Mix 37.5		H301-H312+H332-H315-H317-H319-H340-H350-H361f-H372	P201-P280-P302+P352-P305+P351+P338
AgNO ₃ (Silver nitrate)		H272-H314-H410	P273-P280-P301+P330+P331-P305+P351+P338
Ammonium acetate		H303, H316, H320, H333	P281, P335
Ampicillin		H317-H334	P261-P280-P342+P311
APS (Ammonium persulfate)		H272-H302-H315-H317-H319-H334-H335	P220-P261-P280-P305 + P351 + P338-P342 + P311

β -Mercaptoethanol		H301+H331- H310-H315- H317-H318- H373-H410	P273-P280- P302+P352- P304+P341- P305+P351+P338
CaCl ₂ (Calciumchloride)		H319	P264-P280- P305+P351+P338- P337+P313
Chloroform		H302-H315- H319-H331- H351-H361d- H372	P281-P302+P352- P304+P340- P305+P351+P338- P308-P310
Chloroquine diphosphate		H302	
DAPCO		H228-H302-H 315-H319-H412	P273-P280- P305+P351+P338- P332+P313
DNase Inactivation Reagent		H315-H335- H318	P280 P305 + P351 + P338
DNase I Buffer (10x)		H316	P332 + P313
EDTA		H319-H332- H373	P260-P261-P271- P304+P340- P305+P351+P338- P312
EtBr (Ethidiumbromide)		H302-H330- H341	P281-P302+P352- P304+P340- P305+P351+P338- P309-P310
Ethanol		H225	P210

Formaldehyde		H301+H311+H331-H314-H317-H335-H341-H350	P301+P330+P331-P302+P352-P305+P351+P338-P309-P310
Glutaraldehyde		H302+ H332-H314-H317-H334-H335-H410	P260-P280-P284-P303 + P361 + P353-P304 + P340 + P310-P305 + P351 + P338
Hoechst		H302-H315-H319	P280-P305+P351+P338-P313
Hydrogen peroxide 10%		H302-H318	P280-P305+P351+P338-P313
Hydrochloric acid (HCl)		H290-H314-H335	P280-P301+P330+P331-P305+P351+P338
KOH (Potassium hydroxide)		H290-H302-H314	P280-P301+P330+P331-P305+P351+P338
Lauric Acid		H318	P280-P305 + P351 + P338 + P310
Methanol (MeOH)		H225-H301+H311+H331-H370	P210-P233-P280-P302+P352-P309-P310-P501
Na ₂ CO ₃ (Sodium carbonate)		H319	P260-P305+P351+P338

Nonidet-P40		H302-H318-H411	P280-P301+P312-P305+P351+P338
Osmium tetroxide		300+310+330-314	280-301+330+331-302+352-304+340-305+351+338-308+310
Paraformaldehyde (PFA)		H228-H302-H315-H317-H319-H335-H351	P281-P302+P352-P304+P340-P305+P351+P338-P308+P313
Passive Lysis Buffer 5x		H360	P201-P202-P280-P308+P313-P405-P501
PFA (Paraformaldehyde)		H228-H302-H315-H317-H319-H335-H351	P281-P302+P352-P304+P340-P305+P351+P338-P308+P313
Phenol-Chloroform-Isoamyl alcohol (25:24:1 vol/vol/vol)		H301+H311+H331-H314-H341-H351-H361d-H372	P280b-P301+P330+P331-P305+P351+P338-P309+P311
Phenylmethylsulfonyl fluoride (PMSF)		H301-H314	P280-P305+P351+P338-P310
Phosphoric acid		H290, H314	P280, P305+351+338, P310 ^f
Polybrene (Hexadimethrinbromid)		H302	

Renilla Luciferase Assay Lysis Buffer 5x		H351-H360-H412	P201-P202-P280 P273-P308+P313-P405
Renilla Luciferase Assay Substrate		H225	
RNase Away		H315-H319	
Sodium deoxycholate		H302	P261
Sodium dodecyl sulfate (SDS)		H228-H302+H332-H315-H318-H335-H412	P210-P280-P302+P352-P304+P341-P305+P351+P338
Sodium hydroxide		H290-H314	P280-P301+P330+P331-P305+P351+P338
Sodium hypochlorite		EUH031-H315-H319	P264-P280-P302+P352-P305+P351+P338-P321-P501
Stop &Glo® Substrate		H225	P243-P280-P241-P303+P361+P353 P370+P378 P403+P235
TEMED (Tetramethylethylenediamine)		H225-H302+H332-H314	P210-P233-P280-P301+P330+P331-P305+P351+P338
Thiocarbohydrazide		H300 + H330-H311	P260-P264-P280-P284-P301 + P310-P310

TRI Reagent/Stat60		H301+ H311+ H331-H314- H341-H373- H411	P201-P261-P280-P301 + P310 + P330-P303 + P361 + P353-P305 + P351 + P338
Tris ultrapure (Tris-base)		H315-H319	P302+P352- P305+P351+P338
Triton X-100		H302-H318- H411	P273-P280- P305+P351+P338- P310
Trypan blue solution 0,4%		H350	P201-P308+P313
γ-Linolenic acid		H315-H319- H335	P261-P305 + P351 + P338

GHS pictogram guide



Harmful

Identifies chemicals with the following hazards:
Irritant, skin sensitizer, acute toxicity (harmful), narcotic effects,
respiratory tract infection, hazardous ozone layer.



Toxic

Identifies chemicals with the following hazards:
Acute toxicity (fatal or toxic).



Health Hazard

Identifies chemicals with the following hazards:
Carcinogen, mutagenicity, reproductive toxicity, respiratory
sensitizer, Target organ toxicity, Aspiration toxicity.



Environmental
hazard

Identifies chemicals with the following hazards:
Aquatic toxicity.



Corrosion

Identifies chemicals with the following hazards:
Skin corrosion, Eye damage, Corrosive metals.



Flammable

Identifies chemicals with the following hazards:

Flammables, pyrophorics, self-heating, emits flammable gas, self-reactives, organic peroxides



Oxidizing

Identifies chemicals with the following hazards:

Oxidizers

GHS hazard statements

0	Unstable explosive.
H201	Explosive; mass explosion hazard.
H202	Explosive; severe projection hazard.
H203	Explosive; fire, blast or projection hazard.
H204	Fire or projection hazard.
H205	May mass explode in fire.
H220	Extremely flammable gas.
H221	Flammable gas.
H222	Extremely flammable aerosol.
H223	Flammable aerosol.
H224	Extremely flammable liquid and vapour.
H225	Highly flammable liquid and vapour.
H226	Flammable liquid and vapour.
H227	Combustible liquid.
H228	Flammable solid.
H240	Heating may cause explosion.
H241	Heating may cause fire or explosion.
H242	Heating may cause a fire.
H250	Catches fire spontaneously if exposed to air.
H251	Self-heating; may catch fire.
H252	Self-heating in large quantities; may catch fire.
H260	In contact with water releases flammable gases which may ignite spontaneously.
H261	In contact with water releases flammable gas.
H270	May cause or intensify fire; oxidizer.
H271	May cause fire or explosion; strong oxidizer.
H272	May intensify fire; oxidizer.
H280	Contains gas under pressure; may explode if heated.
H281	Contains refrigerated gas; may cause cryogenic burns or injury.
H290	May be corrosive to metals.
H300	Fatal if swallowed.
H301	Toxic if swallowed.
H302	Harmful if swallowed.
H303	May be harmful if swallowed.

H304	May be fatal if swallowed and enters airways.
H305	May be harmful if swallowed and enters airways.
H310	Fatal in contact with skin.
H311	Toxic in contact with skin.
H312	Harmful in contact with skin.
H313	May be harmful in contact with skin.
H314	Causes severe skin burns and eye damage.
H315	Causes skin irritation.
H316	Causes mild skin irritation.
H317	May cause an allergic skin reaction.
H318	Causes serious eye damage.
H319	Causes serious eye irritation.
H320	Causes eye irritation.
H330	Fatal if inhaled.
H331	Toxic if inhaled.
H333	May be harmful if inhaled.
H334	May cause allergy or asthma symptoms or breathing difficulties if inhaled.
H335	May cause respiratory irritation.
H336	May cause drowsiness or dizziness.
H340	May cause genetic defects.
H341	Suspected of causing genetic defects.
H350	May cause cancer.
H351	Suspected of causing cancer.
H360	May damage fertility or the unborn child.
H361	Suspected of damaging fertility or the unborn child.
H362	May cause harm to breast-fed children.
H370	Causes damage to organs.
H371	May cause damage to organs.
H372	Causes damage to organs through prolonged or repeated exposure.
H373	May cause damage to organs through prolonged or repeated exposure.
H300+H310	Fatal if swallowed or in contact with skin.
H300+H330	Fatal if swallowed or if inhaled.
H310+H330	Fatal in contact with skin or if inhaled.
H300+H310+H330	Fatal if swallowed, in contact with skin or if inhaled.
H301+H311	Toxic if swallowed or in contact with skin.
H301+H331	Toxic if swallowed or if inhaled.
H311+H331	Toxic in contact with skin or if inhaled.
H301+H311+H331	Toxic if swallowed, in contact with skin or if inhaled.
H302+H312	Harmful if swallowed or in contact with skin.
H302+H332	Harmful if swallowed or if inhaled.
H312+H332	Harmful in contact with skin or if inhaled.
H302+H312+H332	Harmful if swallowed, in contact with skin or if inhaled.

H303+H313	May be harmful if swallowed or in contact with skin.
H303+H333	May be harmful if swallowed or if inhaled.
H313+H333	May be harmful in contact with skin or if inhaled.
H303+H313+H333	May be harmful if swallowed, in contact with skin or if inhaled.
H315+H320	Causes skin and eye irritation.
H400	Very toxic to aquatic life.
H401	Toxic to aquatic life.
H402	Harmful to aquatic life.
H410	Very toxic to aquatic life with long lasting effects.
H411	Toxic to aquatic life with long lasting effects.
H412	Harmful to aquatic life with long lasting effects.
H413	May cause long lasting harmful effects to aquatic life.
H420	Harms public health and the environment by destroying ozone in the upper atmosphere.

GHS precautionary statement

P101	If medical advice is needed, have product container or label at hand.
P102	Keep out of reach of children.
P103	Read label before use.
P201	Obtain special instructions before use.
P202	Do not handle until all safety precautions have been read and understood.
P210	Keep away from heat/sparks/open flames/hot surfaces. – No smoking.
P211	Do not spray on an open flame or other ignition source.
P220	Keep/Store away from clothing/.../combustible materials.
P221	Take any precaution to avoid mixing with combustibles/..
P222	Do not allow contact with air.
P230	Keep wetted with ...
P231	Handle under inert gas.
P232	Protect from moisture.
P233	Keep container tightly closed.
P234	Keep only in original container.
P235	Keep cool.
P240	Ground/bond container and receiving equipment.
P241	Use explosion-proof electrical/ventilating/lighting/.../equipment.
P242	Use only non-sparking tools.
P243	Take precautionary measures against static discharge.
P250	Do not subject to grinding/shock/.../friction.
P251	Pressurized container: Do not pierce or burn, even after use.

P260	Do not breathe dust/fume/gas/mist/vapours/spray.
P261	Avoid breathing dust/fume/gas/mist/vapours/spray.
P262	Do not get in eyes, on skin, or on clothing.
P262	Do not get in eyes, on skin, or on clothing.
P263	Avoid contact during pregnancy/while nursing.
P264	Wash...thoroughly after handling
P270	Do not eat, drink or smoke when using this product.
P271	Use only outdoors or in a well-ventilated area
P272	Contaminated work clothing should not be allowed out of the workplace.
P273	Avoid release to the environment.
P280	Wash...thoroughly after handling
P281	Use personal protective equipment as required.
P282	Wear cold insulating gloves/face shield/eye protection.
P283	Wear fire/flame resistant/retardant clothing
P210	Wear respiratory protection.
P284	Keep away from heat/sparks/open flames/hot surfaces. – No smoking.
P285	In case of inadequate ventilation wear respiratory protection.
P231 + P232	Handle under inert gas. Protect from moisture.
P235 + P410	Keep cool. Protect from sunlight.

EU specific hazard statements

EUH001	Explosive when dry
EUH006	Explosive with or without contact with air
EUH014	Reacts violently with water
EUH018	In use may form flammable/explosive vapour-air mixture
EUH019	May form explosive peroxides
EUH044	Risk of explosion if heated under confinement
EUH029	Contact with water liberates toxic gas
EUH031	Contact with acids liberates toxic gas
EUH032	Contact with acids liberates very toxic gas
EUH066	Repeated exposure may cause skin dryness or cracking
EUH070	Toxic by eye contact
EUH071	Corrosive to the respiratory tract
EUH059	Hazardous to the ozone layer
EUH201	Contains lead. Should not be used on surfaces liable to be chewed or sucked by children.

EUH201A	Warning! Contains lead.
EUH202	Cyanoacrylate. Danger. Bonds skin and eyes in seconds. Keep out of the reach of children.
EUH203	Contains chromium(VI). May produce an allergic reaction.
EUH204	Contains isocyanates. May produce an allergic reaction.
EUH205	Contains epoxy constituents. May produce an allergic reaction.
EUH206	Warning! Do not use together with other products. May release dangerous gases (chlorine).
EUH207	Warning! Contains cadmium. Dangerous fumes are formed during use. See information supplied by the manufacturer. Comply with the safety instructions.
EUH208	Contains < <i>name of sensitising substance</i> >. May produce an allergic reaction.
EUH209	Can become highly flammable in use.
EUH209A	Can become flammable in use.
EUH210	Safety data sheet available on request.
EUH401	To avoid risks to human health and the environment, comply with the instructions for use.

Danksagung

Besonders möchte ich mich bei Frau Dr. Eva Herker für das spannende Thema und die Betreuung meiner Arbeit bedanken. Vielen Dank für die tolle Unterstützung und die vielen hilfreichen Ratschläge.

Ich möchte mich bei Herrn PD Dr. Markus Perbandt für die Zweitbetreuung bedanken. Außerdem möchte ich Herrn Prof. Dr. Wolfgang Maison und Herrn Prof. Dr. Wolfram Brune für die Begutachtung meiner Disputation danken.

Ich möchte mich auch bei meinen Kooperationspartnern für die Zusammenarbeit bedanken, denn ohne diese wären einige der Daten nicht zustande gekommen.

Ein großes Dankeschön geht an Anja, Susan, Kathrin und Cordula, sowie an alle Master- und Bachelorstudenten, mit denen ich zusammenarbeiten durfte. Ich möchte mich bei euch für die schöne und unterhaltsame Atmosphäre im Labor und eure Hilfe und Unterstützung bedanken.

Ein herzlicher Dank geht an meine Familie, die mich immer unterstützt und motiviert hat.

Eidesstattliche Versicherung

Hiermit versichere ich an Eides statt, die vorliegende Dissertation selbst verfasst und keine anderen als die angegebenen Hilfsmittel benutzt zu haben. Die eingereichte schriftliche Fassung entspricht der auf dem elektronischen Speichermedium. Ich versichere, dass diese Dissertation nicht in einem früheren Promotionsverfahren eingereicht wurde.

Hamburg, den